MAGNESIUM SILICATE IMPREGNATION ON PALM-SHELL ACTIVATED CARBON POWDER FOR ENHANCED HEAVY METAL ADSORPTION

CHOONG CHOE EARN

FACULTY OF ENGINEERING
UNIVERSITY OF MALAYA
KUALA LUMPUR

2018

MAGNESIUM SILICATE IMPREGNATION ON PALM-SHELL ACTIVATED CARBON POWDER FOR ENHANCED HEAVY METAL ADSORPTION

CHOONG CHOE EARN

THESIS SUBMITTED IN FULFILMENT OF THE REQUIREMENTS FOR THE DEGREE OF DOCTOR OF PHILOSOPHY

FACULTY OF ENGINEERING
UNIVERSITY OF MALAYA
KUALA LUMPUR

2018

UNIVERSITY OF MALAYA

ORIGINAL LITERARY WORK DECLARATION

Name of Candidate: Choong Choe Earn

Matric No: KHA140139

Name of Degree: Doctor of Philosophy

Title of Project Paper/Research Report/Dissertation/Thesis ("this Work"):

MAGNESIUM SILICATE IMPREGNATION ON PALM-SHELL ACTIVATED CARBON POWDER FOR ENHANCED HEAVY METAL ADSORPTION

Field of Study: Environmental Engineering (Civil Engineering)

I do solemnly and sincerely declare that:

(1) I am the sole author/writer of this Work;
(2) This Work is original;
(3) Any use of any work in which copyright exists was done by way of fair dealing and for permitted purposes and any excerpt or extract from, or reference to or reproduction of any copyright work has been disclosed expressly and sufficiently and the title of the Work and its authorship have been acknowledged in this Work;
(4) I do not have any actual knowledge nor do I ought reasonably to know that the making of this work constitutes an infringement of any copyright work;
(5) I hereby assign all and every rights in the copyright to this Work to the University of Malaya ("UM"), who henceforth shall be owner of the copyright in this Work and that any reproduction or use in any form or by any means whatsoever is prohibited without the written consent of UM having been first had and obtained;
(6) I am fully aware that if in the course of making this Work I have infringed any copyright whether intentionally or otherwise, I may be subject to legal action or any other action as may be determined by UM.

Candidate's Signature   Date:

Subscribed and solemnly declared before,

Witness's Signature   Date:

Name:

Designation:

MAGNESIUM SILICATE IMPREGNATION ON PALM-SHELL ACTIVATED CARBON POWDER FOR ENHANCED HEAVY METAL ADSORPTION

ABSTRACT

In this work, palm-shell waste powder activated carbon (PPAC) coated by magnesium silicate (PPAC-MS) were successfully synthesized by the impregnation of magnesium silicate (MgSiO$_3$) using economical material (silicon dioxide powder) via mild hydrothermal approach under one-pot synthesis for the first time. Surprisingly, PPAC-MS exhibited a homogeneous thin plate mesh-like structure, as well as meso- and macro-pores with a high surface area of 772.1 m^2 g^{-1}. Different impregnation ratios of MgSiO$_3$ onto PPAC were tested from 0% to 300%. High amounts of MgSiO$_3$ led to high Cu (II) adsorption capacity. A ratio of 1:1, designated as PPAC-MS 100, was considered optimum because of its chemical stability in solution. The maximum adsorption capacity of PPAC-MS 100 for Cu (II) obtained by isotherm experiments was 369 mg g^{-1}. Kinetic adsorption data fitted to pseudo-second-order revealed chemisorption. Increasing ionic strength reduced Cu (II) adsorption capacity because of the competition effect between Na$^+$ and Cu^{2+}. Three times of regeneration studies were also conducted for Cu (II) removal. In addition, PPAC-MS 100 showed sufficient adsorption capacity on removal Zn (II), Al (III), Fe (II), Mn (II), and As (V) with the adsorption capacity of 373 mg g^{-1}, 244 mg g^{-1}, 234 mg g^{-1}, 562 mg g^{-1}, 191 mg g^{-1}, respectively. As an effective adsorbent, PPAC-MS 100 simultaneously removes Bisphenol A (BPA) and Pb (II) in single and binary mode. Due to its specific morphological characteristics, PPAC-MS 100 had adsorption capacities of Pb (II) as high as 419.9 mg g^{-1} and 408.8 mg g^{-1} in single mode and binary mode based on Freudliuch isotherm model while those for BPA by PPAC-MS were 168.4 mg g^{-1} and 254.7 mg g^{-1} for single mode and binary modes corresponding to Langmuir isotherm model. Experiment results also indicated that the synergistic removal of BPA occurred because the precipitation process of Pb (II) leads to the co-precipitation of BPA with

Pb(OH)$_2$ compound. PPAC-MS showed a good reusability for 5 regeneration cycles using Mg (II) solution followed by thermal treatment. PPAC-MS is characterized by Fourier Transformed Infrareds (FTIR), nitrogen adsorption/desorption analysis, X-Ray powder diffraction (XRD), X-ray photoelectron spectroscopy (XPS) and Field Emission Scanning Electron Microscope (FESEM). Overall, PPAC-MS has a high potential in the treatment process for wastewater containing both toxic heavy metals and emerging pollutants due to its high sorption capacities and reusability, while remaining economical through the reuse of palm-shell waste materials.

Keywords: adsorption, magnesium silicate, palm-shell waste powder activated carbon

PENYALUTAN MAGNESIUM SILIKAT TERHADAP SERBUK KARBON KELAPA SAWIT YANG DIAKTIFKAN UNTUK MENINGKATKAN PENYINGKIRAN LOGAM BERAT

ABSTRAK

Dalam kertas kerja ini, sisa serbuk kelapa sawit karbon aktifan (PPAC) yang dilapisi oleh magnesium silikat (PPAC-MS) dan disintesis oleh penggabungan magnesium silikat (MgSiO$_3$) dengan menggunakan bahan ekonomi (serbuk silion dioksida) melalui cara hidrotermal ringan dalam sintesis satu periuk untuk kali pertama. Yang menghairankan, PPAC-MS mempamerkan struktur semacam plat nipis yang homogen, serta meso- dan makrofora dengan luas permukaan tinggi sebanyak 772.1 m^2 g^{-1}. Nisbah impregnasi yang berbeza dari MgSiO$_3$ ke atas PPAC diujikan dari 0% hingga 300%. Jumlah MgSiO$_3$ yang tinggi menyebabkan kapasiti penjerapan Cu (II) yang tinggi. Nisbah impregnasi 1:1, yang ditetapkan sebagai PPAC-MS 100, dianggap optimum kerana kestabilan kimianya. Kapasiti penjerapan maksimum PPAC-MS 100 untuk Cu (II) yang diperolehi oleh eksperimen isotherm ialah 369 mg g^{-1}. Data penjerapan kinetik yang dipasang pada urutan kedua pseudo mendedahkan jerapan kimia. Peningkatan kekuatan ionik mengurangkan kapasiti penjerapan Cu (II) kerana kesan persaingan antara Na$^+$ dan Cu^{2+}. Tiga kali kajian regenerasi juga dilakukan untuk penyingkiran Cu (II). Di samping itu, PPAC-MS 100 menunjukkan kapasiti penjerapan yang mencukupi untuk penyingkiran Zn (II), Al (III), Fe (II), Mn (II), dan As (V) dengan kapasiti penyerapan 373 mg g^{-1}, 244 mg g^{-1}, 234 mg g^{-1}, 562 mg g^{-1}, 191 mg g^{-1}, masing-masing. Sebagai penyerap berkesan, PPAC-MS 100 secara serentak membuang BPA dan Pb (II) dalam mod tunggal dan mod binari. Oleh kerana ciri-ciri morfologi spesifiknya, PPAC-MS 100 mempunyai kapasiti penjerapan Pb (II) setinggi 419.9 mg g^{-1} dan 408.8 mg g^{-1} dalam mod tunggal dan mod binari berdasarkan model Freudliuch isotherm manakala bagi BPA oleh PPAC-MS adalah 168.4 mg g^{-1} dan 254.7 mg g^{-1} untuk mod tunggal dan mod binari yang sepadan dengan model isoterm Langmuir. Keputusan eksperimen juga

menunjukkan bahawa penyingkiran sinergi BPA berlaku kerana proses pemendapan Pb (II) membawa kepada pengangkatan BPA dengan sebatian $Pb(OH)_2$. PPAC-MS menunjukkan kebolehgunaan semula untuk 5 siklus regenerasi denggan menggunakan penyelesaian Mg (II) diikuti dengan rawatan termal. PPAC-MS dicirikan oleh Inframerah Transformasi Fourier (FTIR), X-Ray difraksi serbuk (XRD), spektroskopi fotoelektron X-ray (XPS) dan Mikroskop Elektronik Pengimbasan Pelepasan Medan (FESEM). Secara keseluruhannya, PPAC-MS mempunyai potensi yang tinggi dalam proses rawatan air kumbahan yang mengandungi kedua-dua logam berat toksik dan pencemaran yang timbul disebabkan oleh kapasiti penyerapan dan kebolehbalapan yang tinggi, sementara mengekalkan ekonomi melalui penggunaan semula bahan sisa kelapa sawit.

Kata Kunci: Penjerapan, magnesium silikat, sisa serbuk kelapa sawit karbon aktifan

ACKNOWLEDGEMENT

TABLE OF CONTENTS

LIST OF FIGURE

LIST OF TABLES

LIST OF SYMBOLS AND ABBREVIATIONS

Symbol/Abbreviations		Meaning
AC	:	Activated carbon
BPA	:	Bisphenol A
Pb	:	Lead
Mg	:	Magnesium
$MgSiO_3$	:	Magnesium silicate
Zn	:	Zinc
Al	:	Aluminium
Cu	:	Copper
Fe	:	Iron
$Mg(OH)_2$	:	Magnesium hydroxide
MgO	:	Magnesium oxide
Mn	:	Manganese
As	:	Arsenic
OH	:	Hydroxyl radical
$Pb(OH)_2$	:	Lead hydroxide
HCl	:	Hydrogen chloride
NaCl	:	Sodium chloride
ZVI	:	Zero valent iron
AMD	:	Acid mine drainage
H^+	:	Hydrogen ion
NaOH	:	Sodium hydroxide
CuO	:	Copper oxide
SI	:	Saturation Index
IAP	:	Ion activity product

p/p$_o$: Relative pressure

SiO$_2$: Silicon dioxide

CHAPTER 1: INTRODUCTION

1.1 Overview

Metals are the essential to life but its high concentration has toxic effects to the environment and living organisms. Effluents discharged from industry wastewater contain high concentrations of heavy metals, causing a serious environmental and health problems. Metals such as arsenic (As), cadmium (Cd), copper (Cu), chromium (Cr), lead (Pb), mercury (Hg) and selenium (Se) are dangerous to humans and animals due to their toxicities (Simate & Ndlovu, 2014).

Especially, Cu (II) and Pb (II) can be frequently found in industrial wastewater from active or abandoned mine, battery industry and metal pelting industry. Several copper mining-factories operating in Malaysia discharge about 30 times higher Cu (II) concentration than Standard B ($<0.2mg.L^{-1}$) (Madzin, Shai-in et al., 2015). Heavy metals such as copper can accumulate in living organism because heavy metals are not biodegradable (Yang X., Li et al., 2017). High concentrations of Pb (II) can give an effect on erythropoiesis that decreases oxygen level in blood circulation, neutral deafness, kidney and liver damage and causes drop in an intelligence quotient (IQ) for children and cause a reduction in numbers of leaves, leaf area, plant height and plant biomass for Portia tree (Chibuike & Obiora, 2014; Mudga V, 2010).

Apart from heavy metals in the wastewater, micropollutants could coexist in industry wastewater (Lee, Liao et al., 2015; Mohapatra, Brar et al., 2011). Especially, bisphenol A (BPA) is one type of endocrine disrupting chemicals (EDCs) which can cause hazardous health effects on humans. As BPA has been widely used in manufacturing of epoxy and polycarbonate, it is highly resistant for chemical degradation. Moreover, even at a low concentration, BPA can disrupt the endocrine system in human being (Liu, Wu et al., 2016).

1.2 Problem statement

Conventional treatment methods including chemical precipitation (Dabrowski, Hubicki et al., 2004), carbon adsorption (Mobasherpour, Salahi et al., 2014), ion exchange, evaporations, membrane (Barakat, 2011) and biological treatments processes are used to remove toxic and other harmful substances. Among these technologies, adsorption technology is a promising method due to its low maintenance cost and high efficiency (Barakat, 2011). However, the adsorption method suffers in terms of developing efficient adsorbents together with reduction of removal capacity in the complex situation while the competition occur competing with chemical component (Fan, Wang et al., 2016). Therefore, it is necessary to develop efficient adsorbents which can adapt complex condition with efficient binding capacity, not only for single-type metal adsorption, but also complex heavy metal compounds.

Porous materials have advantages in adsorption because of high surface area and the ability to bind functional group on the surface (Linares, Silvestre-Albero et al., 2014). Porous material such as zeolite, activated carbon, compost and biomass is reported as a good potential adsorption material for heavy metal removal. Activated carbon is a type of porous material which is widely used for micropollutant adsorption because of its high specific surface area with adequate pore structure and fast adsorption kinetic (Lua & Guo, 2001; Tsai, Chang et al., 2001).

Disparity surface chemistry modification approaches on the activated carbon have been reported for enhancing the adsorption performance including impregnation of organic compound (Gholidoust, Atkinson et al., 2017) and inorganic compound (Mopoung, Moonsri et al., 2015; Przepiórski, Czyżewski, Pietrzak, & Morawski, 2013). A great deal of research has investigated micropollutant removal using modified activated carbon by amine group (Yantasee, Lin et al., 2004), Fe_2O_3 impregnation (Reza & Ahmaruzzaman, 2015), anionic surfactants (Ahn, Park et al., 2009) and others.

However, commercial active carbon is expensive, so several studies have been conducted to investigate economical adsorbents such as bamboo (Liao P., Yuan et al., 2012), nut shell (Shukla & Pai, 2005), sawdust (Hameed & El-Khaiary, 2008), and cotton hull (Sathishkumar, Binupriya et al., 2008). In this study, palm-shell waste powder activated carbon (PPAC) was used, which is a cost-effective material (Jais, Ibrahim et al., 2016).

Moreover, since many surface waters are contaminated by both organic and inorganic toxic compounds, it is necessary to develop high efficiency media that can remove both toxic compounds simultaneously. As one of the most promising methods, adsorption of organic and inorganic micro pollutants by activated carbon has been extensively studied (Bautista-Toledo I., Ferro-García et al., 2005; Gaya, Otene et al., 2015; Kadirvelu, Faur-Brasquet et al., 2000; Shekinah, Kadirvelu et al., 2002; Xu, Wang et al., 2012). However, there are few studies that have been conducted on the simultaneous removal of BPA and Pb (II).

1.3 Objective and Scope of study

The main scope of this study is to develop a new and simple one-pot synthesis methods for coating $MgSiO_3$ onto surface of palm-shell waste powder activated carbon (PPAC) with mild hydrothermal treatment in an economical route using a cheap precursor (silicon dioxide powder) for removal of organic and inorganic micropolluant i.e. heavy metals and BPA. Objectives for this study we shown below:

1. **Synthesis of adsorbent:** To modify the palm-shell waste powder activated carbon (PPAC) using $MgSiO_3$ using simple one pot synthesis method. Optimize the coating ratio of $MgSiO_3$ onto (PPAC) by compare the efficiency of heavy metals adsorption capacity.

2. **Dissection of adsorbents:** To investigate the physical and chemical characterization of prepared adsorbents through crystalline phase analysis,

surface functional group analysis, surface morphology imaging, surface area and pore size characteristics.

3. **Assessment of heavy metals removal performance:** To investigate the effect of pH, temperature, ionic strength and various through adsorption test. To investigate the removal capacity of Pb (II), Cu (II), Mn (IV), Al (III) and As (V) using modified PPAC.

4. **Assessment of pollutant removal performance with the presence of BPA:** To evaluate the influence of the presence of BPA with adsorption of Pb (II) using modified PPAC compare with PPAC.

5. **Assessment of reusability:** To study the regeneration of adsorbent using acid, Mg (II) solution and thermal treatment.

1.4   Thesis Overview

This thesis is divided into 5 chapters. Chapter 1 starts with the introduction and discussion the environmental issues. This is followed by an introductory on adsorption for heavy metals wastewater treatment using porous material as adsorbents. It also presented the major scope and objectives of this study.

Chapter 2 covers the literature survey related to the thesis. In this chapter, a comprehensive literature on effect of heavy metal toward human being, aquatic life and plant, background of heavy metal treatment technologies and finally the performance general adsorbent development and modification approach are discussed.

Chapter 3 outlines the synthesis route of heavy metals adsorbents, followed by surface modification using magnesium silicate. Several analytical techniques were involved in understanding the textural properties and surface chemistry of prepared

adsorbents. This chapter also presents the experiment setup for the adsorption of heavy metals.

Chapter 4 presents the finding of the thesis with detailed discussion. This chapter presents the chemical and physical properties of prepared adsorbents and the results of heavy meal and BPA adsorption capacity. The influence of ionic strength, solution pH and temperature on heavy metal and BPA adsorption was discussed. Moreover, the performance and mechanism of heavy metal and BPA adsorption are presented. Finally, the conclusion is presented in Chapter 5.

2.1 Wastewater sources

Rapid developments in variety of fields such as mining operation, batteries, agriculture industries, and etc, to meet the requirement of mankind has led to the presence of new compounds in the effluent outlet of processing plants which are not degraded by the general wastewater treatment methods. It is very important to discharge the effluent in a proper manner and keep the water quality of effluent comply with environmental laws which not affected to the existing water bodies. However, many recent studies indicated that high concentration of heavy metals have been detected in water sources around the world presented in Table 2.1. Heavy metal toxicity is a serious risk to the plant, human and aquatic life. It is high solubility in aquatic environments and it can be easily absorbed by living species. Therefore, it is compulsory to treat the heavy metal wastewater prior to its discharge to the environment.

Table 2.1: Heavy metals detected in open water sources

Pollutant	Concentration	Sources	Country	Reference
As (III)	0.66 mg.L^{-1}	River	Spain	(Sánchez-Rodas, Luis Gómez-Ariza et al., 2005)
Cd (II)	0.134 mg.L^{-1}	River	Sri Lanka	(Perera, Sundarabarathy et al., 2016)
Cr (VI)	4.82±1.45 mg.L^{-1}	River	Algeria	(Leghouchi, Laib et al., 2008)
Cu (II)	4.29 mg.L^{-1}	Lake	Kenya	(Wambu, Omwoyo et al., 2016)
Pb (II)	17.13 ± 1.58mg.L^{-1}	River	United State	(Kilmer & Bouldin, 2016)
Hg (II)	0.002 mg.L^{-1}	River	Indonesia	(Tjokronegoro & Roosmini, 2010)

2.1.1 Impact of dissolved heavy metals on Human Being

Generally, low concentration of heavy metals can naturally found in the environment but high concentration of heavy metals were detected due to the increased of industrial wastes. There are several routes that the heavy metals can be entering to human body via breathing, eating and drinking. The heavy metals can transfer from soil to human through directly vegetation (Tchounwou, Yedjou et al., 2012). Moreover, heavy metal contaminated soil will continuously stay in the food chain through food crop resulting in phytotoxicity affected to human health (Liao J., Wen et al., 2016). Excess intake of heavy metals component such as As, Cd, Cr, Pb, Hg and Sn are dangerous to human and animals due to toxicity of heavy metal will disrupt the metabolic function as shown in Table 2.2 (Kapaj et al., 2006; Mudgal et al., 2010). In addition, many significant impacts to the health of human being who are exposed to heavy metals due to heavy metal can highly persist in human bodies for a long period of time (Kapaj, Peterson et al., 2006). Therefore, heavy metals will easily accumulate in the organs and disrupt their function and inhibit biological function by interfere or displace the vital nutritional minerals from their original place (Simate & Ndlovu, 2014).

Table 2.2: Disease cause by high level of heavy metal

Heavy metal	Disease cause by high level of heavy metal
Arsenic	Arsenicosis/arsenicalism commonly known as arsenic poisoning, it will led to the problems with circulatory systems and may have increased the risk of gaining cancer.
Cadmium	High level of cadmium in drinking water causes irritates the stomach, leading to vomiting and diarrhea.

Heavy metal	Disease cause by high level of heavy metal
Chromium	High level of chromium can result damage of kidney, liver and nerve tissue.
Lead	High level of lead can effect on erythropoises will decrease oxygen in blood circulation,neural deafness, kidney and liver damage and cause drop in IQ for children.
Mercury	Mercury can accumulation in thyroid cause ocrodynia under continuous expose condition
Selenium	Expose to a high concentration of selenium will cause for hair loss, and neurological abnormalities.

2.1.2. Effect of dissolved heavy metals on plant and soil

Soils can be contaminated by high concentration of heavy metals via disposal of mine tailing, metal wastes, industrial wastewater, sludge and petrochemicals. High concentration of heavy metal contaminated soil resulting long-term difficulties for re-vegetation and rehabilitation. Furthermore, it also reduced the usable land for agricultural purpose due to its creating potential for toxic effect at higher food chain level.

Heavy metal ions can be leached out from contaminated soil in low pH due to the favorable solubility condition for cation. Leaching of heavy metals will be absorbed by plant to translocation and store as micronutrients (Tangahu, Sheikh Abdullah et al., 2011). In addition, imbalance of metal elements can led to acidification of soil where the high amount of metals will tend to retain in soil and easily to be absorbed by plant (Simate & Ndlovu, 2014). Heavy metals affect the plants in diverse ways, however, excess of heavy metals have negative effects on plant biochemical and physical

activities show in Table 2.3. For example, excess intake of arsenic leading to reduction in seed germination, seedling height, lead area and dry matter production for rice. Plants grown in high concentration heavy metal contaminated soil show the symptoms of growth inhibition, and finally death.

Table 2.3: Effect of heavy metal on plant

Heavy metal	Heavy metal effect on plant
Arsenic	Reduction in seed germination; decrease in seedling height; reduced leaf area and dry matter production for rice.
Cadmium	Reduced shoot growth for garlic and maize, cadmium will accumulate in the plant.
Chromium	Reduced shoot and root growth for wheal; Reduce onion biomass
Copper	Copper will accumulate in bean roots; Reduction roots growth for rhode grass.
Lead	Reduction in number of leaves and leaf area; reduced plant height; decrease in plant biomass for Portia tree.
Manganese	Manganese will accumulate in the shoot and root; reduce the growth rate for pea, reduce photosynthesis of oxygen for pea
Mercury	Reduction in germination percentage; reduced plant height; reduction in flowering and fruit weight; chlorosis for tomato plant.
Nickel	Decrease in chlorophyll content and stomata conductance; decreased enzyme activity which affected calvin cycle and CO_2 fixation for Pigeon pea; inhibition for rice to growth root

2.1.3 Effect of dissolved heavy metals on aquatic life

It is well known that metals are easily dissolved in aqueous phase and absorbed by aquatic life. High concentration of heavy metals effluent will accumulate in aquatic

bodies. Furthermore, aquatic life can obtain heavy metal sources through food chain system. In spite of the fact that exposes heavy metals to aquatic life can result the reduction on reproduction, sublethal toxic effect and disturb the organ function. A brief review on the effects caused by heavy metal on aquatic life and plant is shown in Table 2.4. Regulation standard for aquatic life protection for freshwater and seawater described details in Table 2.5 on the concentration limits of heavy metals for fresh water and seawater discharge standard for protection of aquatic system (Canadian Council of Resource and Environment Ministers, 2007). The heavy metal will accumulate from plants to fishes because plants are the essential layer in the food chain system for aquatic life (Simate & Ndlovu, 2014). Moreover, the increased of dissolved oxygen level can decrease the concentration of dissolved heavy metals due to the heavy metal ion tends to be oxidized to form hydroxide compound under sufficient oxygen level.

Table 2.4: Heavy metal effect on aquatic life and plant

Metal	Effect on Aquatic life	Effect on Aquatic Plant
Chromium	Low concentration of Cr (IV) sub lethal toxic effects.	Low concentration of Cr (IV) sub lethal toxic effects, inhabit growth for plant
Lead	Lead concentration excess 100 ppb, gill function will be affected. Lead accumulates in the skin, bones, kidneys, and liver of aquatic life.	Excess 500 ppb of lead will affect the growth of algae
Mercury	Mercury accumulates in aquatic life's tissue, decreased hatching rate of fish.	It will caused folior injury chlorophyll content showed perceptible.

Table 2.5: Canadian Water Quality Standards for aquatic life protection standard

Metal	Freshwater (PPB)	Marine water
Aluminium	5 PPB at pH<6.5; 100 PPB at pH ≥6.5	N
Arsenic	5.0 PPB	12.5PPB
Cadmium	0.017 PPB	0.12 PPB
Chromium	Cr(III) 8.9 PPB Cr(VI) 1.0 PPB	Cr(III) 56 PPB Cr(VI) 1.5 PPB
Copper	2-5 (based on water hardness)	N
Lead	1-7 (based on water hardness)	N
Iron	300 PPB	N
Mercury	0.026	0.016 PPB
Nickel	25-150 (based on water hardness)	N
Selenium	1.0 PPB	N
Silver	0.1 PPB	N
Zinc	30 PPB	N

N-Not stated

PPB – Part per billion

2.2 Heavy metal removal technologies

Tremendous treatment methods though precipitation, ion-exchange, adsorption, electrolysis, membrane filtration and coagulation for efficient removal of heavy metal from wastewater. Treatment can be achieved by either active or passive treatment as described as following:

2.2.1 Active Treatment

Active treatment involved chemical reagent and labor input for continued operation by raise the pH of wastewater and result the dissolved metal to precipitate as hydroxides or carbonates compound. Alkaline material such as lime, slaked lime, calcium carbonate, sodium carbonate, sodium hydroxide, and magnesium oxide and hydroxide widely use as neutralization agent for removal of heavy metals in aqueous phase. This is due to the alkaline material can be produced alkalinity and precipitated the metals ion in wastewater by precipitation and sorption on alkaline material surface. The advantages of active treatment are effective to remove heavy metals and increase the pH rapidly. On the other hand, there are several numbers of disadvantages for active treatment such as operation costs are high for the chemical used in the system, the labor needed for maintenance for this system and mass amount of metal particle sludge need proper care for disposal. Moreover, a range of factors can influence the performance of active treatment system such as total suspension solid, flow rate of the system and the heavy metals concentration. Many researchers investigated the advantages and disadvantages of active treatment system are summarized in Table 2.6 (Taylor et al., 2005; Trumm, 2010).

Table 2.6: Advantages and limitations for Active treatment

Material	Chemical	Saturation pH	Solubility in water (mg.L⁻¹)	Advantages	Limitation
Soda Ash	Na_2CO_3	11.6	75,000	High efficiently to precipitate metal , low sludge volume	Poor on sludge setting, potential toxicity on sodium
Limestone	$CaCO_3$	8-9.4	14	Safe to use, lowest cost among all chemical	Low efficiently , fail to remove manganese, armoring occur
Quicklime	CaO	12.4	1,300-1,850	High efficiently to precipitate metal , low chemical cost	Efficiently reduce when chemical saturated
Ammonia	NH_3	9.2	900,000	Very high efficiently to precipitate metal , low sludge volume	Toxic to aquatic life, low cost ,Poor on sludge setting ,high cost chemical
Caustic Soda	NaOH	14	450,000	Very high efficiently to precipitate metal , low sludge volume	potential toxicity on sodium, highest cost among all chemical
Caustic magnesia	MgO	9.5-10.8	1-50	Very high efficiently to precipitate metal , low sludge volume ,low chemical cost	Lower reaction compare to calcium hydroxide

2.2.2 Passive Treatment

Passive treatment has been developed for acid mine drainage (AMD) treatments at early of 1990. Acid mine drainage effluence consists of high concentration of various heavy metals and low pH solution. The advantages of passive treatment are not requiring constantly labor maintenance and low long-term operation cost. The design of passive system must allow slow reaction rate to minimize the armoring effect. Moreover, organic matter can be introduced to the system to control the redox condition to minimize the armoring effect. Thus, passive treatment approaches are more economical compare to activate treatment; however, there are some significant limitations for this type of treatment system such as it cannot designed for accommodate any acidity, flow rate and daily heavy metal loading. A brief description for different type of passive treatment system using open limestone drain, anoxic limestone drain, aerobic wetlands, reducing and alkalinity producing system (RAPS) and slag leach bed shown in Table 2.7 (Taylor et al., 2005).

Table 2.7 : Characteristic for Passive treatment system

Passive treatment method	Acidity Range (mg $CaCO_3$/L)f or influent	Acidity Load (kg $CaCO_3$/day) for influent	Flow Rate (L/s) for influent	Dissolve Oxygen Concentration	Influent pH range	Max pH for Effluent
Open Limestone Drains	< 500	< 150	< 20	Based on site condition.	> 2	6–8
Anoxic Limestone Drains	< 500	< 150	< 20	< 1	> 2	6–8
Aerobic Wetlands	< 500	≤ 1	1–5 days	Based on site condition.	> 6	n/a

Passive treatment method	Acidity Range (mg CaCO$_3$/L)f or influent	Acidity Load (kg CaCO$_3$/day) for influent	Flow Rate (L/s) for influent	Dissolve Oxygen Concentration	Influent pH range	Max pH for Effluent
Anaerobic Wetlands	< 500	1	1–5 days	Based on site condition.;< 1 mg/L subsurface	> 2.5	6–8
RAPS	< 300	< 100	< 15	< 1-3	> 2.5	6–8
Slag Leach Beds	< 1000	1-2	< 20	Based on site condition.	> 1.5	>10

2.2.3 Anoxic Limestone drain

Anoxic Limestone drain (ALD) consists of a burial limestone bed encapsulation in geotechnical fabric and cover by soil to remain anoxic condition or low dissolve oxygen condition shown in Figure 2.1 (Interstate Technology & Regulatory Council, 2010). The heavy metal effluent pass through the ALD system promoting the limestone layer reacts rapidly to heavy metal wastewater to produce alkalinity via limestone dissolution. Generally, the pH of effluent from limestone drains is in the range of pH 6.8-7.0. In fact, ALD needed to remain low oxygen level to avoiding armoring effect on limestone from metal hydroxide compound. With ALD system can prevent the formation of metal hydroxide compound that can resulting clogging of effluent drain. Generally, the effluent from ALD must be followed by a pond and aerobic wetland to remove the dissolved metal precipitant. Furthermore, ALD is not suitable for wastewater which contain very high concentration of aluminum due to the insoluble pH for aluminum is between pH 4.5-8.5 (Watzlaf, Schroeder et al., 2000). This passive treatment system allows the reduction of treatment system size by decrease the metal ion loading and led to the increase of alkalinity release.
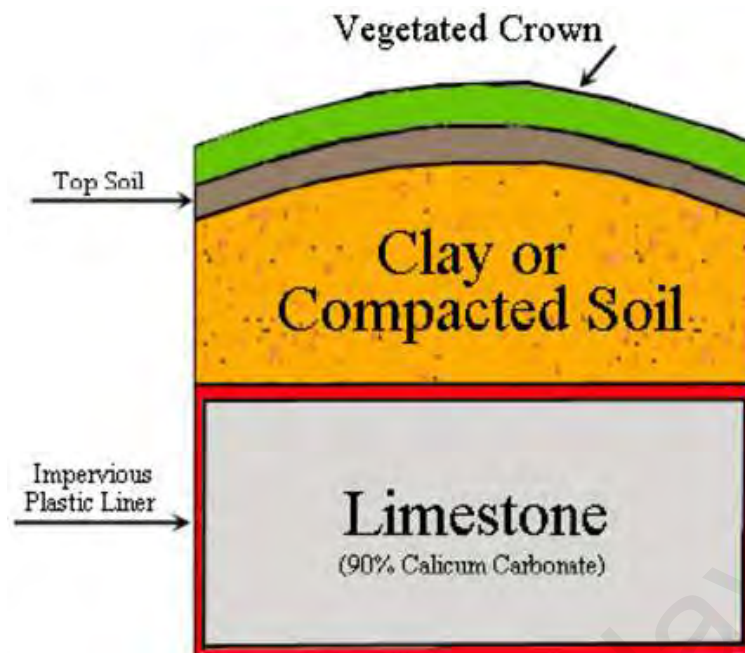
Figure 2.1: Cross section of an anoxic limestone drain

2.2.4 Slag bed

Steel slag is a side product from smelting process for steel-making industry, and huge amount are generated annually. Steel slag is highly alkaline because it contains mixture of oxides compound such as calcium oxide and calcium iron silicate which can undergo dissolution with water and increasing the alkalinity of the solutions. Traditionally, steel slag is used for soil amendment and sintering material for the past decade. The application of steel slag has been extended from the soil amendment system to heavy metal wastewater treatment system (Goetz & Riefler, 2014). The advantages of slag leach beds lied in the low operations and maintenance costs for the overall passive treatment system. The general cut section drawing for steel slag leach bed design is shown in Figure 2.2, the wastewater will penetrate through a layer of steel slag and detent for a specific duration.
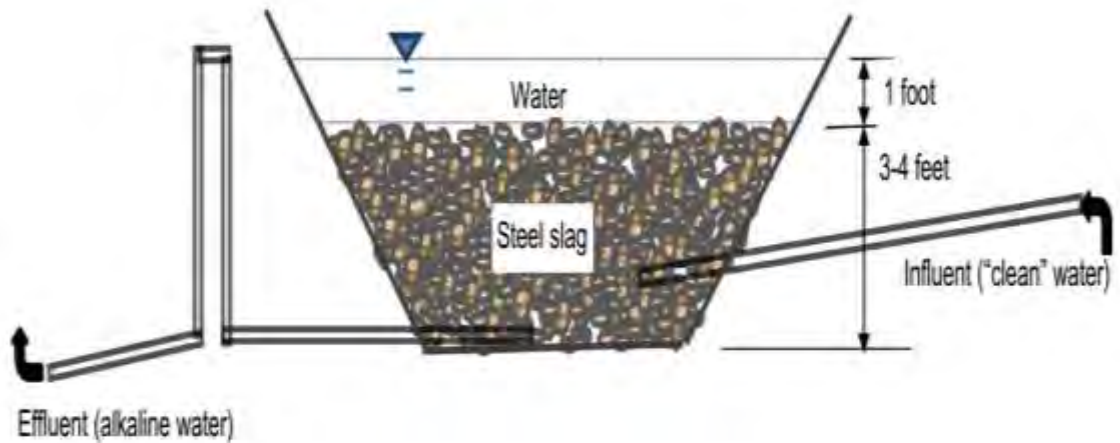
Figure 2.2: Schematic drawing for Steel slag leach bed (Goetz and Riefler, 2014)

The potential of employed steel slag bed for wastewater treatment had been studies by many researchers. Name & Sheridan (2014) conducted a set of experiments on remediation on acid heavy metal wastewater using 2 different types of steel slag which corresponding to stainless steel slag and basic oxygen slag. Basic oxygen slag (BOS) is more significant for the reduction of the iron and sulphate compare to stainless steel slag (Name & Sheridan, 2014). Goetz and Riefler (2014) proposed the optimum ratio of 100g of steel slag to 1L of heavy metal wastewater, the effluent pH value increase from pH 2.5 to pH 12.1.

Furthermore, Goetz and Riefler (2014) reported by reduction of flow rate can enhance the iron and sulphate removal efficiency due to increase the contact time between the steel slag and the heavy metal ions. However, the clogging in the effluent pipe from the steel slag bed will form a thick layer of precipitant due to the armoring effect. Moreover, thick layer of steel slag bed that generated high concentration of carbonate alkalinity will also resulting clogging problem at the effluent pipe (Goetz & Riefler, 2014).

2.2.5 Organic Material

Recently, many researchers attempted to develop low cost organic material (e.g. coal and rice hulls) to treat heavy metal wastewater due to cost effective reason. Kalyoncu Ergüler (2015) investigated on treating acidic heavy metal wastewater using eggshell. The grinded eggshells can increase the solution pH value from 2.3 to pH value of 6-8 for acidic wastewater less than 6 hours. Moreover, the amount of concentrations of some hazardous constituent achieve significant reduction such as 99.2% reduction of Fe (II), 75% reduction of Cu (II), 73% reduction of Zn (II), 54.6% of Pb (II), 31.6% of Ni (II) and 22% of Co (II) using 0.5g of grinded eggshells with 300mL of acidic wastewater (Kalyoncu Ergüler, 2015).

Heviánková (2014) conducted a series of experiments on treating acidic wastewater from brown coal opencast mine using wood ash which obtained from combusted deciduous and coniferous tree wood. Wood ash achieved higher pH value for treated solution, better metals removal efficiency (Fe (II), As (V), Hg (II), Cr (III), Co (II), Cu (II), Ni (II), Pb (II), Al (III), Mn (II), Zn (II), Mg (II) and SO_4^{2-}) and faster sludge setting capacities compared to conventional calcium hydroxide (Heviánková, Bestová et al., 2014). The authors had demonstrated the wood ash can be an alternative source for calcium hydroxide on treating acidic heavy metal wastewater.

2.2.6 Zero Valent Iron (ZVI)

ZVI is an effective media for immobilization of dissolved heavy metal ion and rapidly neutralize acidic wastewater (Lindsay, Ptacek et al., 2008). Lindsay (2008) reported that ZVI is very effective on the removal of Al (III), Zn (II), Cd (II), Ni (II) and Pb (II) elements due to the mechanism of adsorbs metals ion on the iron metal surface and resulting corrosion product. The mechanism for produced primary corrosion product of ZVI is sulfate green rust in sulphate rich solution. Furthermore, the

adsorption process continues and forms co-precipitant with primary corrosion product on ZVI surface (Wilkin & McNeil, 2003). Besides that, the microbial activity was detected in low flow rate column system of ZVI that can enhance metal ion removal and the iron reactivity can remain a longer life span (Bartzas, Komnitsas et al., 2006).

2.2.6 Magnesium oxide (MgO)

Magnesium oxide is an alkaline material which can increase the pH of solution up to 8-10 and decrease the solubility of heavy metal ion. Several researchers conducted lab scale test and field test to treat acidic heavy metal wastewater using MgO powder. Manuel A. Caraballo et al. (2009) conducted laboratory column experiments to test 2 different of MgO rich reagents (Caustic magnesia precipitator dust-CMPD and dolomitic lime precipitator dust-DLPL) for removal of manganese and aluminium from the wastewater. Based on their finding, CMPD and DLPD have similar performance according the reactivity, neutralizing capacity and hydraulic conductivity toward acidic heavy metal wastewater (Caraballo Manuel A., Rötting et al., 2009). Moreover, Caraballo et al found that divalent metals (Fe (II), Zn (II), Cd (II), Ni (II) and Co (II)) were precipitated along a MgO passive pilot system tank wall, infer that MgO is very efficiently on divalent metals removal. Therefore, MgO passive system is suitable to removal of divalent metals compare to trivalent metals ion (Caraballo M. A., Rotting et al., 2010).

2.3 Activated Carbon

2.3.1   Introduction

Activated carbon (AC) is a non-graphitic and porous carbonaceous material. Non-graphitic carbon can be divided into graphitzable and non-grapitizable carbon compound based on the degree of crystallographic order. The schematic representations of the structures of graphitizing and non-graphitizing carbons are shown in Figure 2.3.

Graphitizable carbon is non-graphitic carbon undergone heat treatment (graphitization) which is a non reversible process. Moreover, graphitizing carbon contained a higher number of graphite layer which arranged parallel to each of the layer. Each of these layers is formed by the weak cross linking between the micro-crystallites and minimum of porous structure causing the fragile properties of the carbon. On the other hand, strong linking between crystallites and well developed porous structure made non-graphitizing carbon with hard physical properties. The strong cross-link is bond by the existing oxygen and insufficiency of hydrogen from the initial raw material.
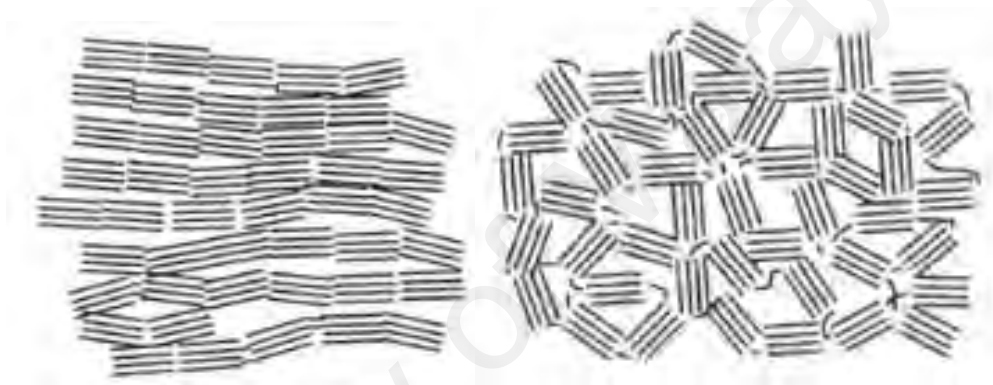
Figure 2.3: Schematic illustration of structure of activated carbon: (a) graphitized carbon (left), and (b) non-graphitized carbon (right)

All the carbon materials are formed by carbon element with unique bonding with other elements. The allotropic forms of carbon are divided into diamond, graphite and fullerenes were illustrated in Figure 2.4 according to Bourrat's figure. Diamond form at sp3 structure which carbon atom bonds with another 4 carbon atoms through sp3 σ bonds. On the hand hand, the graphite consists of sp2 carbon structure with a hexagonal layered structure which the carbon atoms bonded to nearby carbon atoms by sp2 σ and delocalized π bonds. Thus, due to these bonding properties, graphite has better thermal conductivity and electrical conductivity than diamond. Fullerenes are between sp2 and sp3 which resulting re-hybridization and formed sp2+ε. The carbon atoms are bent to form an empty cage of 60 carbons or more carbon atoms 3D carbon structures.
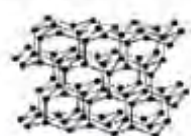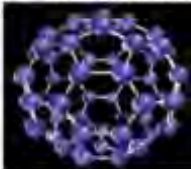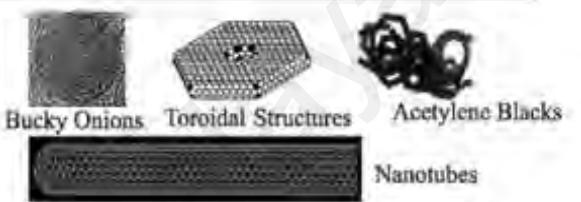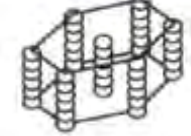
Figure 2.4 : Carbon allotropes (Mochida et al., 2006)

The typical pore size for activated carbon (AC) can be divided to micropores (width < 2 nm), mesopores (width = 2–50 nm) and marcopores (width > 50 nm). The ratio of pore size structure is depending on the precursor material that used to produce AC and also the activation process. The general precursor for activated carbon was from coal material ligno-cellulosic material. The production cost of AC can be reduced by selecting a low cost precursor material, while the reduction of AC production cost can directly decreased the overall treatment cost. A general review on the AC production from different type of waste materials are described in Table 2.8.

Table 2.9: Review on AC produced from different precursor

Activated Carbon	Precursor	Function	References
Palm shell activated carbon	Palm oil shell	Hg (II) removal	(Maarof, Ajeel et al., 2017)
Activated Carbon	Waste bamboo, coconut shell, and palm kernel shell	Cr (II) , Cu (II), Ni (II), Pb (II), Fe (II), and Zn(II)	(Ademiluyi & David-West, 2012)
Activated carbon	Waste coirpith	Hg(II), Pb(II), Cd(II), Ni(II), and Cu(II) removal	(Kadirvelu, Thamaraiselvi et al., 2001)
Activated bamboo waste	Waste bamboo	Ibuprofen and Clofibric Acid removal	(Reza, Ahmaruzzaman et al., 2014)
Nitrogen containing activated carbon	1,3-bis (cynomethyl imidazolium) chloride	Hydrogen gas adsorption	(Sethia & Sayari, 2016)
Chitosan coated acid treated coconut shell carbon	Coconut shell	Zn(II) removal	(Amuda, Giwa et al., 2007)
Powder activated carbon	Palm shell	BPA adsorption	(Soni & Padmaja, 2014)

2.3.2 Preparation of activated carbon

Typically, activated carbon can be obtained through physical and chemical activation. For physical activation method is a two-step process which consist of pyrolysis (carbonation) of the precursor material and gasification with activating agent.

The carbonation process is the raw organic material subjected to a high temperature between 400°C-800°C under atmospheric condition to remove impurity organic matter which the surface area is developed and a carbonaceous residue porosity structure are formed and to produces high percentages of carbon contain char. After carbonation will be followed by gasification, this process using activating agents that can produces high porosity of activated carbon at 800°C-1100°C. Generally, stream, carbon dioxide gas, air or other gases will be used as an activating agent that will penetrate into the internal structure of the char and removes the impurities via combustion which results in opening and widening of inaccessible pore by porosity development. Carbon dioxide gas is the most widely used as an activation gas due to it is ease to handle and easy to control the activation process at high temperatures.

In chemical activation process, acid, bases or salts ($ZnCl_2$) are impregnated on AC precursor at 450°C-900°C. Advantages of chemical activation process compared to physical activation progress are lower activation temperature and duration. The surface properties of AC strongly depended on the impregnated chemical reagent and the pyrolysis temperature. Several researchers reported AC can pollute by zinc chloride which resulting in separation difficulties at 550°C-650°C. Furthermore, corrosion problem appear with the equipment of synthesis at 375°C-500 °C.

2.3.3 Application of activated carbon

Generally, AC is widely used as an adsorbent for water and wastewater treatment, gas storage and air purification. In fact, AC is employed the most for aqueous phase application where various sizes and type of AC used for remove different type of contaminants via adsorption which is a surface interaction between the adsorbent and adsorbate. AC show the satisfactory performance on removal of organic and inorganic pollutant according to literature review. A details review on the application of AC is presented in Table 2.10.

Table 2.10: Review for application of activated carbon in adsorption of pollutant in gas and liquid phase.

Application	References
Hydrogen gas storage	(Ahluwalia & Peng, 2009; Choi B.-U., Choi et al., 2003; de la Casa-Lillo, Lamari-Darkrim et al., 2002; Li Y., Ben et al., 2013; Paggiaro, Bénard et al., 2010; Ramesh, Rajalakshmi et al., 2017; Sun Y., Yang et al., 2011; VASILIEV, KANONCHIK et al., 2007)
Methane gas storage	(Beckner & Dailly, 2016; Biloé, Goetz et al., 2002; Brady, Rostam-Abadi et al., 1996; Choi B.-U. et al., 2003; Dai, Liu et al., 2009; El-Sharkawy, Mansour et al., 2015; Sircar, Golden et al., 1996; Sun J., Rood et al., 1996)
Dye removal	(Albroomi, Elsayed et al., 2017; Asfaram, Ghaedi et al., 2015; Djilani, Zaghdoudi et al., 2015; Khraisheh, Al-Degs et al., 2002; Malik, 2004; Ojedokun & Bello, 2017; Singh, Mohan et al., 2003)
Oil removal	(Fulazzaky & Omar, 2012; Gong, Alef et al., 2007; Sathivel & Prinyawiwatkul, 2004; Silvani, Vrchotova et al., 2017)
EDC removal	(Bautista-Toledo I. et al., 2005; Choi K.-J., Kim et al., 2008; Choi Keun J., Kim et al., 2005; Choi Keun Joo, Kim et al., 2006; Koduru, Lingamdinne et al., 2016; Soni & Padmaja, 2014; Tanghe & Verstraete, 2001; Yamanaka, Moriyoshi et al., 2008)
Heavy metal cation removal	(Ademiluyi & David-West, 2012; Ahn et al., 2009; Amuda et al., 2007; Cataldo, Gianguzza et al., 2016; Gaya et al., 2015; Kadirvelu et al., 2000; Kadirvelu et al., 2001; Karnib, Kabbani et al., 2014; Shekinah et al., 2002; Yantasee et al., 2004)

Table 2.0, continued

Application	References
Heavy metal Anion removal	(Chen, Parette et al., 2007; Jais et al., 2016; Ma, Zhu et al., 2013; Sawana, Somasundar et al., 2017; Velazquez-Jimenez, Hurt et al., 2014; Yang L., Wu et al., 2007)
Microorganism removal	(Bandyopadhyaya, Sivaiah et al., 2008; Nekouei, Kargarzadeh et al., 2016; Shi, Neoh et al., 2007; Yamanaka et al., 2008; Yoon, Byeon et al., 2008)

2.4   Summary

Activated carbon is widely used for organic and inorganic micropollutant adsorption due to its high surface area with fast adsorption rate. However, general AC suffer in term of achieving insufficient of removal capacity in complex scenario while competition occur with co- existing micropollutant (Fan et al., 2016). Many researchers reported impregnation of metal oxide compound on activated carbon can improved the hydrophobic characteristics properties such as coated Iron oxide (Mahmoud, Khalifa et al., 2017), Silica (Karnib et al., 2014), Manganese oxide (Wang M. C., Sheng et al., 2015), magnetite Lanthanum oxide (Jais et al., 2016), and Zinc chloride (Gaya et al., 2015) onto active carbon. Among all, the effectiveness of magnesium silicate ($MgSiO_3$) for heavy metal removal was recently reported by Yu, Hu et al. (2016), and it was noted that $MgSiO_3$ has the capability for ion exchange between Mg (II) and positively charged metal ions. However, nano-sized materials do not have a practical implementation for wastewater treatment because of separation difficulty in the treatment system and insufficient evaluation on assessing the toxicity of nano-sized material (Brar, Verma et al., 2010; Lu, Wang et al., 2016). According to literature finding, $MgSiO_3$ coated onto active carbon for heavy metal removal has not been studied.

CHAPTER 3 : METHODOLOGY

3.1 Materials and Method

3.1.1 Chemical Reagent

PPAC (<75 μm) activated by potassium hydroxide (KOH) was obtained from Bravo Green Sdn. Bhd. Malaysia. Then, it was washed with distilled water for several times until washed water electro-conductivity was less than 300 μs cm^{-1} and oven dried at 70 °C for 24 h. Sodium chloride (NaCl), copper sulphate ($CuSO_4$), silicon powder (SiO_2), magnesium oxide (MgO), methanol, zinc nitrate ($ZnNO_3$), iron sulphate ($FeSO_4$), manganese sulphate ($MnSO_4$), lead nitrate ($PbNO_3$), sodium hydroxide (NaOH) and nitric acid (HNO_3) obtained from R&M chemical were of analytical grade ($>99.99\%$). Bisphenol A (BPA), methanol, aluminium sulphate hydrate ($Al_2(SO_4)_3$) and sodium arsenate (Na_3AsO_4) was purchased from Sigma company ($>99.99\%$). Lead test kit [4-(2'-pyridylazo) resorcinol (PAR)] was obtained from Merck Company.

3.1.2 Preparation of Magnesium silicate impregnated on PPAC

3.3g of MgO and 4.8g of SiO_2 dissolved into 50mL dionized water stirred continuously to obtain magnesium silicate gel. Furthermore, difference mass (3.33g, 5g, 6.67g, 10g, 20g and 40g) of PPAC was added to $MgSiO_3$ gel were assigned as PPAC-MS 300, PPAC-MS 200, PPAC-MS 150, PPAC-MS 100, PPAC-MS 50 and PPAC-MS 25 and stirred for 1 hour at 150rpm at 24 ± 1 °C. The impregnated product was transferred into a stainless steel Teflon-lined autoclave and treated at 150 °C for 10 h. The resulted product was filtered through a 0.45μm-pore Whatman filter paper and washed with distilled water for several times, and dried in an oven at 70 °C for 24 h (referred list of publications).
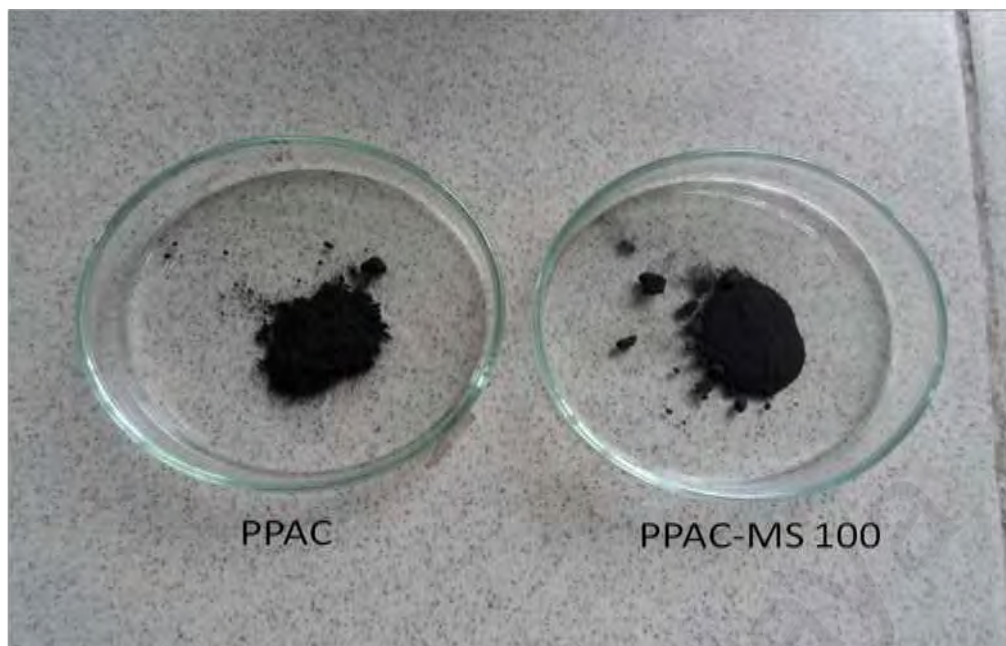
Figure 3.1: Photograph of PPAC and PPAC-MS 100
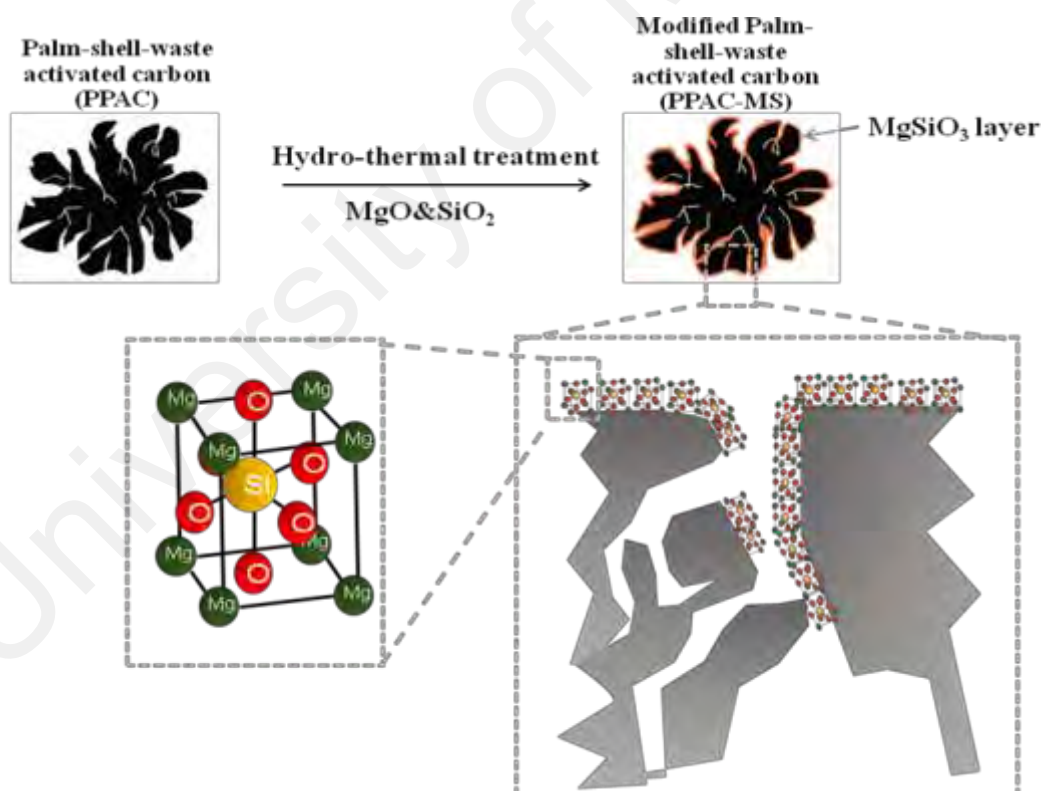
Figure 3.2: Schematic of synthesis route for PPAC-MS

3.2 Material Characterization

Surface functionalize group were determined by Fourier Transformed Infrareds (FTIR) spectroscopy (FTIR-Spectrum 400, Perkin Elmer, Waltham, MA, USA) in the scanning range of $450cm^{-1}$ to $4000cm^{-1}$. The characteristic textural structure of pore of PPAC-MS 100, PPAC-MS 50, PPAC-MS 25 and PPAC was determined by nitrogen adsorption/desorption analyzer (Mircrmeritics ASAP2020, Tristar II 3020, Norcross, GA, USA) to measure surface area, pore volume and pore size distribution with relative pressure from range 0 to 1. The pore size distribution was calculated with Barrett Joyner-Halenda (BJH) equation. Moreover, the surface area was determined by Langmuir and Brunauer-Emmett-Teller (BET). The surface morphologies of PPAC and PPAC-MS were determined by Field Emission Scanning Electron Microscope (FESEM-EDX) (FEG Quanta 450, EDX-OXFORD, Beaverton, OR, USA and Hitachi SU8010, Ibaraki, Japan). X-Ray powder diffraction (XRD)pattern was obtained using (EMPYREAN, PANalytical, Royston, UK) with the operation voltage of 40 kV and 40 mA current of Cu Kα radiation (λ). The XRD data were recorded in the range of 10 ~ 80° at 0.02 step size. The XRD raw data was evaluated using the Highscore software (PANalytical). X-ray photoelectron spectroscopy (XPS) measurements performed with ULVAC-PHI Quantera II using Al-Kα radiation (1486.6eV) operated at 15kV.

3.3 Optimization on impregnated ratio of MgSiO₃ on PPAC.

The experiment of copper adsorption on PPAC with impregnation ratio from 0% - 300% were carried out to investigate the optimum ratio of $MgSiO_3$ impregnated on PPAC. The experiment was conducted using 5mg of absorbent with $500mg.L^{-1}$ of 50mL Cu(II) solution under 150rpm for 24 hours using PPAC-MS 300, PPAC-MS 200, PPAC-MS 150, PPAC-MS 100, PPAC-MS 50 and PPAC-MS 25. After the adsorption, the suspension was filtered out using 0.45um pore size syringe filter and Cu(II)

concentration was determined using inductively coupled plasma optical emission spectrometry (ICP-OES, Optima 5300V, Perkin Elmer) analysis.

3.4 Heavy metal adsorption

3.4.1 Adsorption Isotherms

Adsorption isotherm explains the adsorption molecule on the surface of an absorbent. To compare the Cu(II) removal capacity for PPAC-MS 100, PPAC-MS 50, PPAC-MS 25 and PPAC the adsorption experiment was conducted at different initial concentration. The equilibrium isotherm experiment was conducted with 5mg of adsorbents with 50 mL Cu(II) solution under 150rpm for 24 hours. Cu(II) solutions with 50 mg.L^{-1}, 100 mg.L^{-1}, 200 mg.L^{-1}, 300 mg.L^{-1}, 400 mg.L^{-1} and 500 mg.L^{-1} were prepared and the initial solution was adjusted to pH 4.5 using 0.1M of sodium hydroxide (NaOH) and 0.1M of hydrochloric acid (HCl). After equilibrium reached, the suspension was filtered out using 0.45μm pore size Whatsman filter paper and the copper concentration was determined using ICP-OES analysis.

3.4.2 Effect of ionic strength on Cu(II) adsorption kinetic

Kinetic adsorption experiments were conducted with 5mg of absorbent with 50mL of pollutant under 150rpm at room temperature. 500mg.L^{-1} of copper solution with 0 M NaCl, 0.01M NaCl and 0.1M NaCl were prepared to investigate the influence of ionic strength on copper removal. Samples were collected at 30 minutes, 60 minutes, 90 minutes, 120 minutes, 150 minutes and 180 minutes were analyzed for copper concentration.

3.4.3 Influence of pH on PPAC-MS-100 for Cu(II) removal

The experiment was carried out to determine the influence of pH for copper removal using PPAC-MS 100 was investigated. 100mg.L^{-1} of Cu (II) solution was prepared and the initial pH was adjusted to 2, 3, 4, 5, 6 using 0.1M of NaOH and 0.1M

of HCl. Adsorption experiment was conducted with 5mg of absorbent with 50mL of Cu (II) solution with 150rpm for 24 hours at room temperature. Suspension filtered through 0.45µm pore size of Whatsman filter paper then proceeds with ICP-OED analysis for Cu(II) concentration tracing.

3.4.4 Regeneration of PPAC-MS 100 for Cu adsorption

Three cycles of regeneration were performed to investigate the reusability of PPAC-MS 100 for Cu(II) removal. 5mg of PPAC-MS 100 were added to a 50mL solution containing 400 mg.L^{-1} of Cu(II) was shaken under 150rpm for 24 hours. After adsorption, the suspension was filtered and treated with 100mL of 50 mg.L^{-1} of Mg (II) solution or 0.1M HCl solution, shaken under 150rpm for 1 hour at room temperature. The absorbent was washed for several times with distilled water and dried in an oven at 70°C for another adsorption cycle.

3.4.5 Adsorption study of dissociated heavy metals by PPAC-MS 100

Langmuir and Freundlich isotherm modelling have been used to investigate adsorption capacities of PPAC-MS 100 to 5 types of different heavy metals. 5mg of PPAC-MS 100 were added to the solution of heavy metals: Zn (II) from 50 to 600 mg.L^{-1}, Al (III)50-500 mg.L^{-1}, Fe (II) from 50 to 600 mg.L^{-1}, Mn (II) from 50-500 mg.L^{-1} and As (V) from 25 to 400 mg.L^{-1}. 5mg of PPAC-MS 100 was placed in 50mL centrifuge tube shake under 150rpm for 24 hours at room temperature. Initial solution pH was not adjusted (pH 5-7). After the suspension filtered, the concentration of the pollutant was determined using ICP-OES.

3.5 Heavy metal adsorption with the presence of BPA

3.5.1 Adsorption isotherms single and binary mode

The isotherm experiments were carried out with 5mg of adsorbents with 50 mL of single pollutant [either BPA or Pb (II)] or mixed pollutants [BPA and Pb (II)]

containing solutions under 150 rpm for 24 hours (Shaker, Lab Companion, SK-300). The Pb (II) solution ($25 \sim 400$ mg.L^{-1}) was prepared using $Pb(NO_3)_2$ in deionized water. The prepared concentration of BPA solution was $10 \sim 100$ mg.L^{-1}. The combined solution of BPA and Pb (II) was designated as 'x+y' where 'x' is the concentration of BPA and 'y' is the concentration of Pb (II). The concentrations (mg.L^{-1}) of binary pollutants in solution were expressed e.g. "100+400", "80+300", "60+200", "40+100", "20+50" and "10+25" (Liu et al., 2016). All the solutions were adjusted to pH 4.5 using 0.1 M of sodium hydroxide (NaOH) and nitric acid (HNO_3) at 24 ± 1 °C. When the reaction was completed, the suspension was collected and filtered through a 0.45 μm-pore Whatman filter paper. After isotherm experiments, Pb (II) concentrations were determined using the 4-(2'-pyridylazo) resorcinol (PAR) colorimetric method using standard Merck kit with UV spectrophotometer (Merck, Spectoquant Pharo-300) and BPA concentrations were measured using a UV spectrophotometer at 276 nm wavelength with no interference for measuring both pollutants (Li J., Zhou et al., 2007; Li S., Zhang et al., 2016). The calibration curved generated for the quantification of BPA concentration is shown in Figure 3.3.
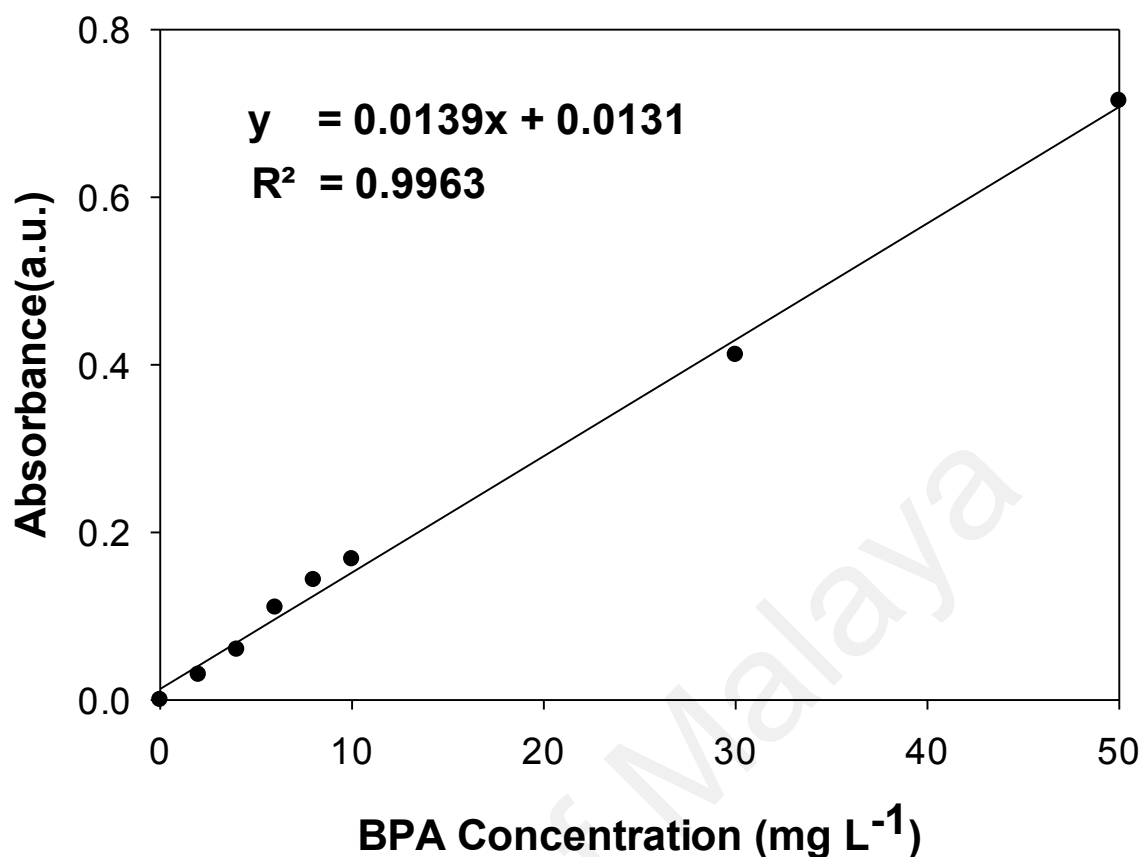
Figure 3.3 :Calibration Curve for BPA

3.5.2 Adsorption kinetics single and binary mode

Adsorption kinetics experiments were performed using 5mg of PPAC and PPAC-MS with 50 mL of pollutant solutions under 150 rpm at 25°C. Two hundred mg.L^{-1} of Pb (II) and 50 mg.L^{-1} of BPA solutions with pH 4.5 were prepared for kinetics in both single and binary pollutant modes to investigate the influences of BPA in Pb (II) removal. Samples were collected at a different time interval in the range of 10 minutes to 3 hours. And then, the collected samples were analyzed for Pb (II) and BPA concentrations. To analyze kinetic adsorption process, the pseudo-first and pseudo-second order kinetics models were applied.

32

3.5.3 Influence of ionic strength effect in binary mode adsorption

The influences of ionic strength on the removal of BPA and Pb (II) by PPAC and PPAC-MS were investigated. Five mg of absorbent was added into 50 mL solution containing 400 $mg.L^{-1}$ Pb (II) and 100 $mg.L^{-1}$ BPA with various concentrations (0.01 ~ 0.05 mM) of ionic strength by sodium chloride (NaCl).

3.5.4 Effect of Pb (II) precipitation on BPA removal

Different initial concentration of Pb (II) (25 ~ 400 $mg.L^{-1}$) and BPA (10 ~ 100 $mg.L^{-1}$) solution were prepared and its pH was adjusted to 4.5 to avoid metal hydrolysis. Meanwhile, in order to investigate the co-precipitation of BPA by $Pb(OH)_2$, Pb (II) was precipitated by adjusting solution pH to 7 without adding sorption media under 150 rpm for 24 hours at room temperature. The supernatant was drawn out for BPA concentration measurement at pH 7. Then, the remaining suspension was treated using 0.1 M of HNO_3 to adjusting pH to 2.5 under 150 rpm for 24 hours at room temperature. The suspension was collected and filtered through a 0.45 μm-pore Whatman filter paper to measure concentration of BPA. The residual BPA concentrations were measured using a UV-spectrophotometer (Merck, Spectoquant Pharo-300) at 276 nm wavelength according Standard Methods(Greenberg, Clesceri et al., 1992).

The surface characteristics of Pb (II) and BPA precipitant (designated as PLB) were determined by FTIR analysis. The Visual MINTEQ 3.1 was used to calculate the saturation index (SI) and ion activity product (IAP). If the SI is > 0, it means that the minerals are oversaturated, if SI is < 0, it represents that the phases of minerals are under saturated. On the other hand, if SI is equal to 0, the solid reaches equilibrium.

3.5.5 Regeneration of PPAC-MS 100

To investigate the reusability of PPAC-MS 100, 5 cycles of adsorption and desorption experiments were conducted. To the best of our knowledge, the present study

was the first reported study that the absorbent was desorbed by Mg (II) solution followed by thermal treatment. Five mg with 50 mL solution containing 400 mg.L^{-1} Pb (II) and 100 mg.L^{-1} BPA was shaken under 150 rpm at 24 ± 1 °C for 24 h. After adsorption, pollutants retained media were treated with 50 mg.L^{-1} of Mg (II) solution. This suspension was shaken under 150 rpm at 24 ± 1 °C for 1 hour. Then, the absorbent was heated at 350 °C for 3hours. The absorbent was washed several times with distilled water and dried in oven at 70 °C for 24 hours for another adsorption.

3.6 Adsorption Isotherm

3.6.1 Adsorption Capacity

In order to ascertain the adsorption capacity of the adsorbent q_e was calculated as:

$$q_e = \frac{(C_o - C_e)V}{M} \tag{3.1}$$

Where q_e is the adsorption capacity of solute absorbed at equilibrium (mg g^{-1}), C_e is the equilibrium concentration (mg.L^{-1}), C_o is the initial solution concentration (mg.L^{-1}), M is the mass of absorbent (g) and V is the volume of solution (L). The isotherm data experiments were fitted to Langmuir and Freundlich isotherms modeling.

3.6.2 Langmuir Isotherm

The linear form of the Langmuir model can be depicted as follows.

$$\frac{C_e}{q_e} = \frac{1}{Q_{max}K_L} + \frac{C_e}{q_e} \tag{3.2}$$

where Q_{max} is the maximum adsorption capacity (mg g^{-1}) and K_L (L mg^{-1}) is the Langmuir constant related to the energy of adsorption. When adsorption is held to a

monolayer and uniform surface, the Langmuir model fits the isotherm data. The maximum adsorption capacity will be achieved when all sorption sites are saturated.

3.6.3 Freundlich Isotherm

The linear form of Freundlich isotherm was calculated as:

$$\log q_e = \log K_F + \frac{1}{n} \log C_e \qquad (3.3)$$

where K_F and n are Freundlich isotherm constants related to adsorption capacity and adsorption intensity, respectively.

3.7 Adsorption Kinetic

To study the kinetic adsorption can lead to better understanding of the adsorption mechanism of the process. The kinetic adsorption experiments provide the rate of adsorption, equilibrium time and also provide the output of the adsorption.

3.7.1 Pseudo-First-Order Kinetic Model

To analyze kinetic adsorption process, the pseudo-first and pseudo-second order kinetics models. The pseudo first order kinetic model is expressed as:

$$\log (q_{e1} - q_t) = \log q_{e1} - \frac{K_1}{2.303} t \qquad (3.4)$$

3.7.2 Pseudo-Second-Order Kinetic Model

The pseudo second order kinetic model is expressed as:

$$\frac{t}{q_e^{exp}} = \frac{1}{K_2 q_{e2}^2} + \frac{t}{q_{e2}} \qquad (3.5)$$

Where q_{e1} and q_{e2} (mg g^{-1}) is the adsorption capacity at equilibrium, q_e^{exp} (mg g^{-1}) is the amount of solute absorbed at time t, K_1 (min^{-1}) and K_2 (g mg^{-1} min^{-1}) are the reaction rate constants for the pseudo-first and pseudo-second order kinetic models, respectively.

CHAPTER 4: RESULTS AND DISCUSSION

4.1 Optimization on impregnated ratio of MgSiO₃ on PPAC

In order to find the optimum ratio between $MgSiO_3$ and PPAC, several weight ratios of $MgSiO_3$/PPAC, which are 0, 25, 50, 100, 150, 200 and 300 %, of $MgSiO_3$ impregnated onto PPAC were tested for Cu (II) removal. The results for effect of impregnation ratio of $MgSiO_3$ on PPAC on Cu (II) adsorption is illustrated in Figure 4.1. In the Figure 4.1, it is clear that impregnation ratio and Cu (II) removal capacity promoted a direct proportional relationship; the experimental results indicated increasing of impregnation ratio will also increase of Cu (II) removal capacity. The highest impregnation ratio shows the highest Cu (II) removal capacity. Main removal mechanisms were adsorption and precipitation verified through FTIR, FESEM-EDX, XRD, and XPS. Material synthesis difficulty was encountered when the impregnation ratio went beyond 300% due to segregation between PPAC and excess of $MgSiO_3$ gel. Moreover, the gradient in Figure 4.1 curve decreases from 2.096 to 0.684 when the impregnation ratio is over 100%. Experimental results indicated Cu (II) removal capacity with less increment when the impregnation ratio more than 100% due to the limitation of impregnation area on PPAC. Furthermore, $MgSiO_3$ leaching out from PPAC-MS when the impregnated ratio higher than 100%. Therefore, the following Cu (II) adsorption studies will focus on 0%-100% of $MgSiO_3$ impregnation ratio.
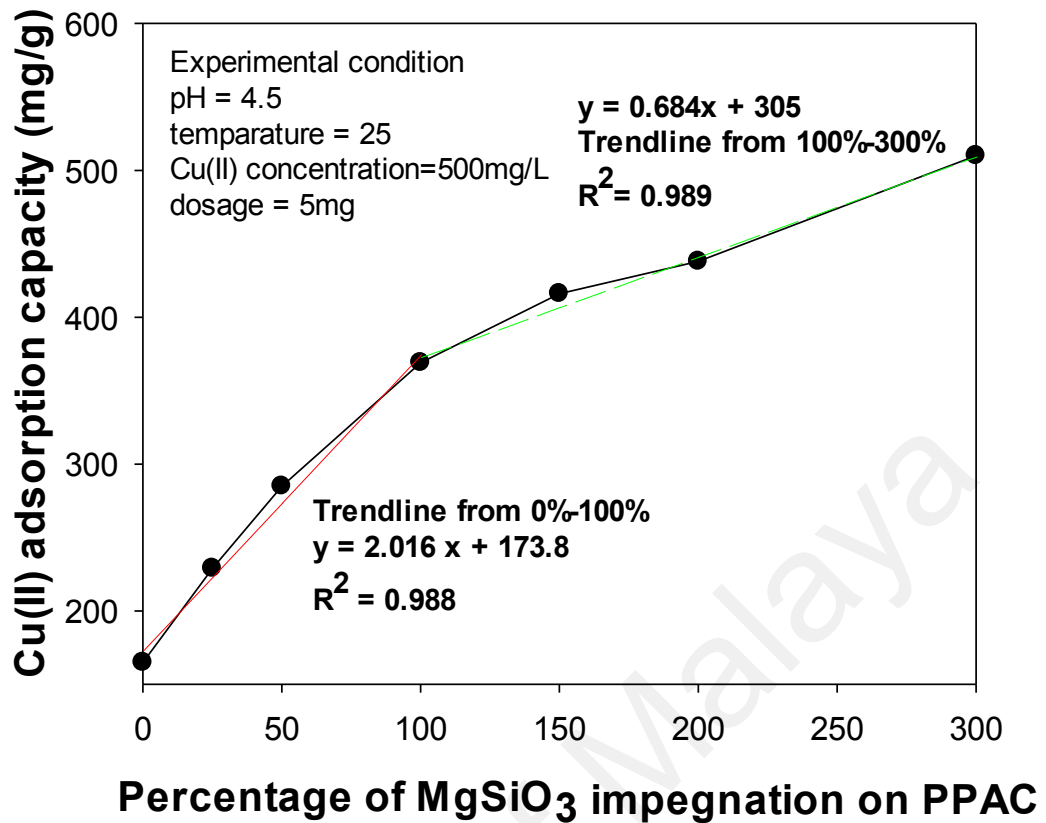
Figure 4.1: Adsorption isotherms of Cu(II) by different impregnation ratio of MgSiO₃ on PPAC

4.2 Heavy Metal Adsorption

4.2.1 Adsorption Isotherms Cu (II)

Cu (II) adsorption by PPAC-MS 100, PPAC-MS50, PPAC-MS 25 and PPAC were fitted to Langmuir and Freundlich isotherm model to describe the interactive behavior between absorbent and pollutant. Figure 4.2 compares the Langmuir and Freundlich isotherm curves for PPAC-MS 100, PPAC-MS 50, PPAC-MS25 and PPAC. Table 4.1 displays the adsorption isotherm parameters. The adsorption capacity from the experiment for Cu (II) removal was 369 mg g^{-1} for PPAC-MS 100, 285 mg g^{-1} for PPAC-MS50, 220 mg g^{-1} for PPAC-25, and 165mg g^{-1} for PPAC. Isotherm results show that by increasing impregnation ratios of MgSiO₃, resulting in more Mg^{2+} and OH$^-$ release and causes the increase of solution pH and Cu (II) removal capacity. This

reveals the fact that $MgSiO_3$ play a crucial role on Cu (II) removal capacity. Thus, PPAC-MS 100 has the highest Cu (II) removal capacity compared to PPAC-MS 50, PPAC-MS 25 and PPAC because PPAC-MS 100 has the highest $MgSiO_3$ impregnation ratio. Compared to the other absorbent media, PPAC-MS 100 showed high Cu (II) adsorption capacity except powdered MgO (Rafiq, Nazir et al., 2014). Although many factors may contribute adsorption performance including surface area and impregnation compound on based material (Kadirvelu et al., 2000; Wang P., Ye et al., 2016; Zhang K., Li et al., 2016), it is clear that granular adsorbent has higher practical implementation for water treatment, but the available sorption area is lower than nano-particles (Khodaie, Ghasemi et al., 2013). Furthermore, due to the fact that KOH has high efficiency on heavy metal adsorption, PPAC activated by KOH exhibited good performance of Cu (II) removal.

According to the coefficient of determination (R^2) in Table 4.1, the adsorption of Cu (II) by PPAC-MS 50, PPAC-MS 25 and PPAC fitted well to Langmuir isotherm while PPAC-MS-100 fitted better with Freundlich isotherm. Theoretically, the Langmuir model is suitable for the monolayer adsorption on homogenous surfaces (Langmuir, 1918), whereas the Freundlich model assumes the multilayer adsorption on heterogeneous surfaces (Freundlich, 1906). The Langmuir isotherm model suggests the monolayer coverage of Cu (II) binding onto PPAC-MS 50, PPAC-MS 25 and PPAC surface homogeneously, while heterogeneous adsorption occurs onto PPAC-MS 100 surface with multiplayer coverage of Cu (II). Moreover, Freundlich isotherm constant, the n value present in Table 4.1 for PPAC-MS 100 above describes the favorability of Cu (II) adsorption (Rafiq et al., 2014).
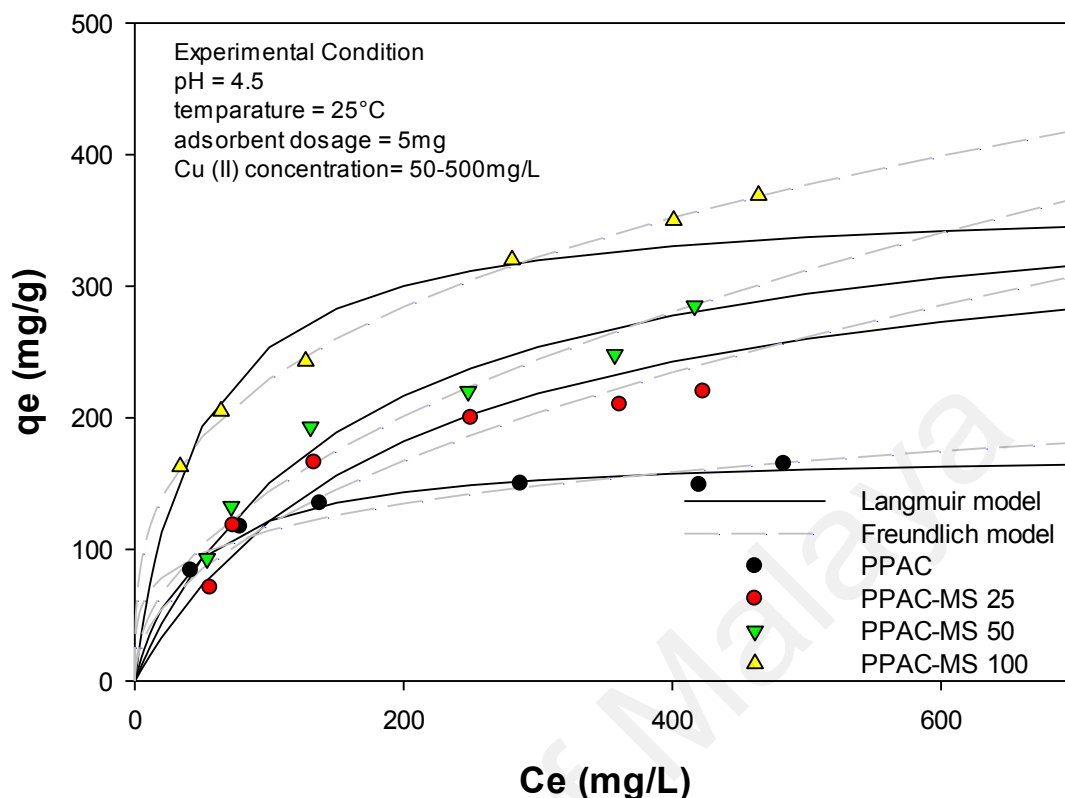
Figure 4.2: Adsorption isotherms of Cu (II) on PPAC and PPAC-MS 25, PPAC-MS 50 and PPAC-MS 100 with Langmuir modeling and Freundlich modeling

Table 4.1:Modeling of isotherm result for PPAC, PPAC-MS 25, PPAC-MS 50, and PPAC-MS 100

Type of adsorbent	Langmuir Parameter			Frendlich Parameter				Experiment
	q_m	K_L	R^2	q_m	K_F	n	R^2	q_{exp}
PPAC	174.774	0.023	0.983	97.431	38.778	4.246	0.894	165
PPAC-MS 25	363.438	0.005	0.901	85.549	12.806	2.060	0.866	220
PPAC-MS 50	386.556	0.006	0.965	103.784	15.964	2.090	0.936	285
PPAC-MS 100	367.601	0.022	0.956	185.766	55.714	3.249	0.998	369

4.2.2 Adsorption Kinetics with different ionic strength

Kinetic adsorption studies were carried out using PPAC-MS 100, PPAC-MS 50,

PPAC-MS 25 and PPAC with different ionic strengths of 0 M, 0.01 M, and 0.1 M NaCl.

The kinetic experiment results were fitted to pseudo first order modeling and pseudo second order modeling, as illustrated in Figure 4.3. Kinetic constants for pseudo first-order and second-order are summarized in Table 4.2. The kinetic experiment data were fitted to pseudo second-order modeling with R^2 from 0.972 to 0.996. Furthermore, the kinetic results indicate that the overall adsorption process is closer to the chemisorptions process than physisorption process (Yakout & Borai, 2014), means that $MgSiO_3$ may be a main component for Cu (II) adsorption compared to PPAC.

As shown in Figure 4.3, ionic strength significantly influences the adsorption capacity of Cu (II). Compared with different ionic strength condition, Cu (II) removal capacity decrease whiles the ionic strength increases. This phenomenon can be explained by the positively charged sodium ion contributed repulsive force at the outer layer of the absorbent and repel positively charged copper ion (Xu et al., 2012). Therefore, the available sorption surface decreases, resulting in a decrease of Cu (II) adsorption capacity.

Moreover, the adsorption reached equilibrium at 60 minutes for all absorbents with 0M, 0.01M and 0.1M ionic strength. It is found that higher ionic strength concentrations can increase adsorption equilibrium rate. This phenomena can be explained by the competitive effect between the Cu (II) and Na+ to compete for available adsorption site (Nouri, Ghodbane et al., 2007). The adsorption rate can be increased when the ionic strength increases.

Table 4.2: Modeling of Kinetic result for PPAC, PPAC-MS 25, PPAC-MS 50 and PPAC-MS 100

Cu removal	Pseudo-first-order model			Pseudo-second-order model			
0M NaCl	k_1(min^{-1})	*Slope*	R^2	k_2(g mg^{-1} min^{-1})	V_0	R^2	q_{e2}
PPAC	0.0264	0.0115	0.5409	0.0004	19.1843	0.972	225.450
PPAC-MS 25	0.0177	0.0077	0.8731	0.0003	21.1844	0.995	256.859
PPAC-MS 50	0.0161	0.0070	0.7980	0.0003	22.4362	0.984	284.257
PPAC-MS 100	0.0192	0.0084	0.7177	0.0005	57.0002	0.996	338.041
0.01M NaCl							
PPAC	0.023	0.010	0.941	0.0010	23.710	0.995	153.066
PPAC-MS 25	0.021	0.009	0.303	0.0005	15.638	0.991	184.616
PPAC-MS 50	0.016	0.007	0.734	0.0004	16.257	0.983	213.899
PPAC-MS 100	0.017	0.007	0.850	0.0005	29.110	0.994	241.733
0.1M NaCl							
PPAC	0.021	0.009	0.896	0.0005	10.239	0.972	147.246
PPAC-MS 25	0.018	0.008	0.698	0.0007	12.813	0.993	137.088
PPAC-MS 50	0.015	0.007	0.821	0.0005	14.073	0.982	175.348
PPAC-MS 100	0.016	0.007	0.907	0.0004	17.659	0.986	199.550
Initial sorption rate, $V_o = k_2 q_{e2}$							
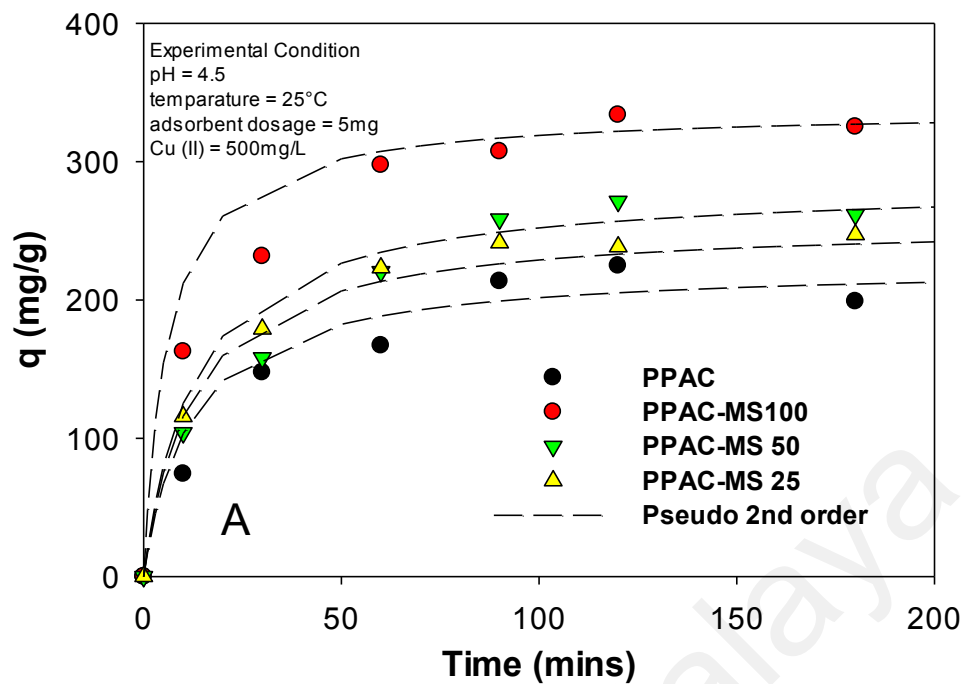
(a)
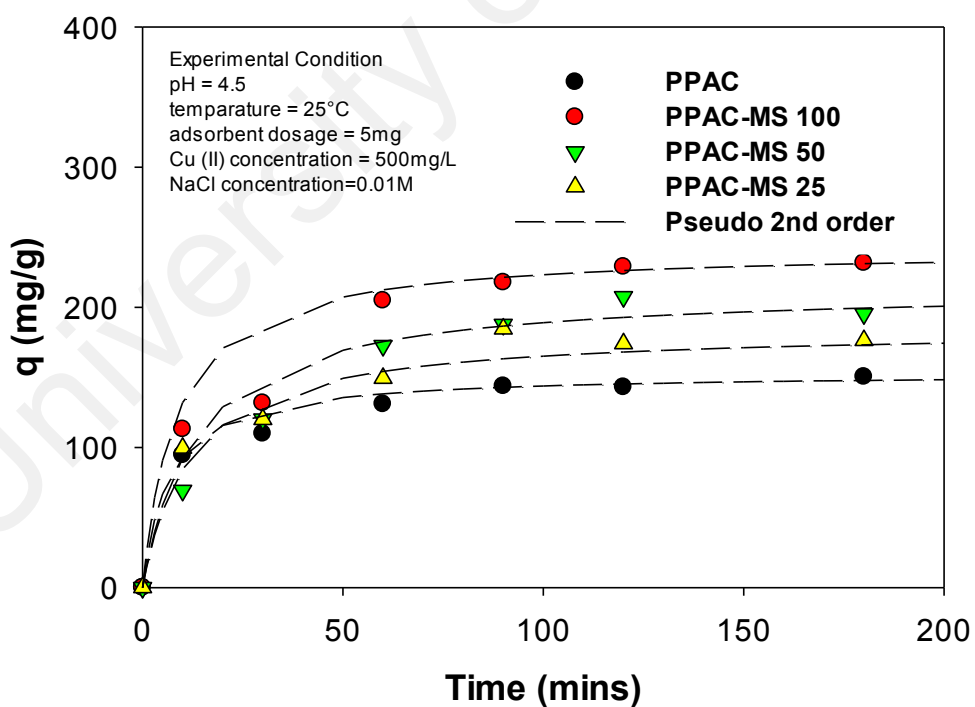
(b)

Figure 4.3 :Effects of ionic strength on adsorption kinetics of Cu (II) by PPAC, PPAC-MS 100 , PPAC-MS 50 and PPAC-MS 25 (A) no NaCl added, (B) 0.01M NaCl (B) and (C) 0.1M NaCl
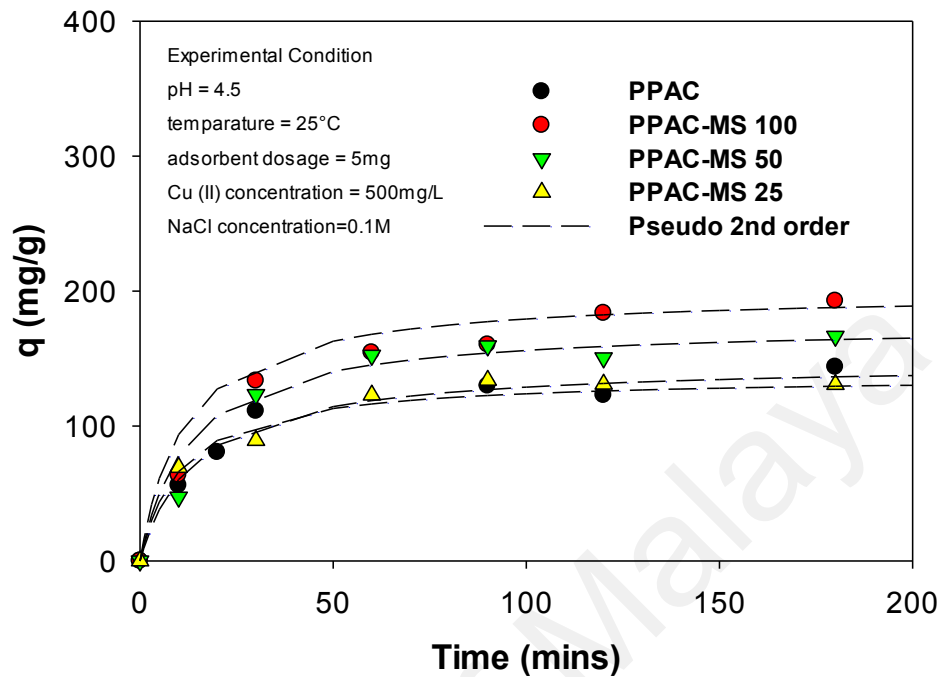
(c)

Figure 4.3, continued

4.2.3 Influence of pH for Cu(II) removal using PPAC-MS 100

The influence of the pH value on Cu (II) adsorption capacity by PPAC-MS 100 was investigated in a range of pH 2 – 6 as shown in Figure 4.4. The Cu (II) adsorption capacity increases when the pH of initial solution increased. It can be explained that the PPAC-MS surface tends to be protonated by hydrogen ion (H^+) which promoted the competition between H^+ and Cu (II) at low pH. Al-Homaindan et al. (2014) have also explained the reduced of heavy metal sorption because of the available active sorption site for heavy metal are occupied by proton in low pH. Therefore, adsorption capacity for Cu (II) was reduced at pH 2 because hydrogen ion (H^+) tends to compete with positively charged copper ions in solution. However, high initial solution might lead to metal ion precipitation to form insoluble salts because of low amount of proton but with

high amount of OH⁻ ion (Johnson, Watson et al., 2002). Therefore, Cu (II) removes capacity increase with an increase in the pH of the initial solution using PPAC-MS 100.

Experimental condition
pH=2-6
temparature = 25 C
Cu(II) concentration= 500mg/L
dosage=5mg
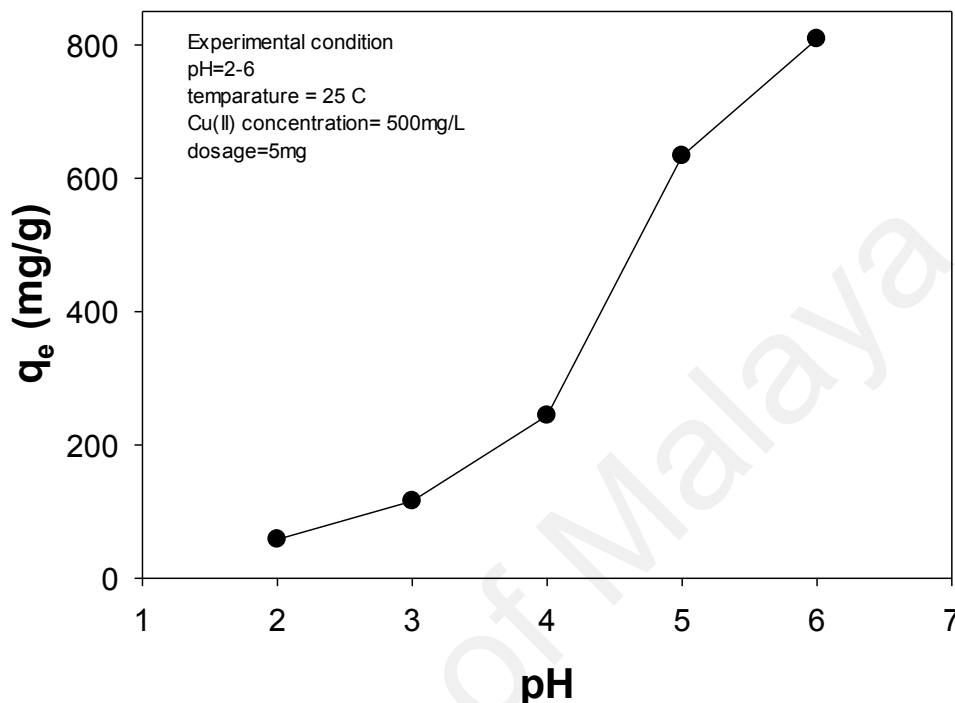
Figure 4.4: Effects of solution pH to Cu (II) adsorption on PPAC-MS 100

4.2.4 Regeneration PPAC-MS 100

A regeneration study of PPAC-MS 100 on Cu (II) removal was conducted using a comparison study of Mg(II) and HCl solution as desorption reagents. PPAC-MS 100 could be regenerated 3 times, and the last adsorption capacity at the third cycle decreased 40% for Mg (II) solution and 60% for HCl solution in Figure 4.5. Using Mg (II) solution for Cu (II) desorption process, competition occurred between Cu (II) and Mg (II) as the main reasons for desorption (Ou, Zhou et al., 2012). Mg (II) tends to replace Cu (II) to form CuO on the surface of absorbents. While using HCl as a desorption reagent, high H^+ concentration mainly causes metal desorption (Sharma, Srivastava et al., 2009). PPAC-MS 100 removed Cu (II) three times using metal

desorption reagents, indicating the economic benefits of using a palm-shell waste material.
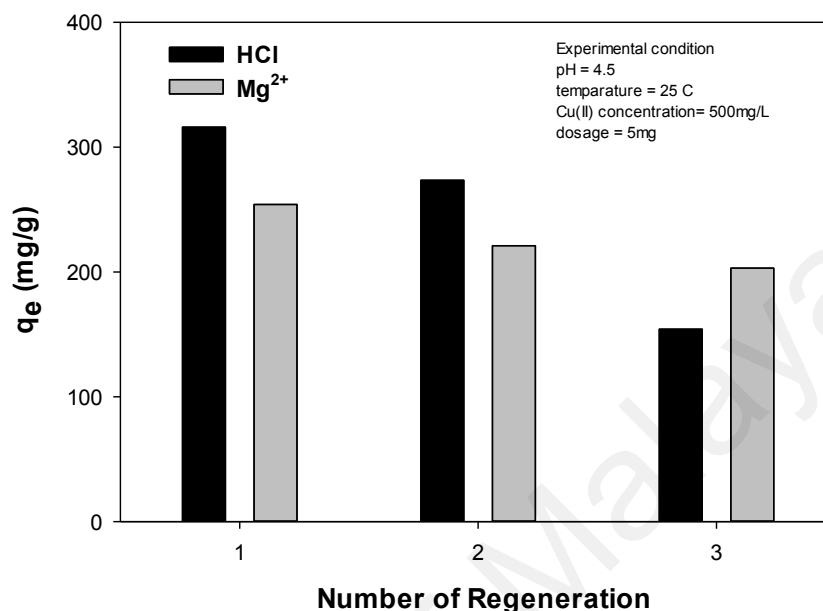
Figure 4.5: Regeneration of PPAC-MS 100 using Mg^{2+} solution and HCl for 3 cycles

4.3 Adsorption study of dissociated heavy metals by PPAC-MS 100

4.3.1 Adsorption isotherms studies on Zn, Al, Fe, Mn and As

PPAC-MS 100 was used to remove 5 different heavy metals in solution, as shown in Figure 4.6. Table 4.3 summarizes the Langmuir and Freundlich adsorption constant on dissociated heavy metal. Heavy metal adsorption capacity (mg g^{-1}) for Zn (II), Al (III), Mn (II), Fe (II) and As (V) were 373 mg g^{-1}, 244 mg g^{-1}, 234 mg g^{-1}, 562 mg g^{-1}, and 191 mg g^{-1}, respectively. Overall, the sequence of adsorption capacities of PPAC-MS 100 for different heavy metal ion is: Fe (II) > Zn (II) > Al (III) > Mn (II) > As (V). Al (III), Mn (II), Fe (II) and As (V) adsorption data fitted well to Langmuir isotherm, while Zn(II) adsorption fitted well to the Freundlich isotherm. PPAC-MS 100 was efficient in removal on cation and also anion heavy metal species.

Experimental Condition
pH = 5-7
temparature = 25°C
adsorbent dosage = 5mg
Zn (II) = 50-600mg/L
Al (III) = 50-500mg/L
Fe (II) = 50-600mg/L
Mn(II) = 50-500mg'L

Langmuir
Freundlich
Zn removal
Al removal
Fe removal
Mn removal
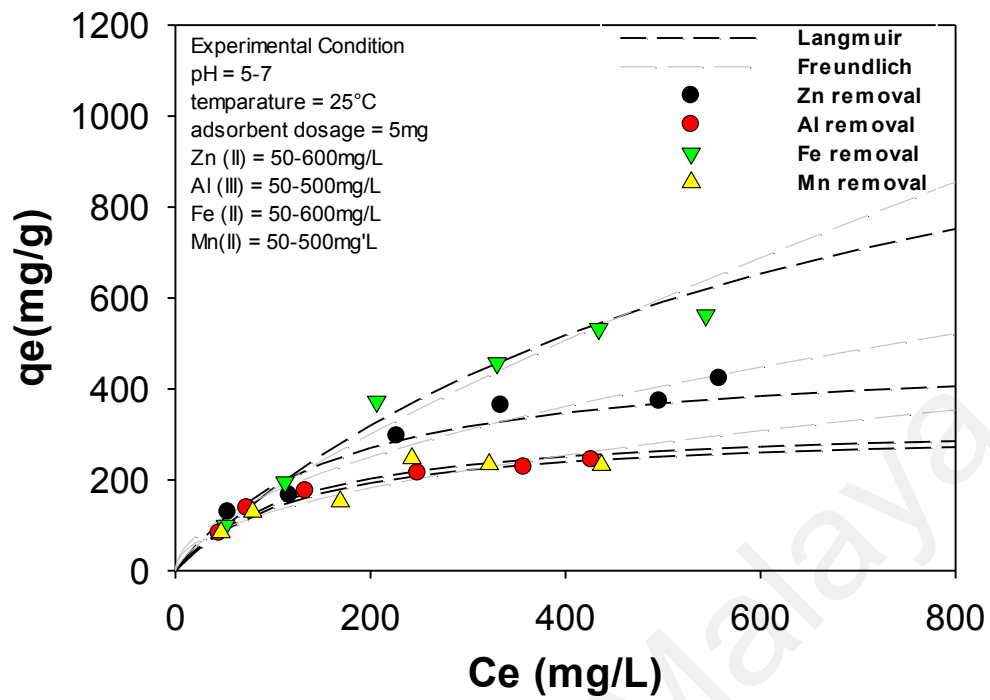
(a)

Figure 4.6: PPAC-MS 100 for (A) cation contaminates and (B) anion contaminates with Langmuir modeling and Freundlich modeling
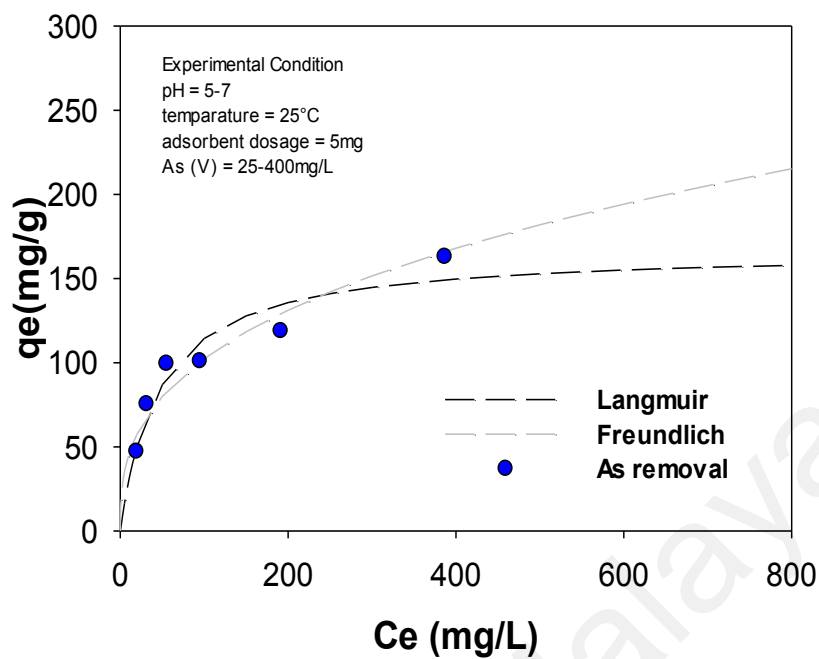
(b)

Figure 4.6, continued

Table 4.3: Isotherm result for PPAC-MS 100 for As, Zn, Al, Fe and Mn removal

Pollutant	Langmuir Parameter			Frendlich Parameter				q_{exp}
	q_m	K_L	R^2	q_m	K_F	n	R^2	
Zn (II)	487.563	0.006	0.931	120.819	15.331	1.895	0.962	373
Al (III)	330.431	0.008	0.968	102.695	18.801	2.304	0.919	244
Mn (II)	315.539	0.008	0.957	94.551	14.671	2.100	0.904	234
Fe (II)	1367.727	0.002	0.997	105.954	5.559	1.327	0.974	562
As (V)	167.039	0.022	0.955	80.073	19.829	2.803	0.902	191

4.3.2 Copper removal mechanisms and material characteristics

The removal mechanisms of Cu(II) by PPAC-MS 100 were verified using FTIR, BET, XRD, FESEM-EDS and XPS. The functional groups of the adsorbents surface were identified through FTIR, as depicted in Figure 4.7. Main different findings are both Cu-O band after treatment and Mg-O (or Mg-OH) band in PPAC-MC. The adsorption peaks of Cu-O were observed at 500 cm^{-1} after treatment, indicating the presence of $Cu(OH)_2$ (Zhang Y. X., Huang et al., 2013). In PPAC-MS 100, the vibration of Si-O-Si, Mg-OH, and Mg-O groups observed at peak 1004 cm^{-1} (Tao, Zhu et al., 2010), 1410 cm^{-1} (Cao H., Zheng et al., 2010), and 680 cm^{-1} (Dhaouadi, Chaabane et al., 2011). The peak of 820 cm^{-1} also proves the existence of Mg-O group (Hassouna, Hedia et al., 2011; Pei, Yin et al., 2010), but the peak may overlap with wide vibration of Si-O-Si at 1004 cm^{-1}(Tao et al., 2010). After adsorption onto PPAC-MS 100, the intensity of Si-O-Si bond for PPAC-MS 100 reduced at peak 1004 cm^{-1} and C-H stretching disappeared, suggesting that the CuO precipitant covered the overall surface. PPAC and PPAC-MS 100 exhibit a broad peak at 3737, 3729 and 3854 cm^{-1} assigned to Si-OH stretching vibration. Besides that, C-H stretching vibration peak were found at 2924/2853 cm^{-1} on PPAC and PPAC-MS 100 (Viana, da Silva et al., 2012). C=C group and C-O-H group were found at 1556 cm^{-1} and 1448 cm^{-1} on PPAC, respectively (Barth, 2007). After impregnation of $MgSiO_3$ on PPAC, the C-O-H group and C=C bond still remain but are shifted to $1555cm^{-1}$ and $1435cm^{-1}$. Overall, the FTIR results can verify Cu(II) adsorption by Cu-OH bonding onto the surface of PPAC-MS.
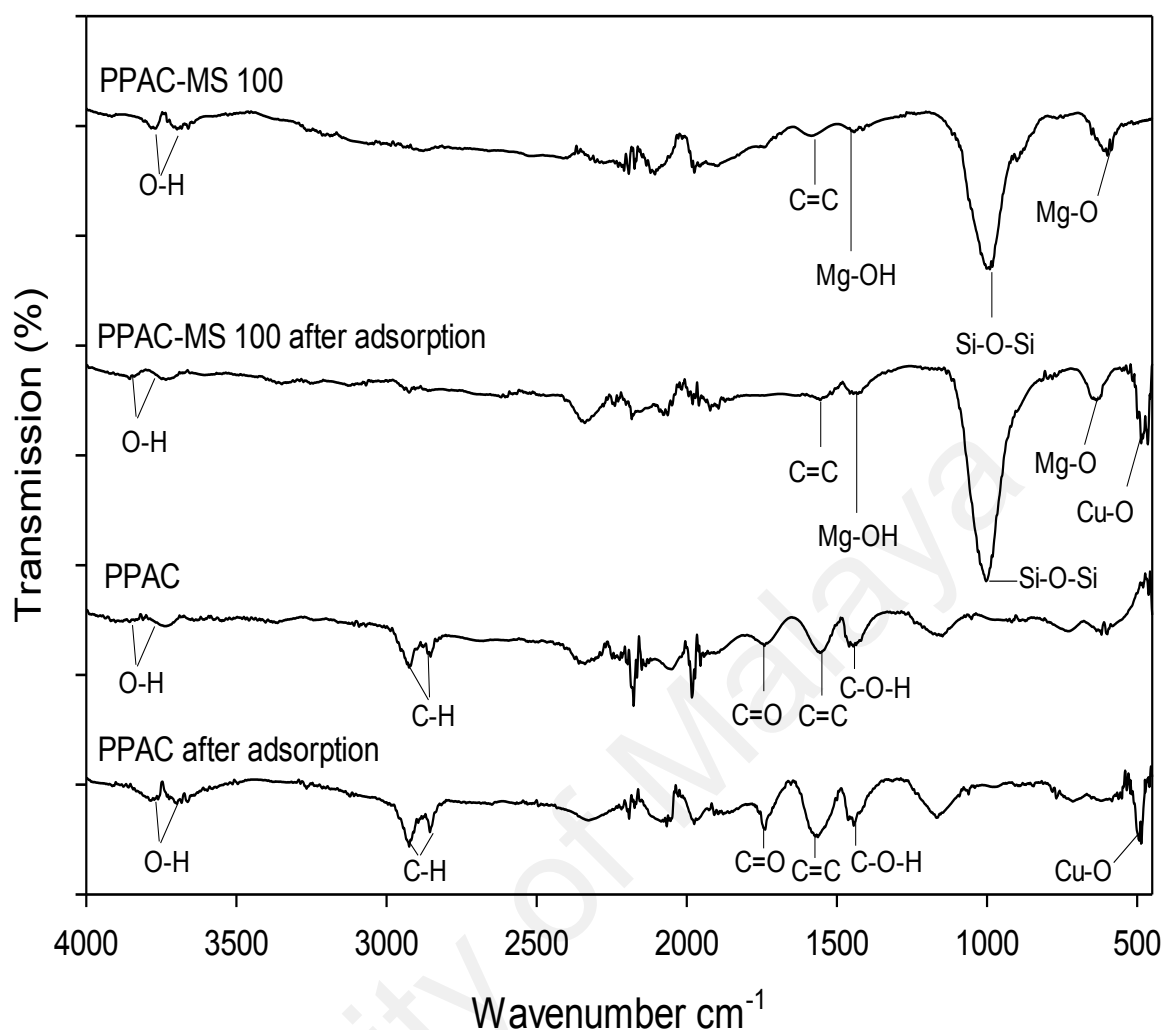
Figure 4.7: FTIR results of PPAC and PPAC-MS 100 before and after adsorption

Nitrogen adsorption-desorption isotherms of PPAC-MS 100, PPAC-MS 50, PPAC-MS 25 and PPAC were measured to further illuminate the pore characteristic (Figure 4.8A). Figure 4.8A showed that the quantity adsorbed volume is decreased as the increase of $MgSiO_3$ ratio due to the increase of Mg compound on the surface of PPAC (refer to Figure 4.9J, 4.9K, 4.9L). Therefore, the increase of $MgSiO_3$ ratio can enhance adsorption capacity of Cu (II), but it results the decrease of the adsorbed volume. Because of this phenomenon, it is important to find an optimal ratio between $MgSiO_3$ and PPAC. Based on International Union of Pure and Applied Chemistry (IUPAC) classification, PPAC, PPAC-MS 25 and PPAC-MS 50 were classified as type I isotherm. Type I isotherm exhibited with a low slope at 0.8-1.0 of p/po and

49

characteristic for high micro-porous material. On the other hand, PPAC-MS 100 exhibited the characteristic of type IV isotherm with it significant had a high slope in 0.8-1.0 p/p_o, indicating the filling of the meso-pore by capillary condensation (Wang K., Zhao et al., 2016). PPAC-MS 100 exhibited H4 hysteresis loop and it associated with the parallel line on nitrogen adsorption-desorption curve.
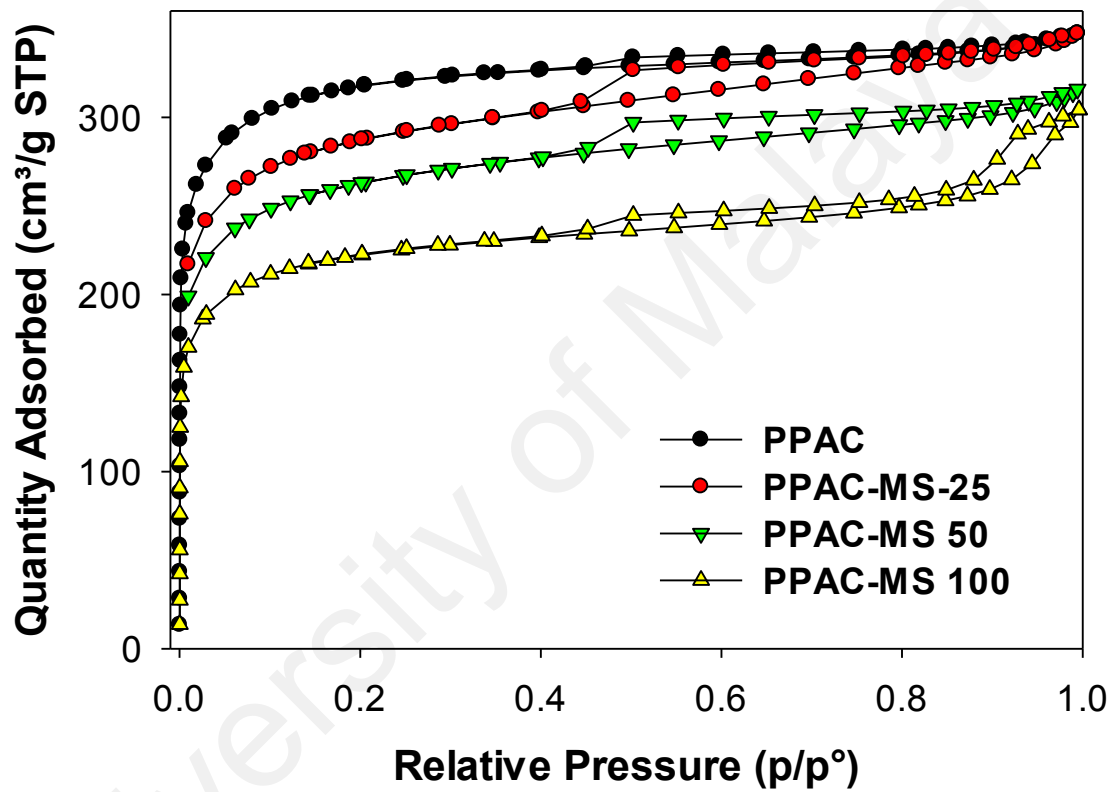
(a)

Figure 4.4: (A) N$_2$ gas adsorption-desorption isotherms of PPAC, PPAC-MS 100, PPAC-MS 50 and PPAC-MS 25 and (B) differential pore volume vs pore width
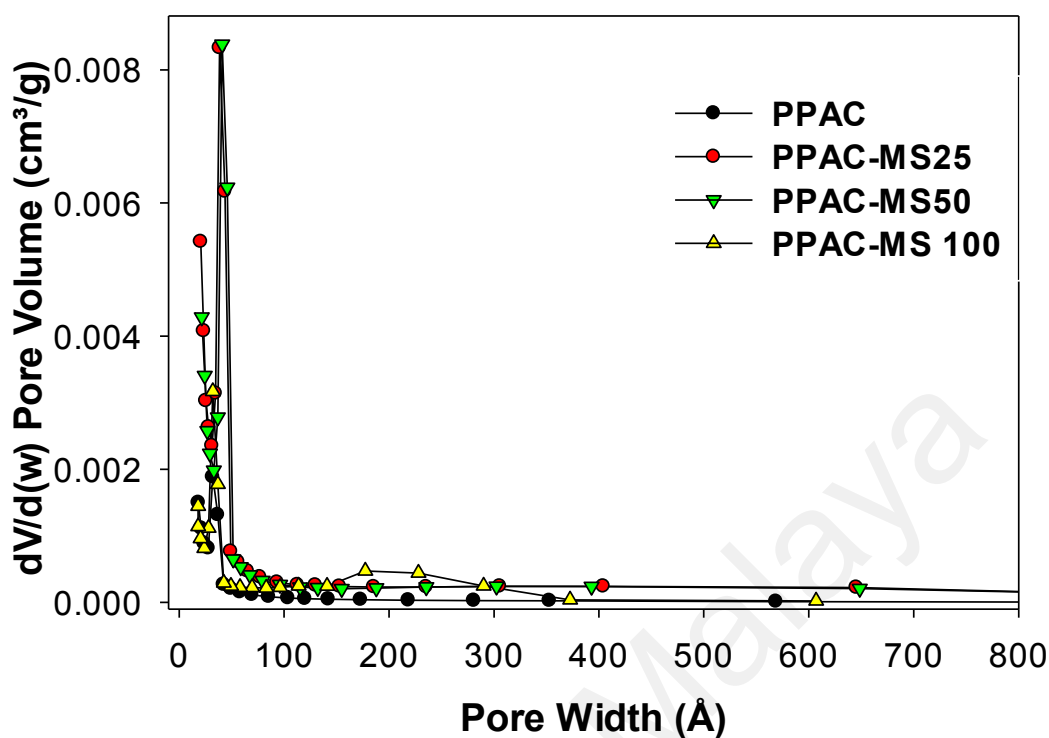
(b)

Figure 4.8, continued

Figure 4.8 (B) depicts the pore size distribution for PPAC, PPAC-MS25, PPAC-MS 50 and PPAC-MS 100. All adsorbents had a similar peak at 32 Å. $MgSiO_3$ impregnation enhances the mesopore and macropore from at 140 - 370 Å. Przepiórski, Czyżewski, Pietrzak, and Tryba (2013) reported carbon material coating with magnesium oxide capable of creating more mesopores under thermal treatment. Table 4.4 lists the textural characteristics for all absorbents on the total surface area, BET surface area, micropore surface area, total pore volume and micropore volume. $MgSiO_3$ impregnation ratio increased, while the total surface area and BET surface area decreased. Compared to PPAC, the average pore width and pore volume increase after $MgSiO_3$ impregnated. Although the BET surface area and pore volume of modified activated carbon is lesser than PPAC but the Cu (II) removal capacity for modified

51

activated carbon is better than PPAC. Thus, the results are proving the magnesium silicates play a significant rule for Cu (II) removal.

Table 4.4: Pore characteristic of PPAC, PPAC-MS 25, PPAC-MS 50, and PPAC-MS 100

Sample	PPAC	PPAC-MS 25	PPAC-MS 50	PPAC-MS 100
Total surface area(m^2/g)	1,099.80	992.97	910.32	772.10
BET surface area (m_2/g)	1,207.70	1,056.8	966.87	831.7
Microspore surface area (m_2/g)	966.55	684.87	620.8	650.1
Total pore volume(cm_3/g)	0.54	0.537	0.489	0.470
Microspore volume (cm_3/g)	0.38	0.28	0.256	0.263
Average pore diameter (Å)	31.96	34.33	37.13	59.76

The FESEM images and EDX of PPAC, PPAC-25, PPAC-MS 50 and PPAC-MS 100 were analyzed (Fig 4.9). The FESEM images illustrate that PPAC exhibited micropore with smooth surface honeycomb like structure (Figure 4.9A and 4.9B). After MgSiO$_3$ impregnation on PPAC, a rough and thin sheet structure form on top of PPAC-MS 100, PPAC-MS 50 and PPAC-MS 25 homogeneously. Interestingly, after impregnation with MgSiO$_3$, the pore structures still remain without blocking. FESEM results (Figure 4.9) reveal the plate-like thin sheet structure formed by interwoven of the MgSiO$_3$ plate within 14nm diameter (Gui, Wang et al., 2014). The EDX results show that PPAC-MS 100, PPAC-MS 50 and PPAC-MS 25 had different amounts of Si, Mg, and O compound, which infers that MgSiO$_3$ is impregnated on the surface. In another FESEM results (refer Figure 4.10), the surface of PPAC-MS 100 and PPAC become rough and the pore is filling with small crystal plate structure. Compared to PPAC-MS 100, the crystal plate structure is lesser on the surface of PPAC. From the EDX result,

Cu and O were detected for both adsorbents. Therefore, Cu (II) in solution was successfully removed by adsorption on the surface of PPAC and PPAC-MS 100.
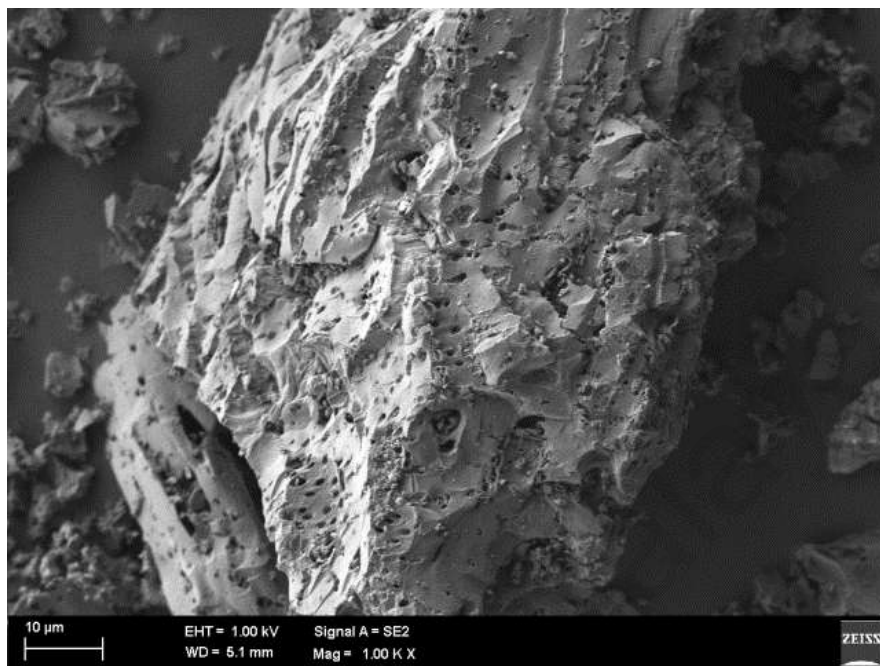
(a)
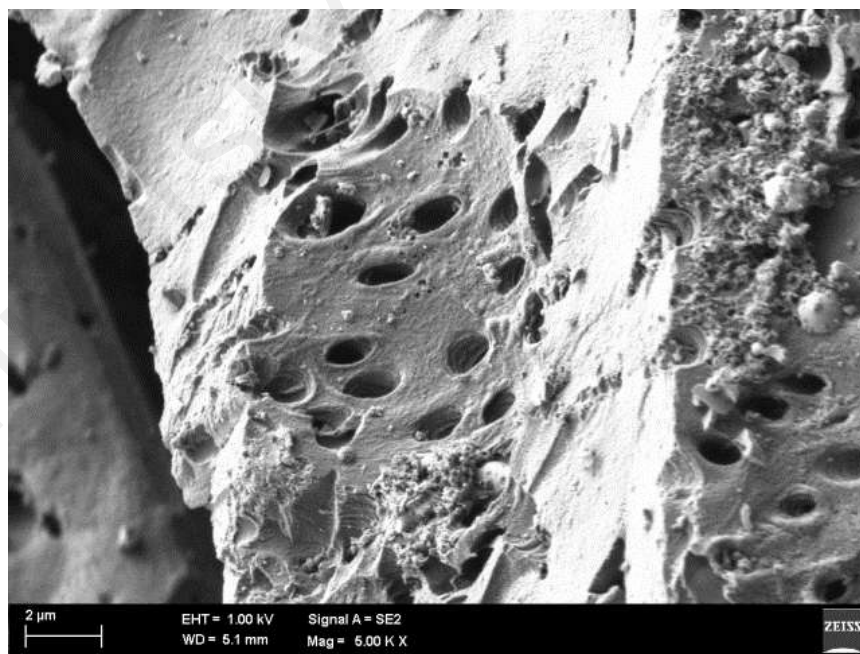
(b)

Figure 4.9: FESEM image of (A,B) PPAC and (C, D, E, F) PPAC-MS 100, and EDX analysis and its detecting area of (G,J) PPAC-MS 100, (H,K) PPAC-MS 50, and (I,L) PPAC-MS25

(c)

(d)

Figure 4.9, continued

HTI LAB 2.0kV 2.4mm x80.0k SE(U) 500nm

(e)

11.0nm 15.0nm 14.0nm 14.0nm

HTI LAB 2.0kV 2.4mm x200k SE(U) 200nm
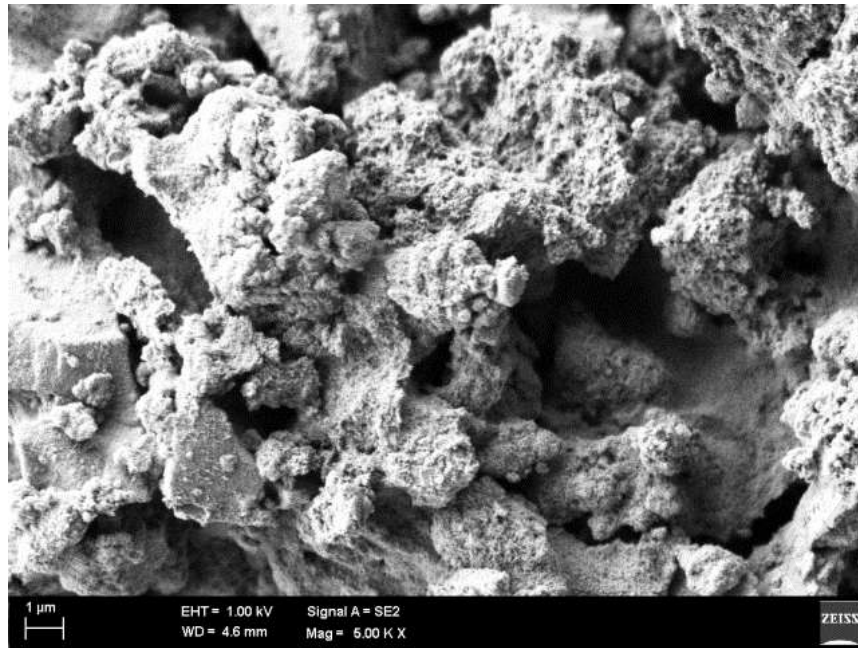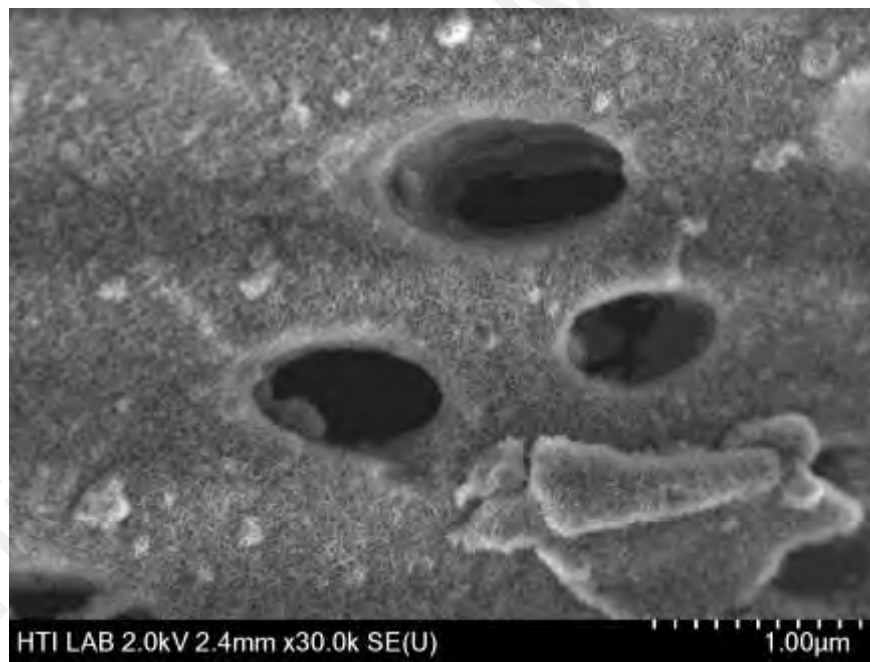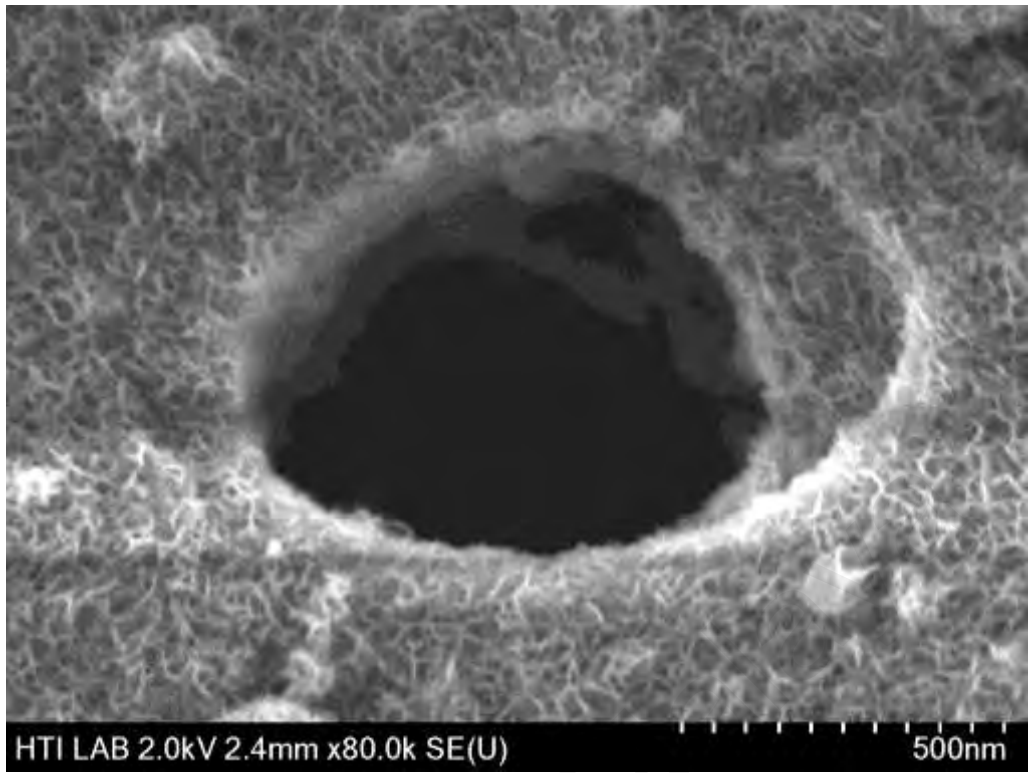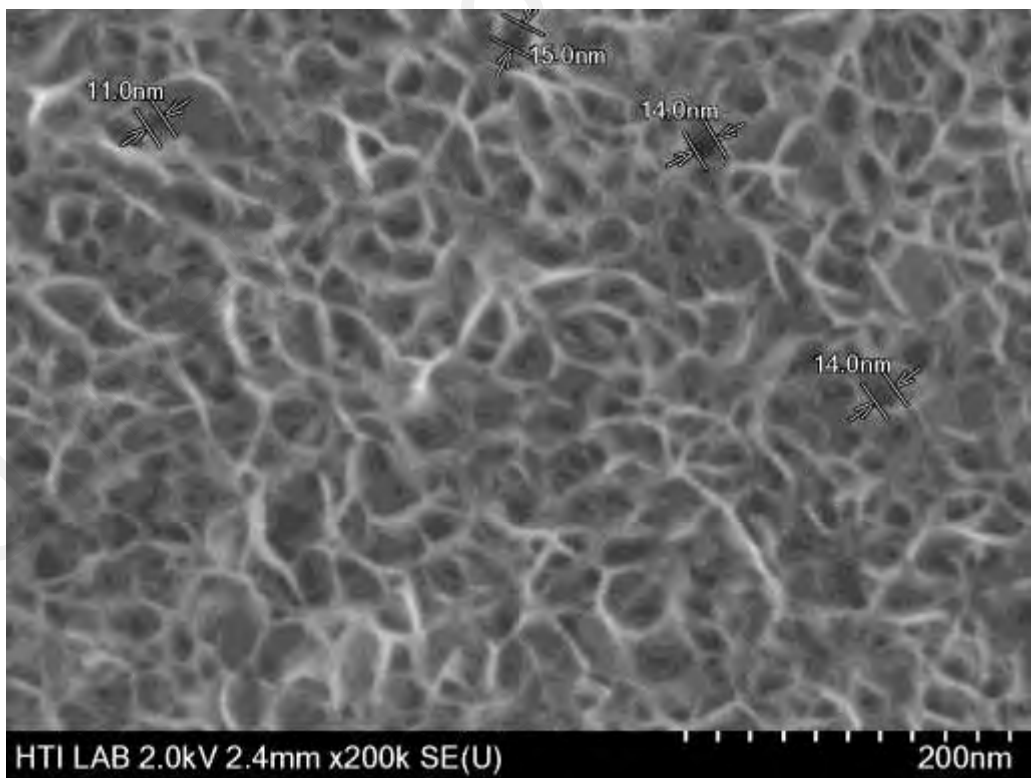
(f)

Figure 4.9, continued

(g)

(h)

Figure 4.9, continued

(i)

Element	Wt%	At%
C	60.78	71.27
O	22.35	19.68
Mg	07.66	04.44
Si	09.21	04.62
Matrix	Correction	ZAF

(j)

Figure 4.9, continued

Element	Wt%	At%
C	78.55	85.42
O	12.45	10.16
Mg	03.18	01.71
Si	05.81	02.70
Matrix	Correction	ZAF

(k)

Element	Wt%	At%
C	89.91	92.96
O	07.57	05.88
Mg	00.78	00.40
Si	01.74	00.77
Matrix	Correction	ZAF
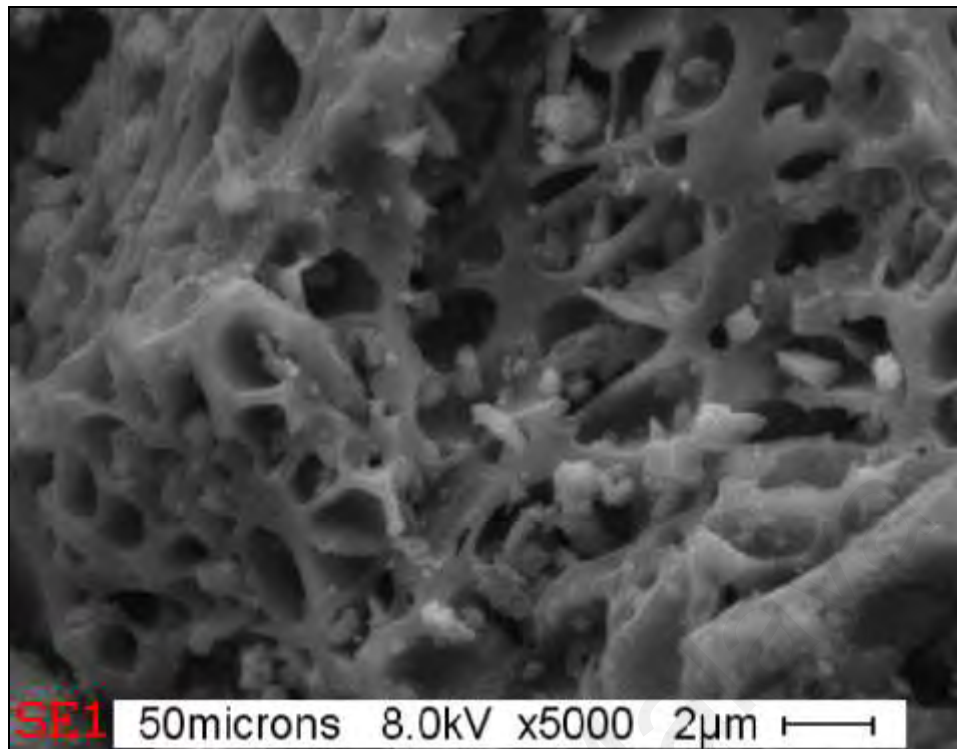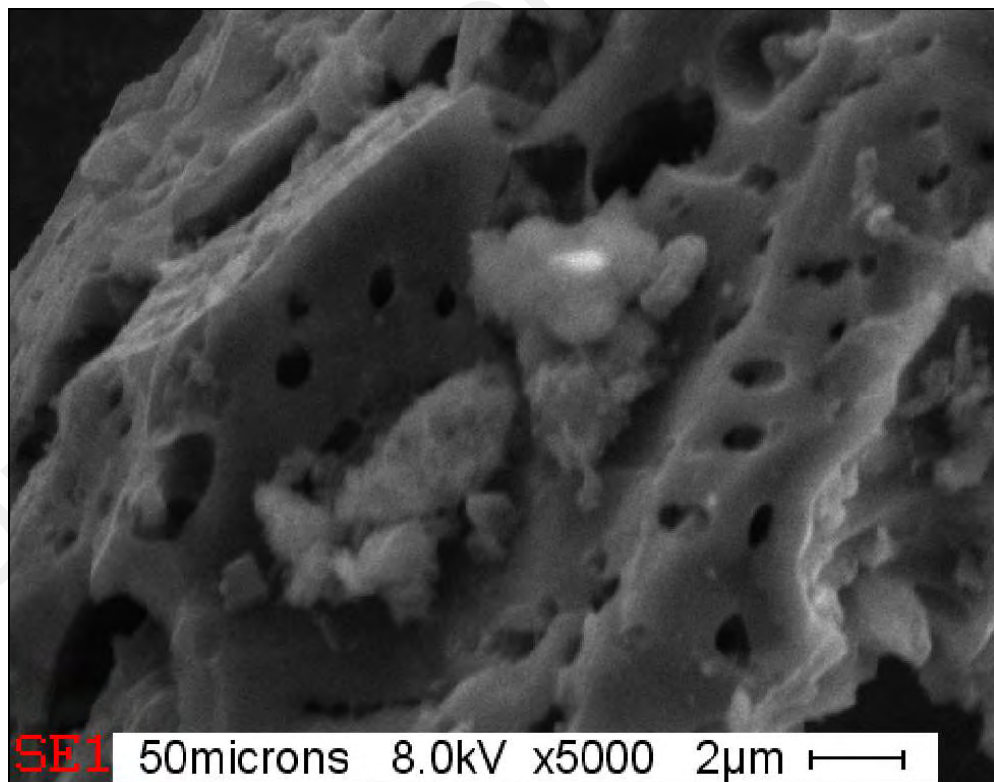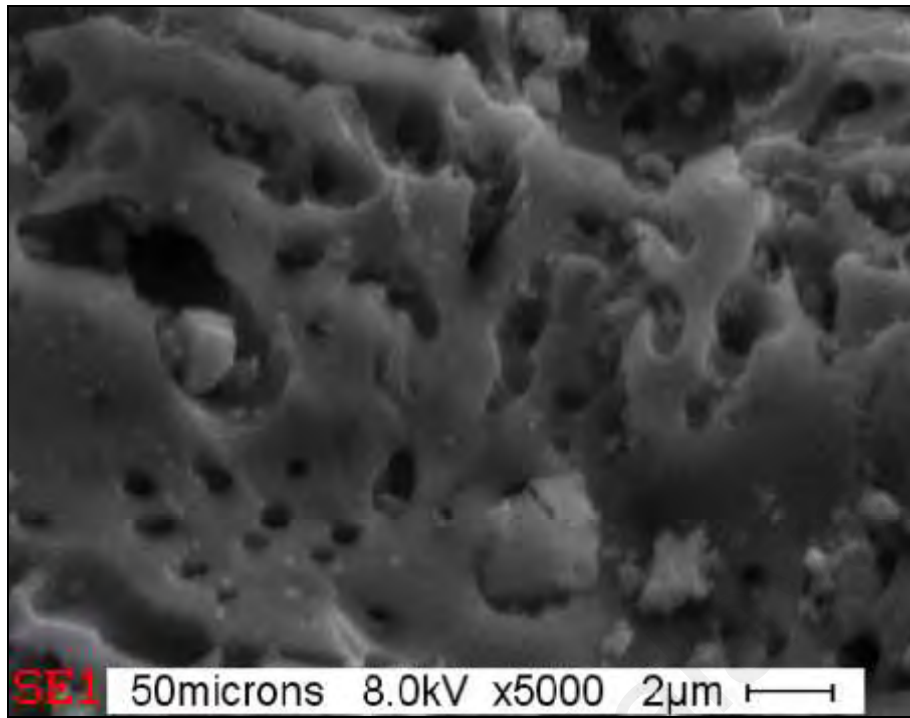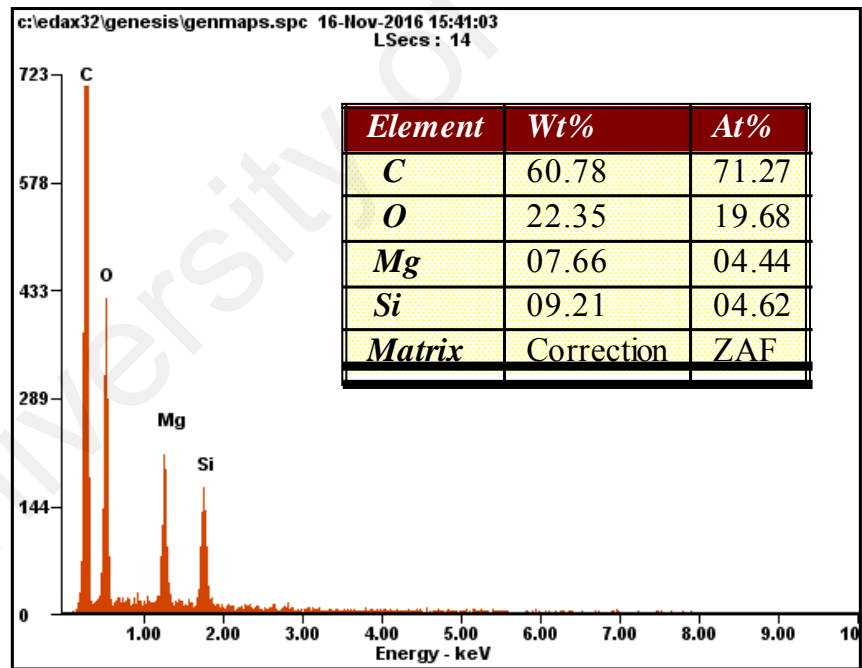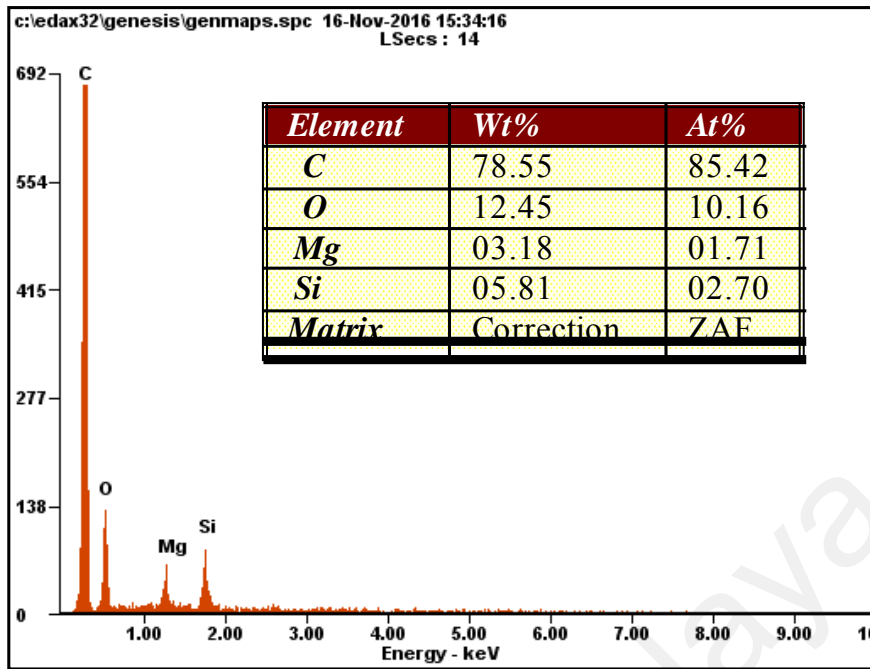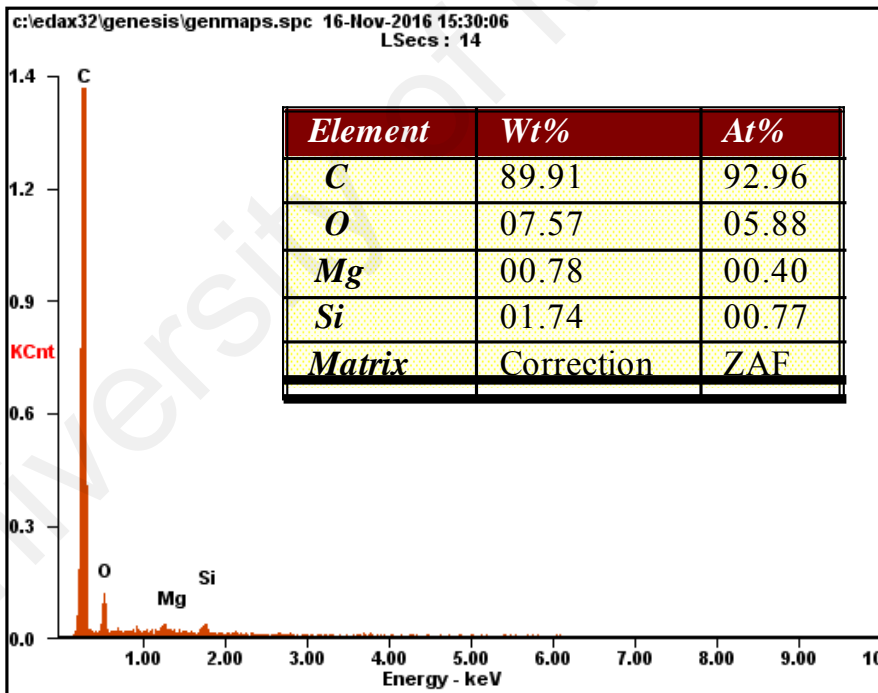
(l)

Figure 4.9, continued
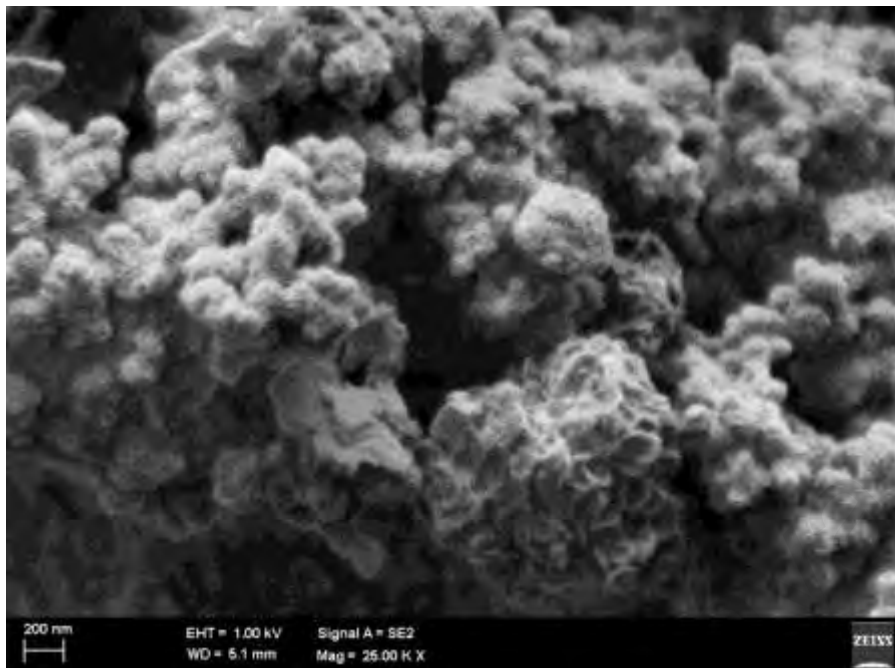
(a)
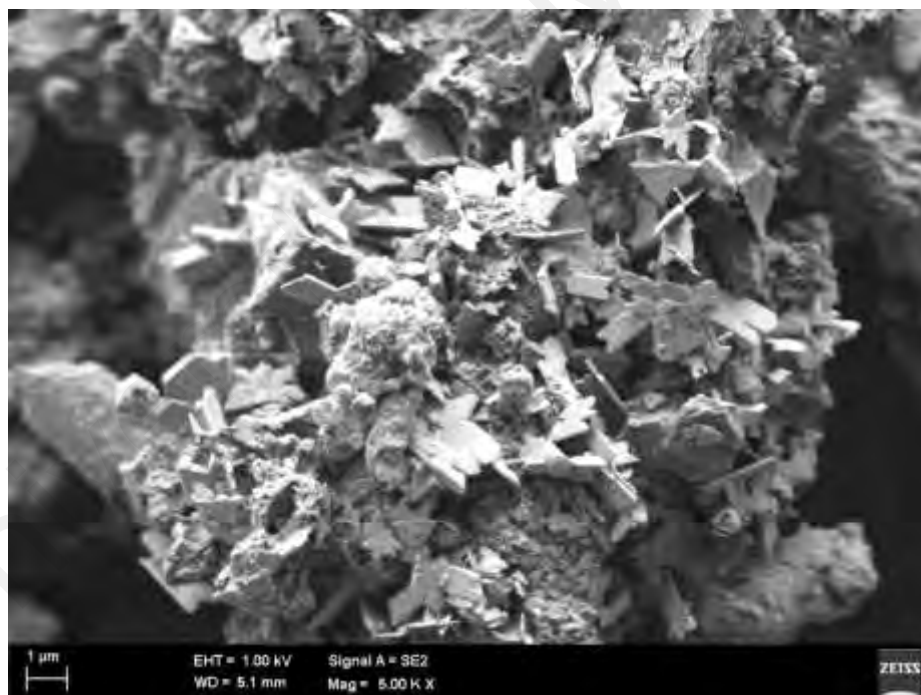
(b)

Figure 4.10:FESEM image after Cu(II) adsorption for (A-C) PPAC and (D-F) PPAC-MS 100

Element	Wt%	At%
C	25.09	40.41
O	31.82	38.47
Cu	24.64	07.50
Mg	08.44	06.71
Si	10.01	06.90
Matrix	Correction	ZAF

(c)

(d)

Figure 4.10, continued

(e)

Element	Wt%	At%
C	91.78	94.80
O	06.19	04.80
Cu	02.03	00.40
Matrix	Correction	ZAF
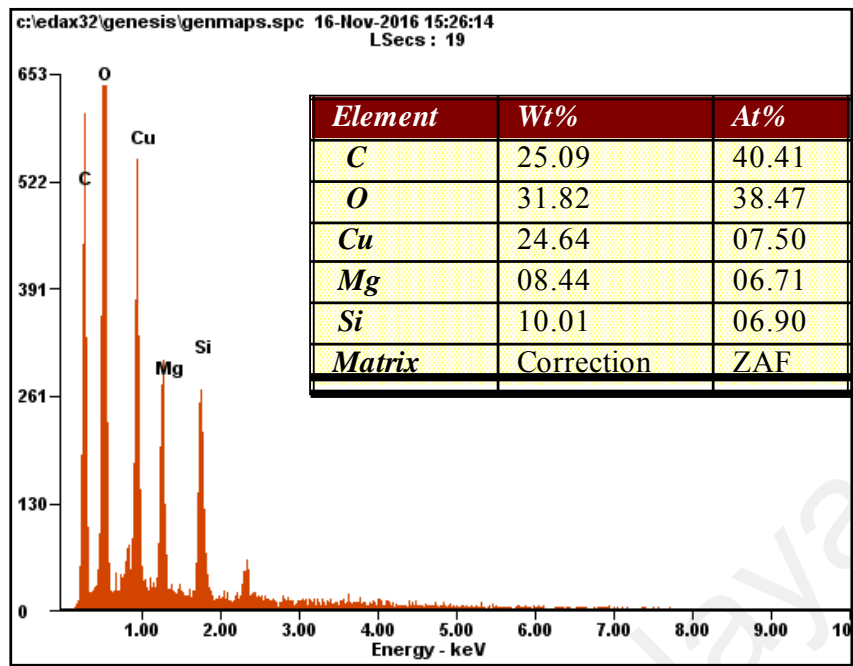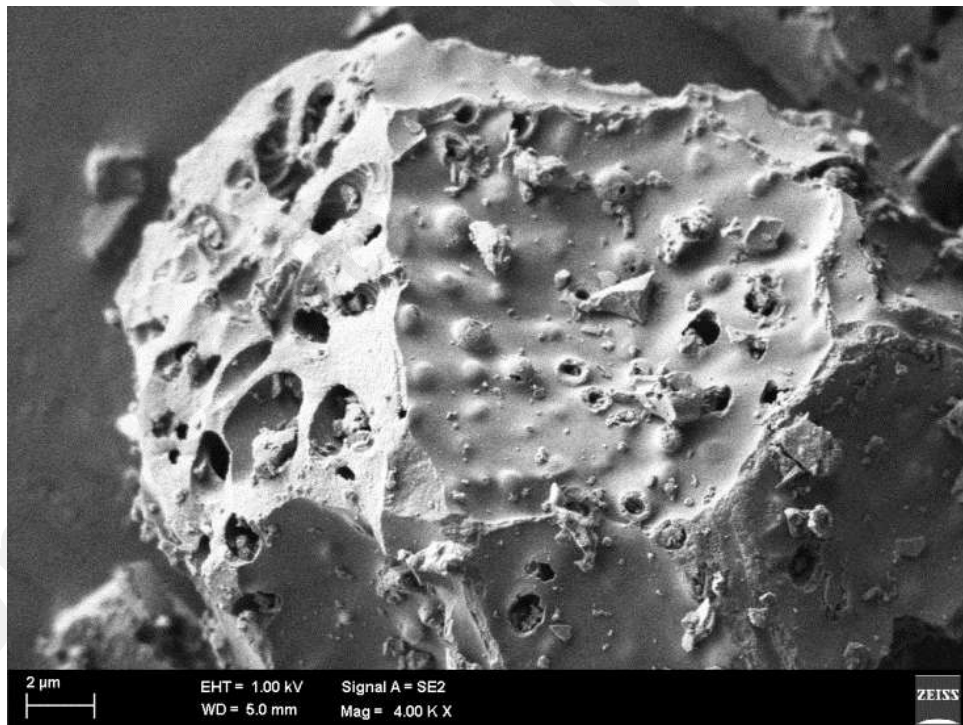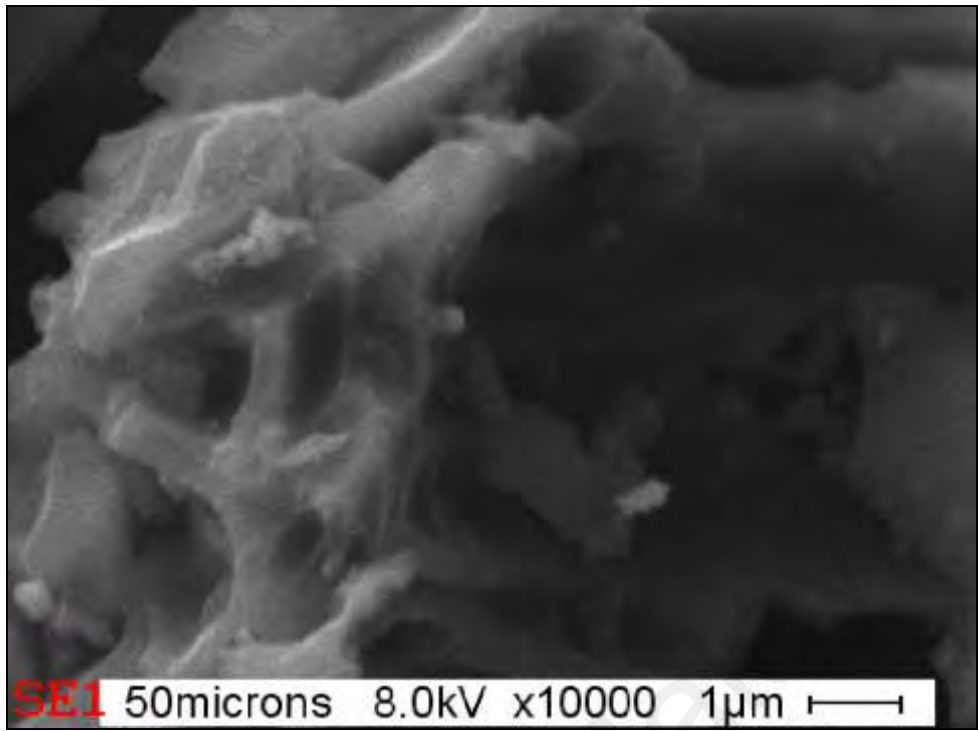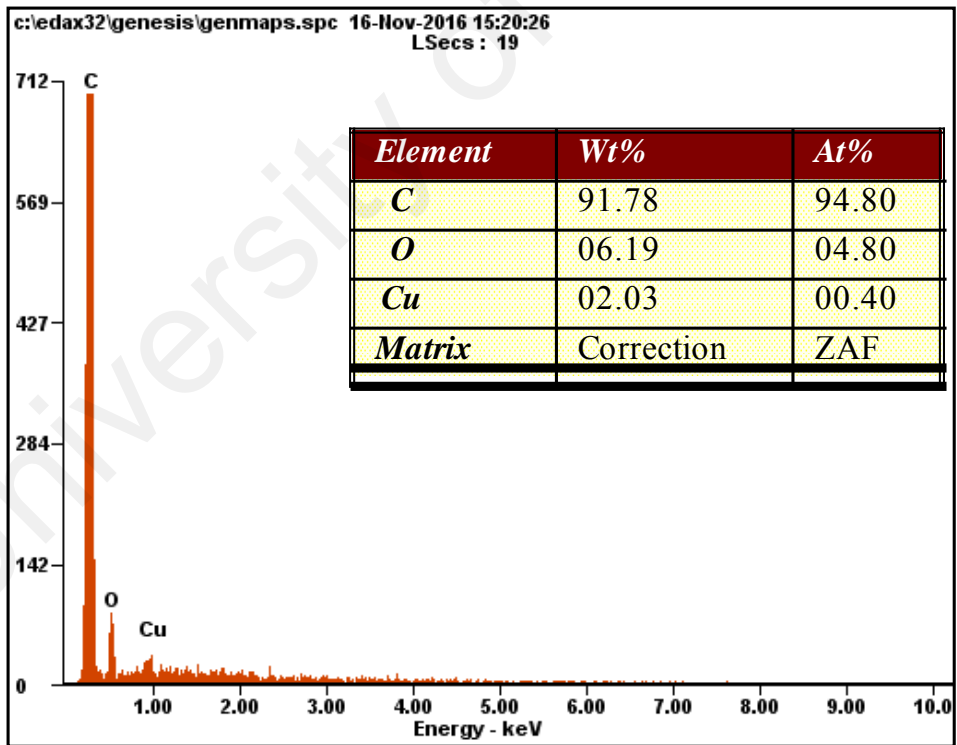
(f)

Figure 4.10, continued

XRD analysis was performed to investigate the chemical compound of PPAC and PPAC-MS 100 before and after adsorption (Figure 4.11). XRD pattern suggests that PPAC sample has asymmetric peaks from 25° - 50° assigned as indexed to Graphite (ISCD: 88813). Meanwhile, the PPAC-MS shows peaks at 20.07°, 33.39°, 46.4° and 60.14° corresponding to $MgSiO_3$ and peaks at 38.09°, 58.79° and 62.29° (ISCD 171782) assigned as magnesium hydroxide (ICSD 34401). SiO_2 was also detected on PPAC-MS 100 at peaks of 24.7° and 58.79°. This result proves that $MgSiO_3$ was successfully impregnated on PPAC after hydrothermal treatment. Compared to PPAC, the graphite peak in PPAC-MS 100 is weak but still exist because of the $MgSiO_3$ might not occupy fully on PPAC-MS 100. After Cu (II) adsorption, PPAC and PPAC-MS 100 present significant peak at 69.1° and 76.3° assigned as CuO (ISCD: 628614). This proven that the precipitation might involve for Cu (II) removal on PPAC and PPAC-MS 100.
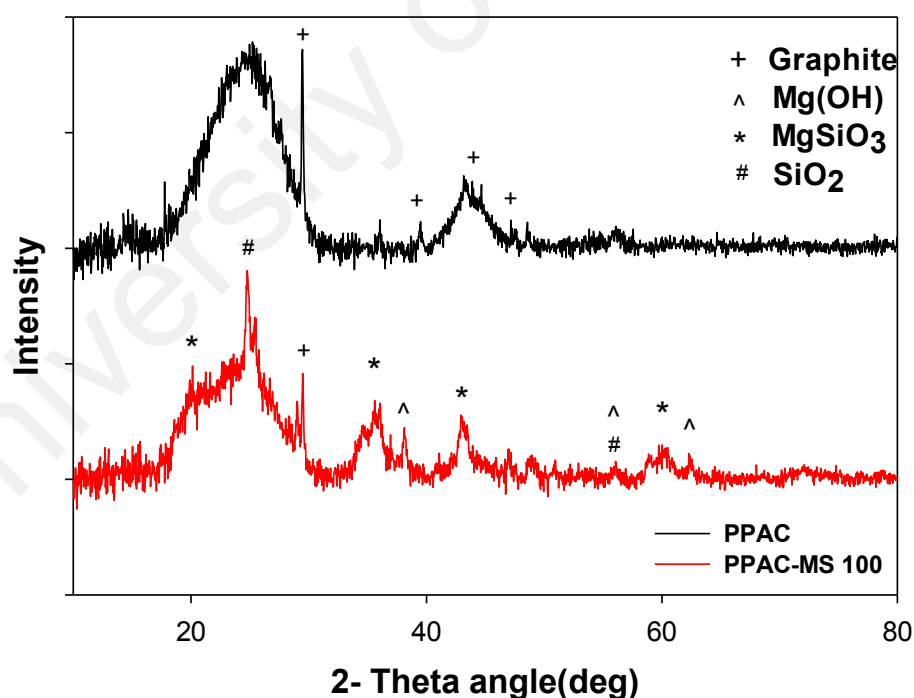
(a)

Figure 4.11:XRD results of PPAC and PPAC-MS 100 (A) before adsorption and (B) after adsorption
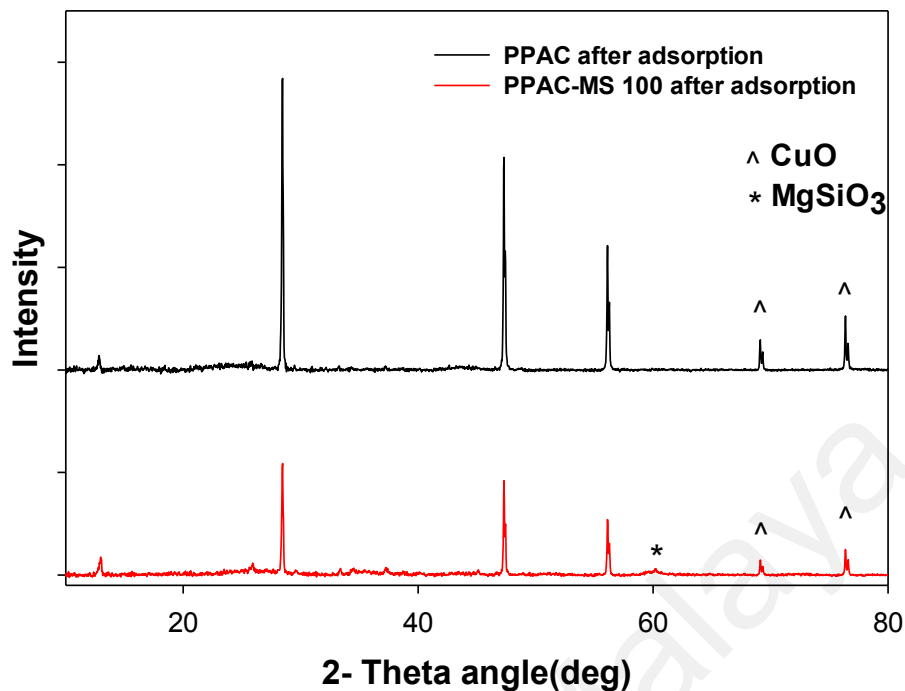
(b)

Figure 4.11, continued

To understand the electron structure of Cu (II) compound form on PPAC and PPAC-MS 100 after adsorption, Cu core level XPS spectra were studied. Wide scan analysis and Cu core level XPS spectra for PPAC and PPAC-MS 100 depict in Figure 4.12. Wide scan XPS spectrum of PPAC indicates O, C and Cu existence while Si, O, Cu, Mg existence on PPAC-MS 100. As shown in Figure 4.12(A), the peak at 935eV and 953eV and 937eV and 955eV associated to the binding energy of Cu $2p^{3/2}$ and Cu $2p^{1/2}$ for PPAC and PPAC-MS 100. The Cu component with low binding energy of Cu $2p^{3/2}$ can be assigned as a tetracoordinated Cu(I) ion species, while PPAC-MS 100 and PPAC Cu component can be assigned as acta coordinated Cu(II) ion species because the Cu $2p^{3/2}$ for PPAC-MS 100 and PPAC is located above 935eV(Li B., Luo et al., 2015). Moreover, Figure 4.12 indicated bivalent CuO form on PPAC and PPAC-MS 100. Therefore, it is proven that CuO was formed on the PPAC and PPAC-MS 100 surface. Moreover, a satellite peak appeared at the Cu core level XPS spectra for both PPAC and

63

PPAC-MS 100. The appearance of the satellite peak indicated CuO have a d9 configuration in a ground state between Cu $2p^{3/2}$ and Cu $2p^{1/2}$ peak (Hu, Shi et al., 2010).
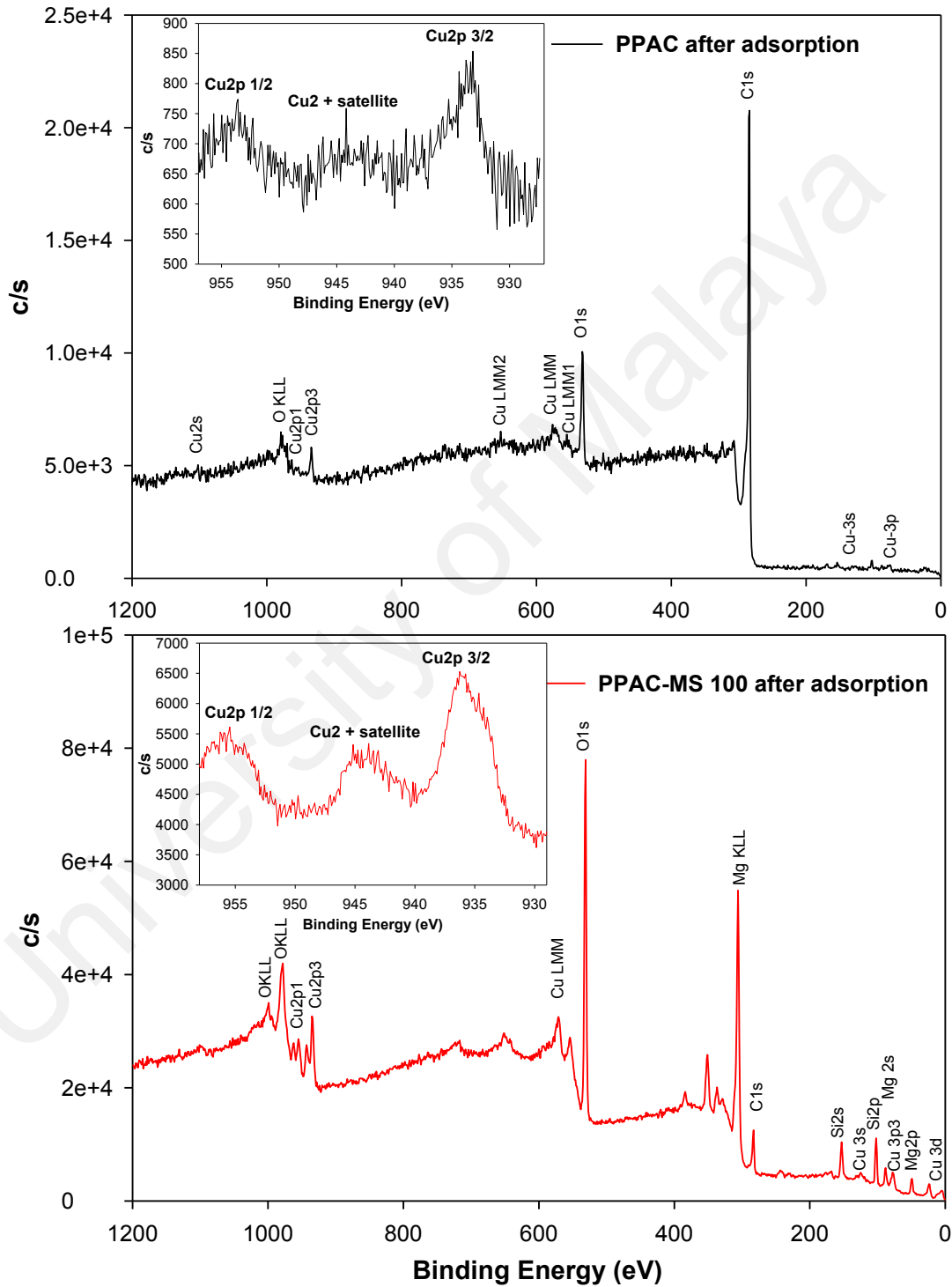
Figure 4.12: XPS wide scan analysis for PPAC and PPAC-MS 100 after adsorption
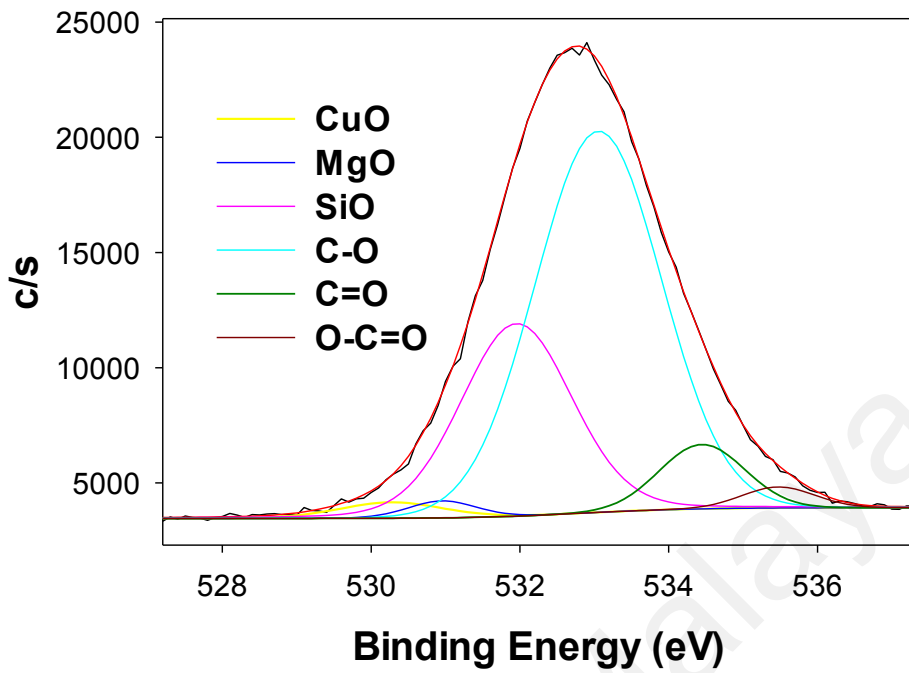
(a)
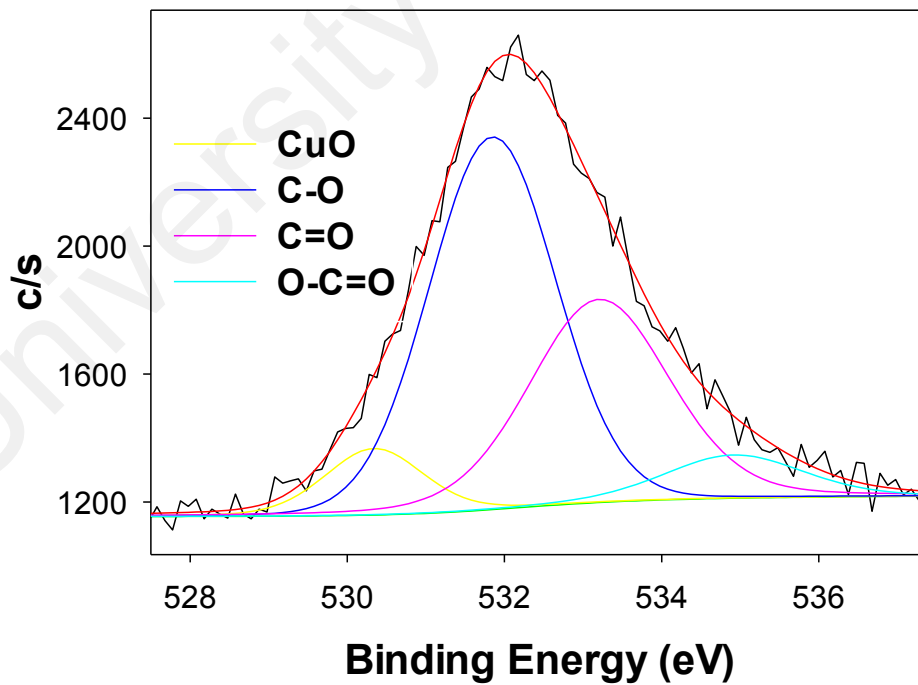
(b)

Figure 4.13: XPS analysis binding energy after adsorption (A) PPAC-MS 100 and (B) PPAC

Based on the characterization of materials, Cu (II) removal can be proposed as adsorption together with ion-exchange and precipitation for PPAC-MS 100. First, dissolution of Mg(OH)$_2$ releases hydroxide and Mg (II) ions to the surface of impregnated PPAC-MS 100, so the pH of solution increases. Thus, Cu (II) could be precipitation at this stage. XPS and XRD result have sufficient agreement to support that CuO component was precipitated and adsorbed on PPAC-MS 100. Second, ion exchange can occur between Mg and Cu ions on the solid surface. Thus, the mechanism of Cu (II) removal by PPAC-MS can be considered adsorption together with precipitation and ion-exchange. The adsorption of Cu (II) ion on PPAC is strongly influenced by the pH of the solution. PPAC is activated by KOH, OH$^-$ release and increased solution pH, resulting in precipitation. Besides that, the negatively charged C-O group can attract positively charged Cu (II) ions in adsorption as detected on PPAC through FTIR analysis.

4.4 Heavy metal adsorption with the presence of BPA

4.4.1 Adsorption isotherms single and binary mode

Figure 4.14 and 4.15 present adsorption isotherms of Pb (II) and BPA by PPAC and PPAC-MS 100 in single and binary modes, as well as data fits by use of Langmuir and Freundlich models. According to the determination coefficient (R^2) in Table 4.5, the adsorption of Pb (II) by PPAC apparently fitted well to the Langmuir isotherm while that of PPAC-MS 100 better fitted with the Freundlich isotherm. Thus, these fitting results inferred that Pb (II) can absorb as homogeneously monolayer on PPAC while it retains as heterogeneous multilayer for PPAC-MS 100 both in single and binary mode (Cataldo et al., 2016). On the other hand, the adsorption of BPA by PPAC and PPAC-MS 100 fitted well with Langmuir model both in single and binary modes (Table 4.5). These results concluded that the adsorption of BPA occurs on the surface of PPAC and PPAC-MS 100 as homogeneous monolayer adsorption. The q$_e$ (based on the Langmuir

model) of Pb (II) removals by PPAC were 391.3 and 194.5 mg g^{-1} in single and binary modes, respectively, while those by PPAC-MS 100 were 419.9 and 408.8 mg g^{-1} based on the Freudlich model. And, the maximum adsorptions of BPA in single and binary modes by the Langmuir model were 359.6 mg g^{-1} and 360.7 mg g^{-1} for PPAC while those by PPAC-MS 100 were 168.4 mg g^{-1} and 254.7 mg g^{-1}, correspondingly.

PPAC had the similar adsorption capacities of BPA in both single and binary modes, but had lower sorption capacity of Pb (II) in binary mode than single mode. Remarkably, however, the isotherm results indicated that Pb (II) removals by PPAC-MS 100 both in single and binary modes were much higher than those by PPAC. Especially, it was found that the adsorption capacities of Pb (II) by PPAC-MS 100 were not reduced in binary mode, but even increased, while those by PPAC greatly reduced. Accordingly, it infers that when Pb (II) and BPA coexist in the solution, they compete for available adsorption sites on the surface of PPAC. Pb (II) might be removed at the same adsorption sites with BPA at PPAC, but the PPAC surface had higher preference on BPA. Therefore, the presence of BPA reduces the number of available adsorption sites in binary mode, decreasing the adsorption capacity of Pb (II) on PPAC (Bonvin, Jost et al., 2016). Meanwhile, PPAC-MS 100 might have different sorption sites for Pb (II) and BPA since Pb (II) and BPA removals were not reduced and even increased in binary mode, respectively.

The sorption capacities of pollutants by PPAC and PPAC-MS100 were evaluated based on the surface area and pore volume. As a result, PPAC-MS100 has a lower surface area (772.1 m²g^{-1}) and microspore volume (0.263 cm^{3}g^{-1}) compared to PPAC (1,099.8 m²g^{-1} and 0.38 cm^{3}g^{-1}). This could be primary reason that PPAC had better sorption of BPA for both single and binary modes than PPAC-MS 100. Moreover, when the mineral material like magnesium silicate exist in PPAC, activated carbon become more hydrophilic to reduce the adsorption capacity of BPA (Bautista-Toledo I.

et al., 2005). On the other hand, PPAC-MS 100 sorption capacity increased 50 % for the BPA removal in binary mode, while PPAC remains similar adsorption capacity. This is due to the fact that the surface of PPAC-MS 100 can release hydroxide (OH⁻), resulting in the precipitation of Pb (II) ions. While the precipitation process of Pb (II) occurs, BPA can co-precipitate with the Pb(OH)$_2$ compounds. Therefore, in the present of Pb (II) ions, the sorption capacity of BPA by PPAC-MS 100 greatly increased. The effect of Pb (II) precipitation on BPA removal has been separately tested and its results were described at the section 3.3. Comparison of Pb (II) adsorption capacities between PPAC, PPAC-MS 100 and other absorbents was presented at Table 4.6. Sorption capacities of Pb (II) by PPAC-MS 100 and PPAC were higher than other materials, except synthetic reduced graphane oxide (Gaya et al., 2015; Gui et al., 2014; Jafari, Tanguy et al., 2012; Saeidi, Parvini et al., 2015; Yang Y., Xie et al., 2013).
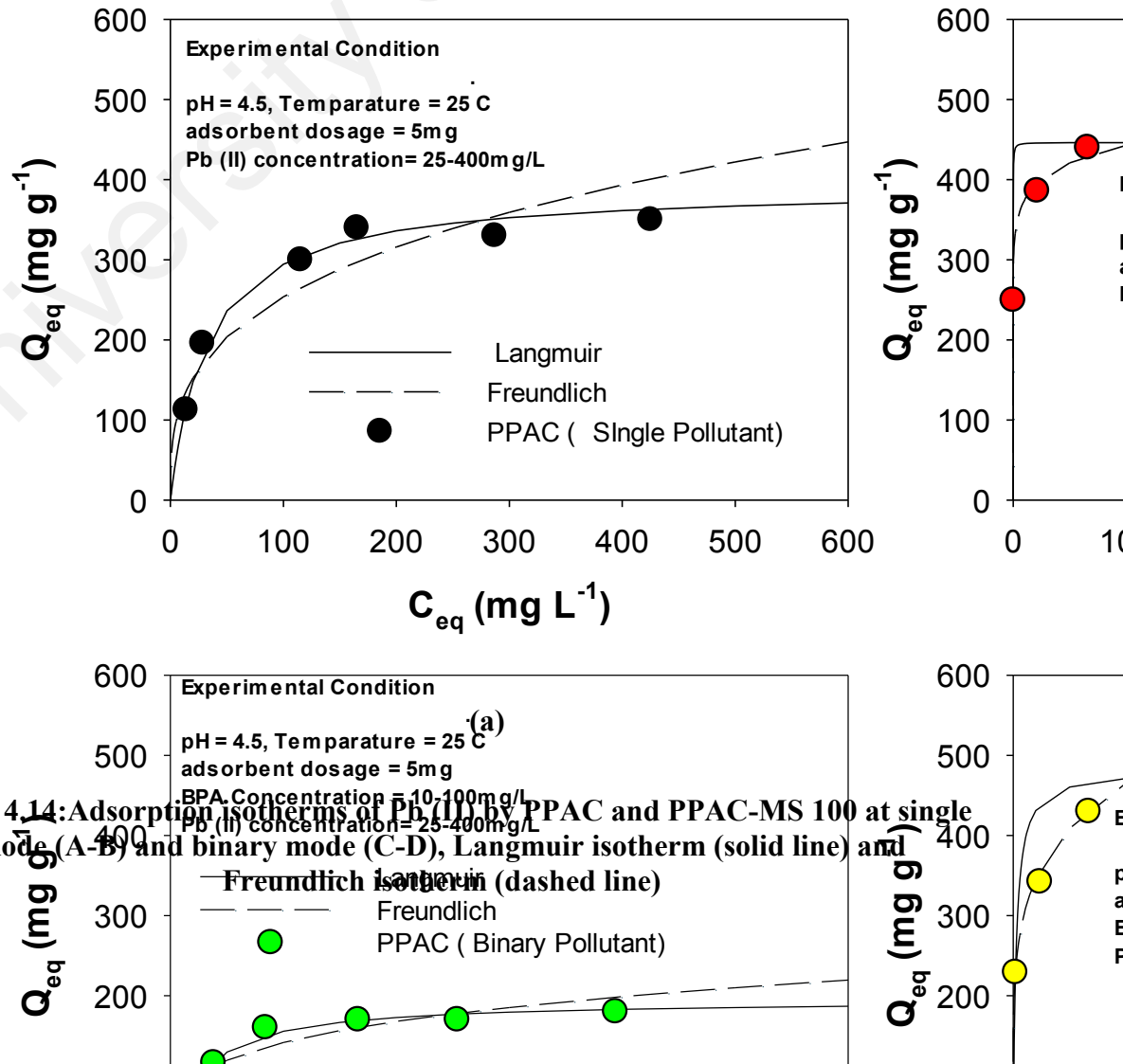
Figure 4.14: Adsorption isotherms of Pb (II) by PPAC and PPAC-MS 100 at single mode (A-B) and binary mode (C-D), Langmuir isotherm (solid line) and Freundlich isotherm (dashed line)

(c)

Figure 4.14, continued

300   400   500   600

(mg L^{-1})

C$_{eq}$ (mg L^{-1})

Experimental Condition

pH = 4.5, Temparature = 25 C
adsorbent dosage = 5mg
BPA Concentration = 10-100mg/L
Pb (II) concentration= 25-400mg/L

— Langmuir
--- Freundlich
○ PPAC-MS (Bianry Pollutant)

(d)

Figure 4.14, continued

Experimental Condition

pH =4.5, Temparature = 25 C
Adsorbent dosage=5mg
BPA concentration= 10-100mg/L

— Langmuir
--- Freundlich
● PPAC - Single Pollutant

(a)
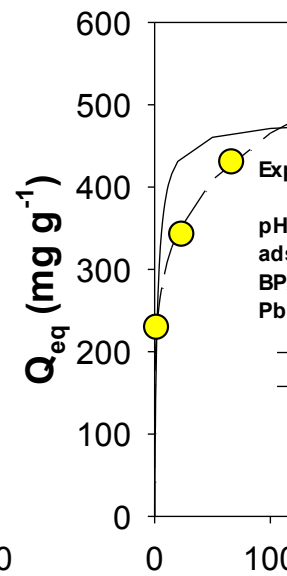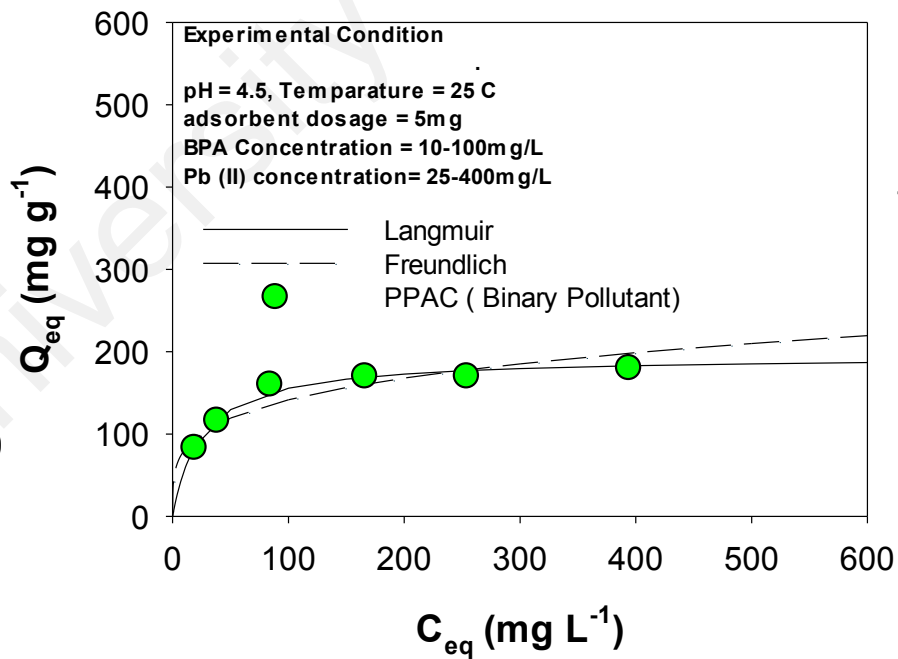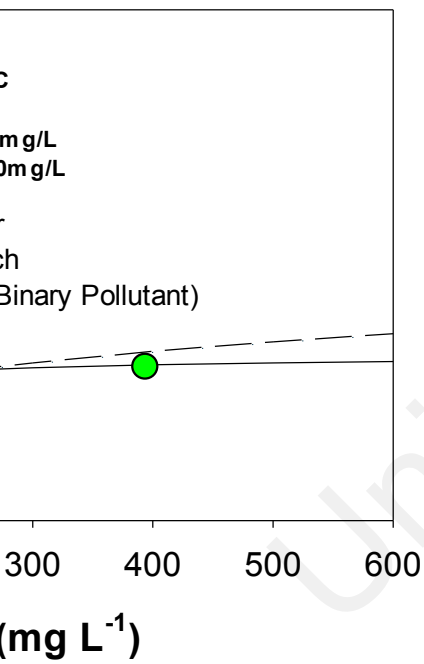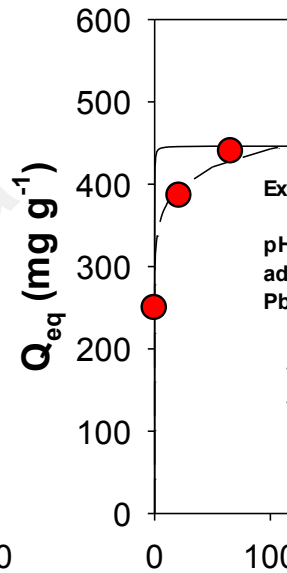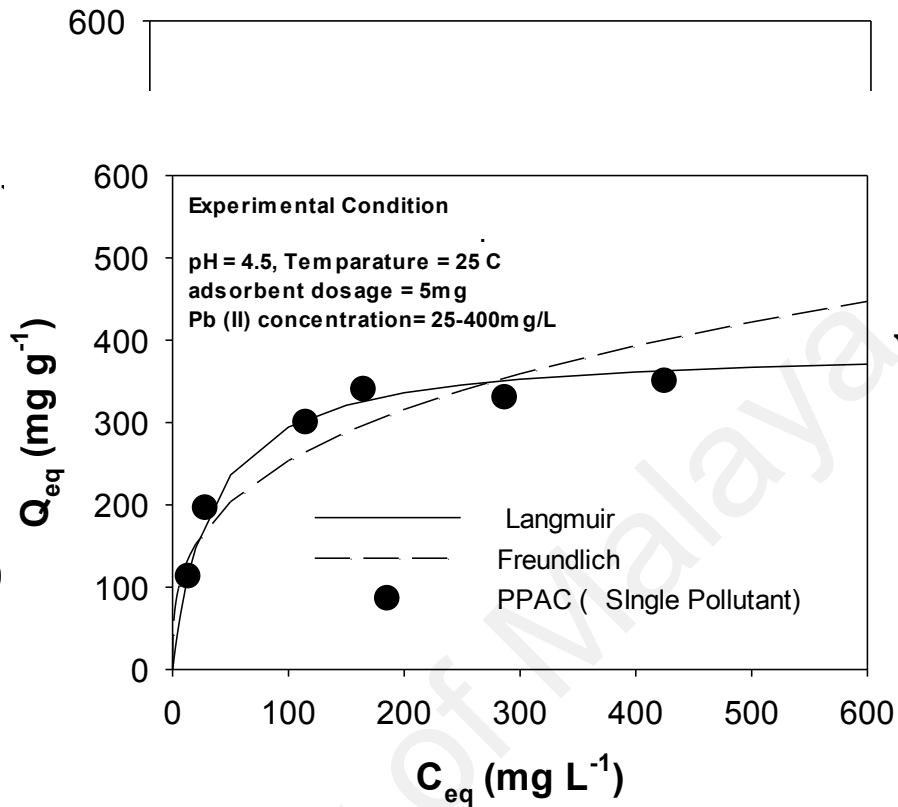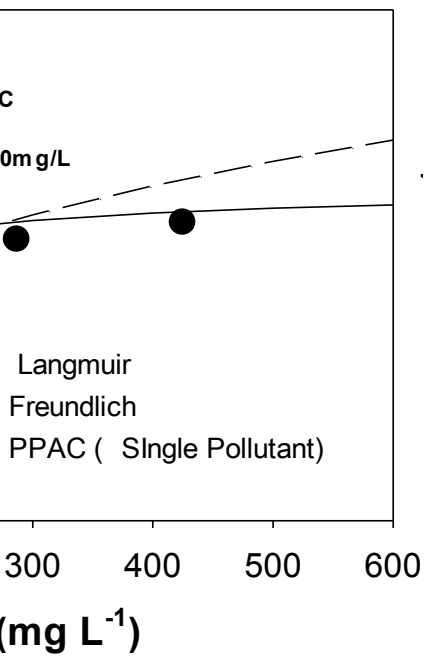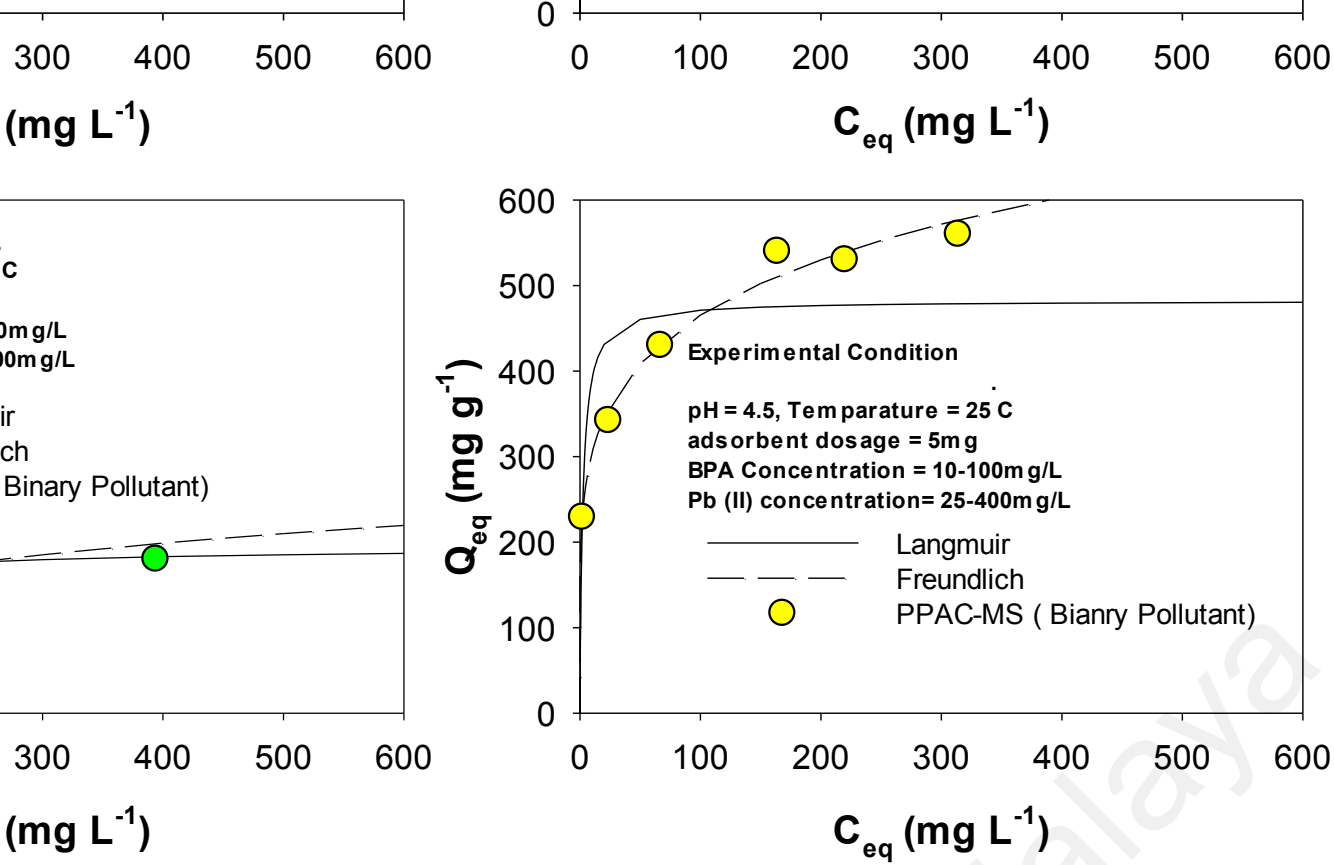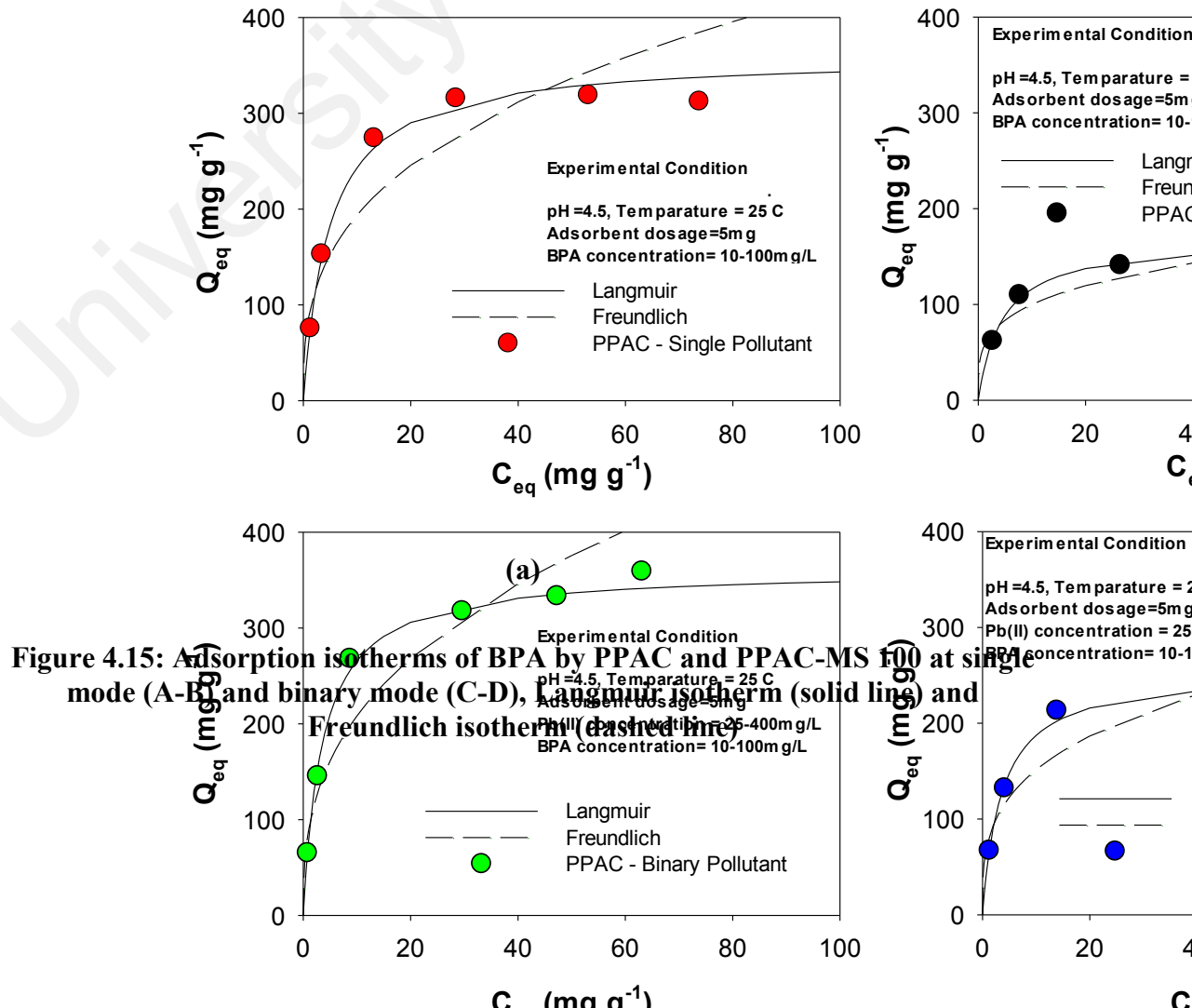
Figure 4.15: Adsorption isotherms of BPA by PPAC and PPAC-MS at single mode (A-B) and binary mode (C-D), Langmuir isotherm (solid line) and Freundlich isotherm (dashed line)

Experimental Condition

pH =4.5, Temparature = 25 C
Adsorbent dosage=5mg
Pb(II) concentration = 25-400mg/L
BPA concentration= 10-100mg/L

— Langmuir
--- Freundlich
○ PPAC - Binary Pollutant

Figure 4.15, continued

(d)

Figure 4.15, continued

Table 4.5: Parameters of adsorption isotherms of Pb (II) and BPA by PPAC and PPAC-MS 100 in single and binary modes

mode	Pollutants	media	Langmuir Parameter			Frendlich Parameter			
			q_e	K_L	R^2	q_e	K_F	n	R^2
Single	BPA	PPAC	359.6	0.209	0.998	336.9	88.1	2.916	0.880
		PPAC-MS 100	168.4	0.222	0.992	152.1	55.1	3.857	0.916
Binary	BPA	PPAC	360.7	0.279	0.998	375.7	89.4	2.726	0.916
		PPAC-MS100	254.7	0.277	0.996	246.4	75.2	3.295	0.893
Single	Pb (II)	PPAC	391.3	0.031	0.99	204.2	59.4	3.167	0.89
		PPAC-MS 100	446.5	31.68	0.93	419.9	315.8	13.73	0.98
Binary	Pb (II)	PPAC	194.5	0.04	0.99	119.4	45.8	4.081	0.87
		PPAC-MS 100	482.3	0.42	0.87	408.8	196.5	5.341	0.99

Table 4.6:Comparison of Pb (II) adsorption capacities between PPAC, PPAC-MS and other absorbents

Adsorbents	Pb (II) concentration (mg.L^{-1}) applied	Q$_{max}$ (mg g^{-1})	Reference
Magnesium silicate coated on reduced graphane oxide	-	416	(Gui et al., 2014)
Graphene composite	100	217.00	(Saeidi et al., 2015)
Fe$_3$O$_4$@MgSiO$_3$	12.9-1036.0	242.1	(Jafari et al., 2012)
Doum palm shells activated carbon activated by KOH	40-80	333	(Gaya et al., 2015)
Synthetic reduced graphene oxide	80-1500	500	(Yang Y. et al., 2013)
PPAC-MS	25-400	446.50	This work
PPAC	25-400	391.26	This work

4.4.2 Adsorption kinetics single and binary mode

Figure 4.16 presents the results of kinetics of Pb (II) and BPA by PPAC and PPAC-MS 100 in single and binary modes. The data of adsorption kinetics were modeled using the Pseudo-first and Pseudo-second order kinetic models, in which parameters were shown in Table 4.7. The determination coefficients (R^2) of Pseudo-second order kinetic model were much higher than those of Pseudo-first order. As a result, overall of Pb (II) and BPA adsorption process by PPAC and PPAC-MS 100 can be concluded as chemisorption (Yakout & Borai, 2014). As the similar results with isotherms, PPAC-MS 100 had the calculated q$_{eq}$ of Pb (II) (479.7 mg g^{-1}), which was higher than PPAC (373.4 mg g^{-1}) in single mode. The equilibrium adsorption for Pb (II) was obtained after 90 minutes for PPAC-MS 100 and PPAC in single mode. On the other hand, q$_{eq}$ of Pb (II) by PPAC in the binary mode was 101.74 mg g^{-1} which was only 73 % of q$_e$ obtained at single mode whiles q$_{eq}$ (485.9 mg g^{-1}) for PPAC-MS 100 in binary mode was higher than that in single mode. The equilibrium adsorptions of Pb (II) by both PPAC and PPAC-MS 100 were obtained at 60 minutes in the binary mode. Thus, Pb (II) equilibrium adsorption by PPAC and PPAC-MS 100 occurred faster in

binary mode compare to single mode. This behavior can be explained by the competition effect between BPA and Pb (II) to compete for available adsorption site (Nouri et al., 2007).Meanwhile, q_{eq} for BPA removal by PPAC-MS 100 was 101.5 mg g^{-1} which was lower than q_{eq} for PPAC (273.1 mg g^{-1}) in single mode. The q_{eq} of BPA removal by PPAC remains as 277.5 mg g^{-1} but PPAC was greatly increased to 121.9 mg g^{-1} in binary mode. The equilibrium adsorption was obtained after 90 minutes for single and bina___ ___ _ ___ ___ ___ ___ _ ___ ___

(a)

Figure 4.16:Adsorption kinetics of Pb (II) and BPA by PPAC and PPAC-MS 100 (dot lines fitted to Pseudo-second order kinetic model): (A) BPA removal in the single mode and (B) binary mode, (C) Pb (II) removal in the single mode and (D) binary mode
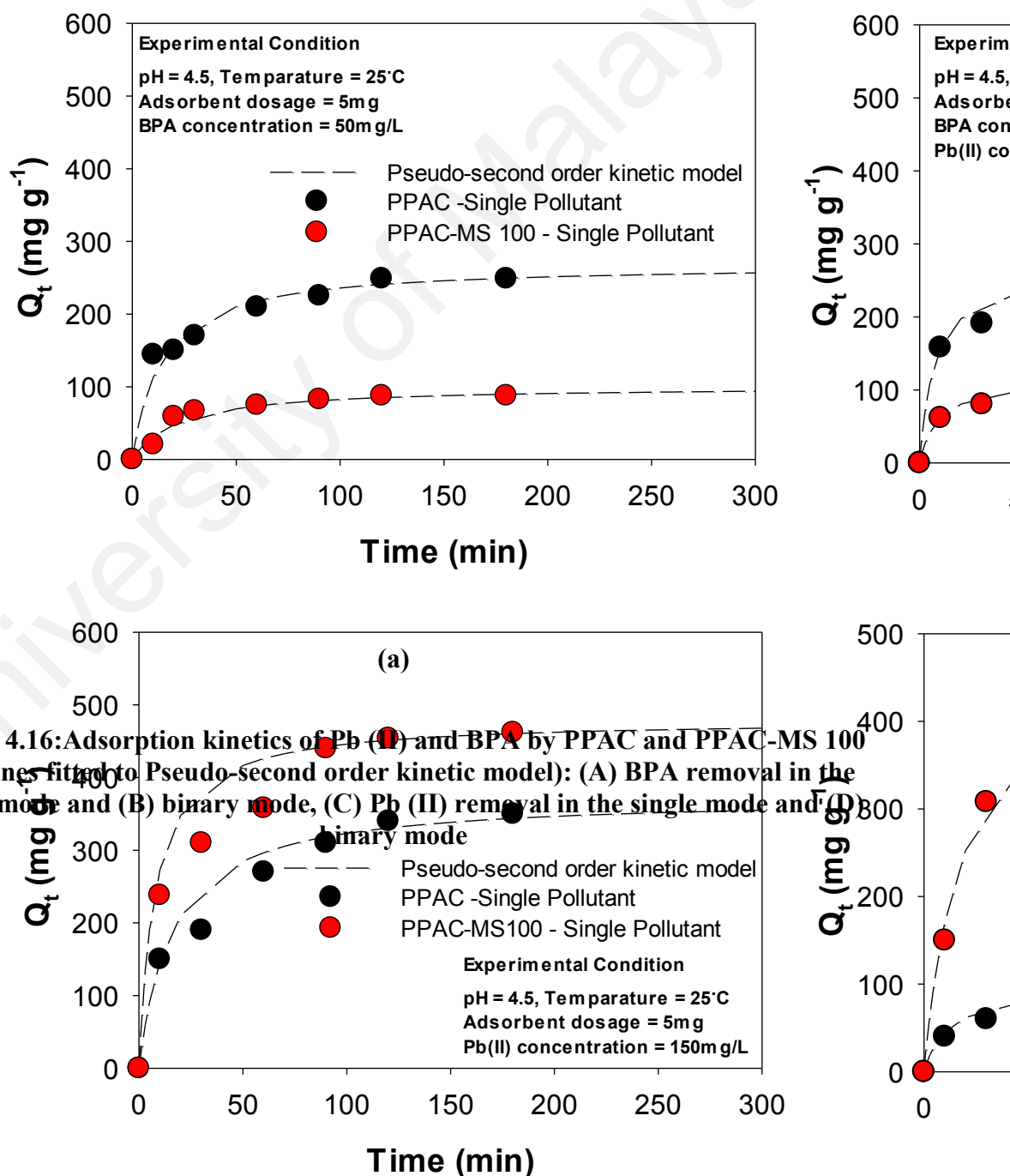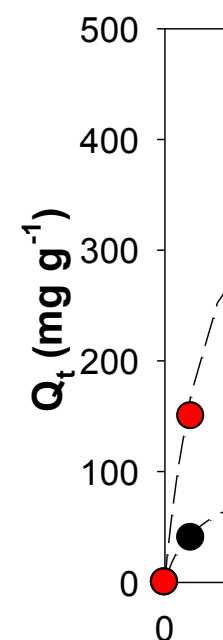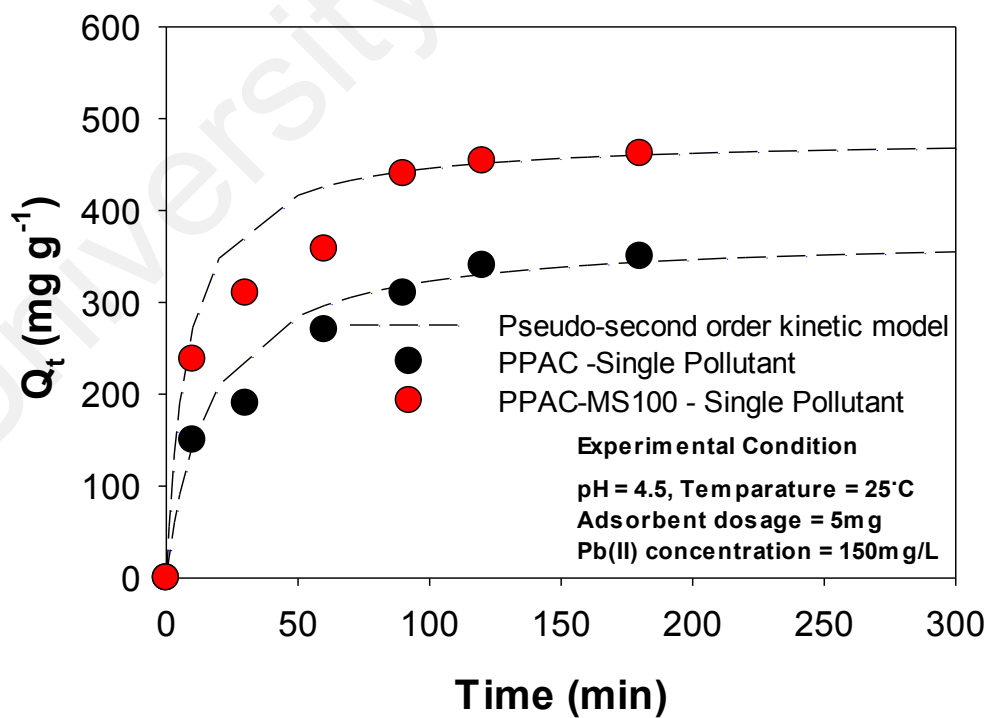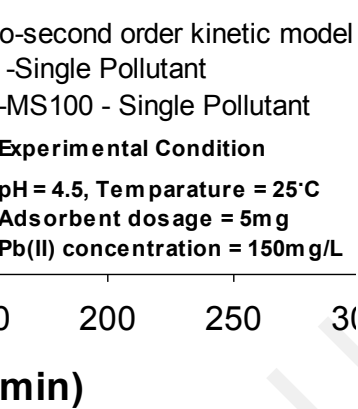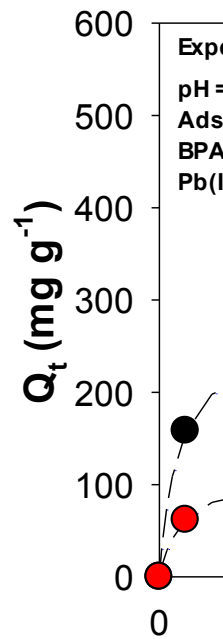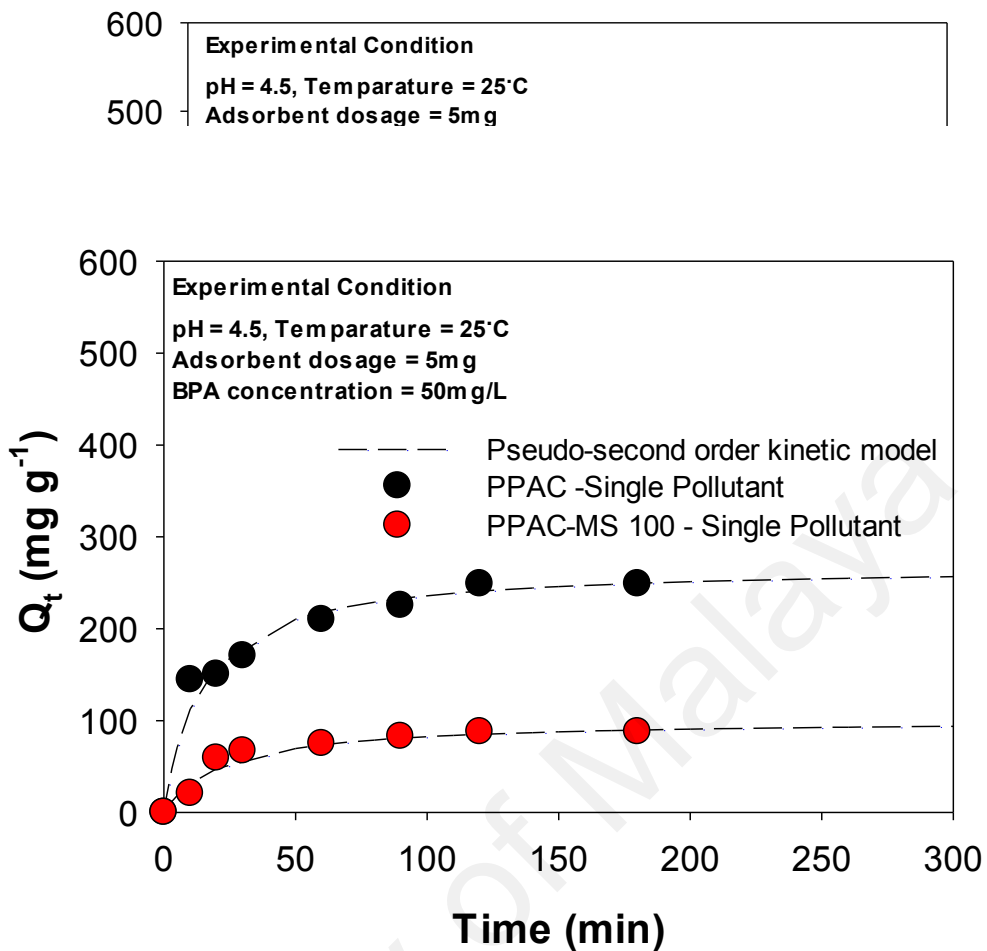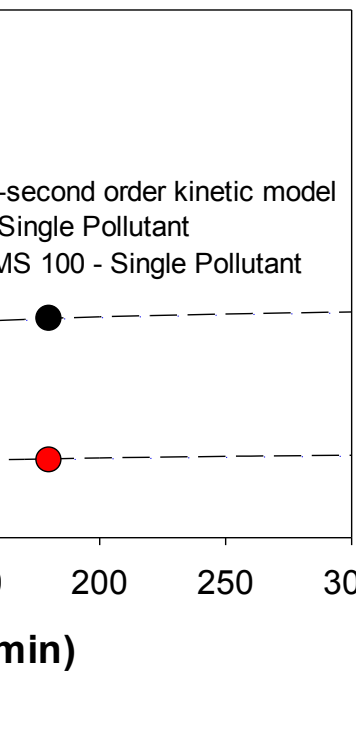
(c)

Figure 4.16, continued
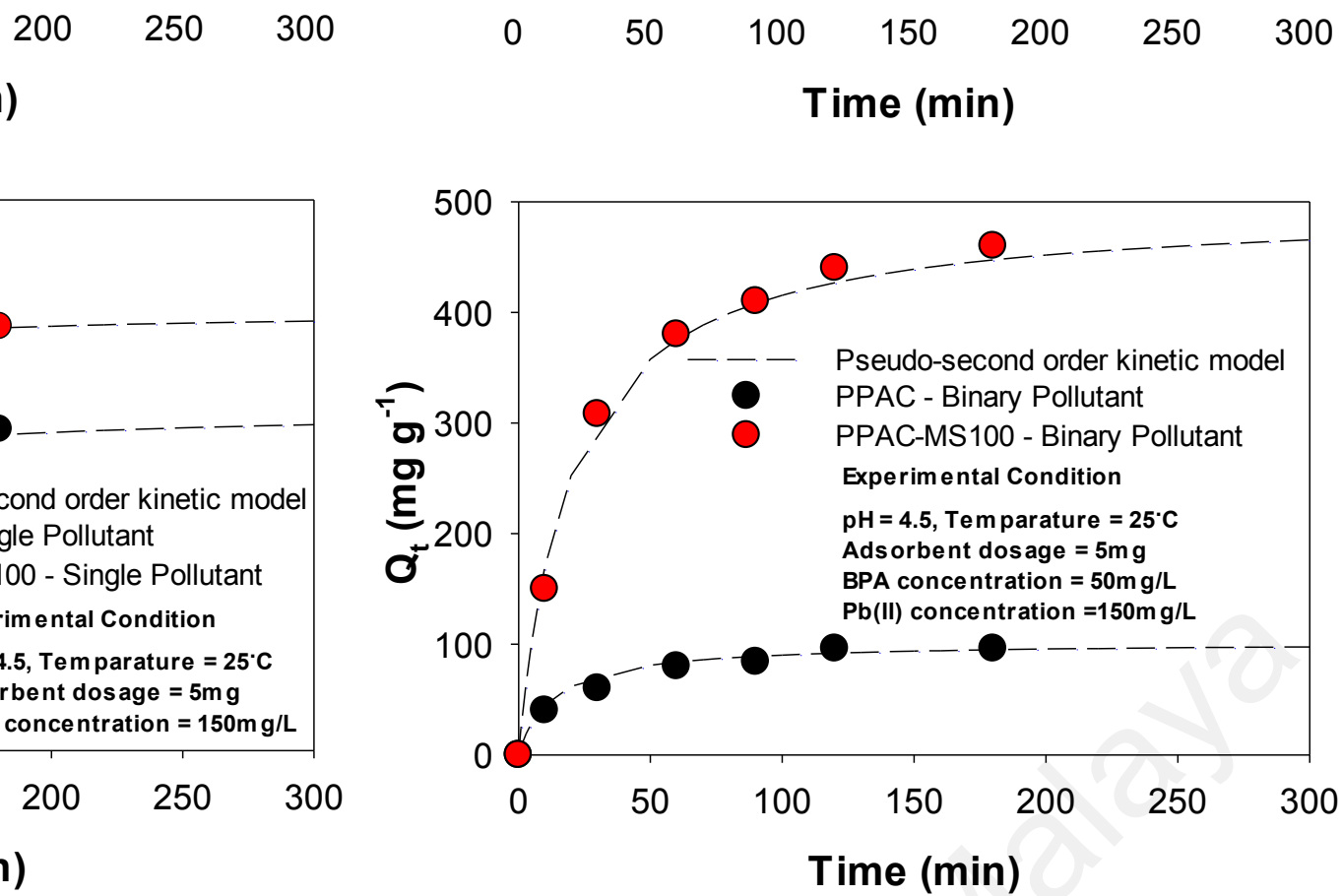
(d)

Figure 4.16, continued

Table 4.7:Parameters of Pseudo-first and Pseudo-second order kinetic models for BPA and Pb (II) removal by PPAC and PPAC-MS 100 in single and binary modes

mode	pollutants	media	Pseudo-first-order model		Pseudo-second-order model			q_e^{exp}
			K_1 (min^{-1})	R^2	K_2 (g·mg^{-1}·min^{-1})	q_{eq}	R^2	
Single	BPA	PPAC	0.013	0.89	0.0003	268.8	0.99	248.92
		PPAC-MS 100	0.011	0.81	0.0004	101.0	0.98	87.769
Binary	BPA	PPAC	0.016	0.85	0.0005	272.2	0.99	260.43
		PPAC-MS 100	0.015	0.85	0.0009	118.8	0.99	112.23
Single	Pb (II)	PPAC	0.015	0.95	0.0002	373.4	0.98	350
		PPAC-MS 100	0.017	0.91	0.0003	479.7	0.99	462
Binary	Pb (II)	PPAC	0.016	0.91	0.0008	101.8	0.98	96
		PPAC-MS 100	0.015	0.95	0.0001	485.9	0.98	460

4.4.3 Influence of ionic strength effect in binary mode adsorption

Figure 4.17(A) represents the effect of ionic strength on the Pb (II) and BPA removal by PPAC and PPAC-MS 100. As a result, the adsorption capacity of Pb (II) by PPAC was reduced by 33% while PPAC-MS 100 had 46% reduction at 0.1 M of ionic strength. Therefore, PPAC-MS has a high sensitivity on the cationic competition compared to PPAC for Pb (II) removal. Several authors reported a high concentration of Na$^+$ contributes a repulsive force for Pb (II) at outer layer of the adsorbent surface,

77

resulting in the decrease of Pb (II) adsorption capacities (Cybelle Morales Futalan, Wan-Chi Tsai et al., 2012; Hayes, Papelis et al., 1988). On the other hand, the adsorption capacities for BPA by PPAC and PPAC-MS 100 were also significant reduced by 62% and 47%, respectively, at 0.1 M of ionic strength. When the concentration of ionic strength increases, BPA adsorption capacity reduces because of the screening effect between the adsorbent surface and BPA molecules (Bautista-Toledo M. I., Rivera-Utrilla et al., 2014). This phenomenon can be also explained by the competition between Na^+ and BPA for the available adsorption site on PPAC and PPAC-MS 100 (Xu et al., 2012). Therefore, available sorption sites for BPA were occupied by NaCl causing the reduction of BPA adsorption on PPAC and PPAC-MS 100.

(a)
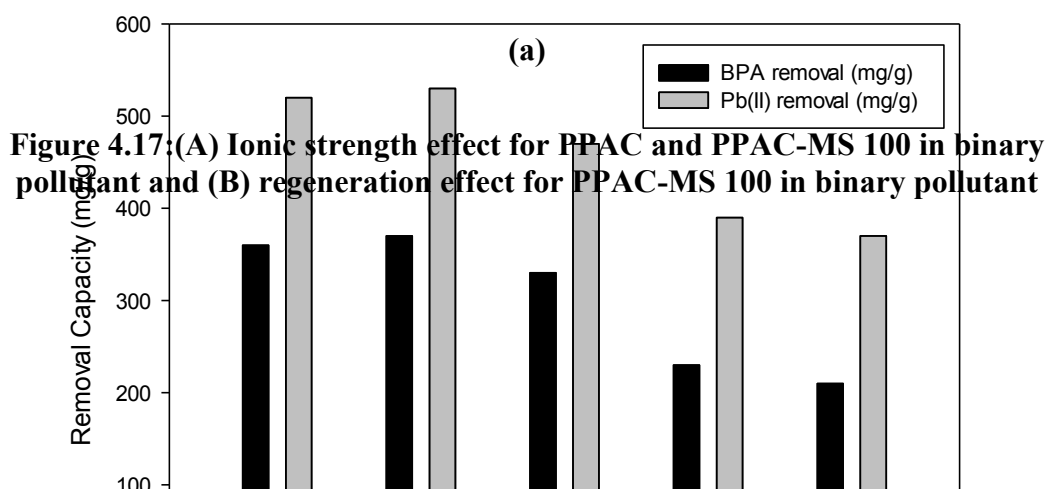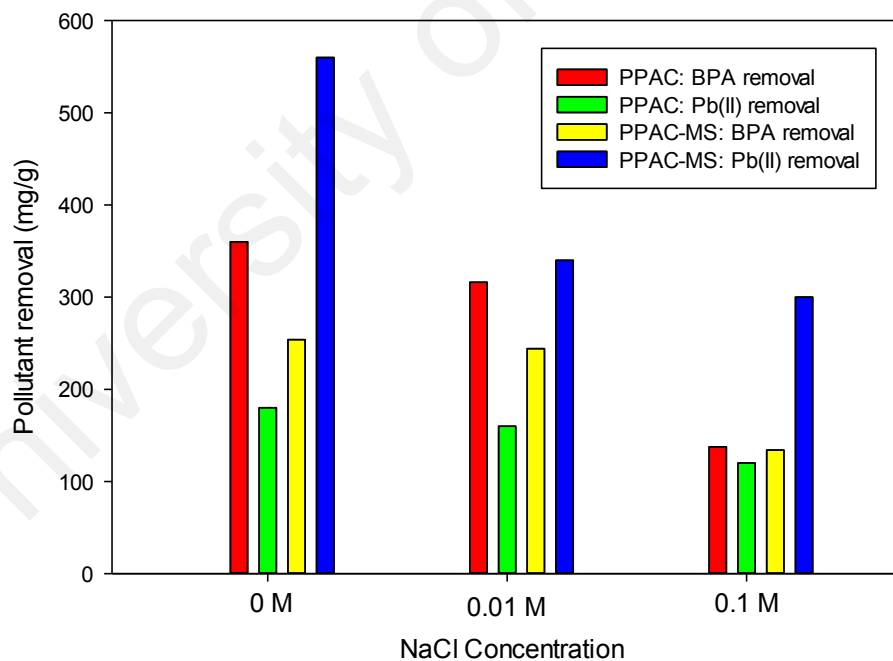
Figure 4.17:(A) Ionic strength effect for PPAC and PPAC-MS 100 in binary pollutant and (B) regeneration effect for PPAC-MS 100 in binary pollutant

78
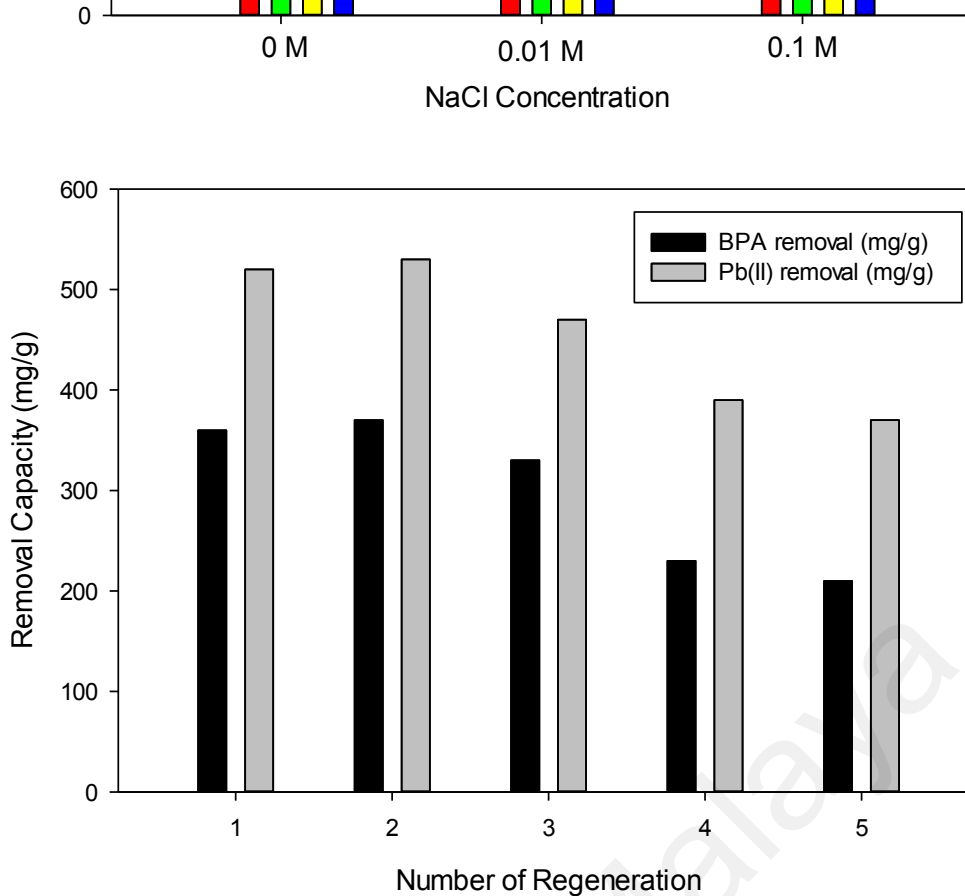
(b)

Figure 4.17, continued

4.4.5 Effect Pb (II) precipitation on BPA removal

To investigate the BPA removal on Pb (II) precipitation, we further carried out an experiment to evaluate the relationship between Pb (II) precipitation and BPA removal. Table 4.8 shows that the remained concentrations of BPA at various pHs. The experiment results indicated that BPA concentrations greatly reduced at pH 7 and remained almost same as the initial concentration at pH 2.5. The SI calculated by the Visual MINTEQ 3.1 for all Pb (II) solution at pH 7 is more than zero which indicated the $Pb(OH)_2$ mineral phase is supersaturated. Moreover, the SI for all Pb (II) solution at pH 2.5 is less than zero, indicating that the $Pb(OH)_2$ is undersaturated (refer Table 4.9).

4.4.5 Regeneration of PPAC-MS 100

As shown in Figure 4.17B, 5 cycles of adsorption-desorption were conducted to find out the reusability of PPAC-MS in binary mode. PPAC-MS had more than 80% of

Pb (II) removal capacities during three cycles, but reduced to 65% at 5th cycle. Ou et. al. (2012) reported that magnetite–magnesium silicate had about 70% of Pb (II) adsorption capacities for first 3 cycles, but reduced to 60% at fifth regeneration cycle using Mg (II) solution as desorption agent. Furthermore, thermal treatment to PPAC-MS 100 had higher than 80% of BPA removal for 5 cycles. Therefore, it can infer that PPAC-MS 100 can be reusable and maintain the sorption capacities using Mg (II) solution and thermal treatment

.

Table 4.8:Effect of pH on BPA with the present of Pb (II)

Pb (mg.L^{-1})	Remained concentrations of BPA (mg.L^{-1}) in aqueous phase		
	pH 2.5	pH 4.5	pH 7
400	117.8	101	18
300	73.3	72	29
200	67.1	66	38.9
100	34.9	35.2	13.3
50	16.4	17.3	16.5
25	7	8	6.9

Table 4.9:Visual MINTEQ 3.1 analysis of Pb (II) at different pH.

pH	400 mg L^{-1}			300 mg L^{-1}		
	Pb(OH)$_2$(s) Saturation index	Pb(OH)$_2$(s) log IAP	Pb+2 Conc.	Pb(OH)$_2$(s) Saturation index	Pb(OH)$_2$(s) log IAP	Pb+2 Conc.
2.5	-6.003	2.147	0.00193	-6.116	2.034	0.0014
3.0	-4.989	3.161	0.00193	-5.1	3.05	0.0014
3.5	-3.984	4.166	0.00193	-4.095	4.055	0.0014
4.0	-2.982	5.168	0.00193	-3.093	5.057	0.0014
4.5	-1.982	6.168	0.00193	-2.092	6.058	0.0014
5.0	-0.983	7.167	0.00193	-1.093	7.057	0.0014
5.5	0.016	8.166	0.00192	-0.095	8.055	0.0014
6.0	1.01	9.16	0.00189	0.899	9.049	0.0014
6.5	1.99	10.14	0.00180	1.88	10.03	0.0013
7.0	2.879	11.029	0.00138	2.794	10.944	0.0011
7.5	3.503	11.653	0.00057	3.455	11.605	0.0005
8.0	3.969	12.119	0.00016	3.927	12.077	0.0001

Table 4.9: Visual MINTEQ 3.1 analysis of Pb (II) at different pH continued.

pH	200 mg L^{-1}			100 mg L^{-1}		
	Pb(OH)$_2$(s) Saturation index	Pb(OH)$_2$(s) log IAP	Pb+2 Conc.	Pb(OH)$_2$(s) Saturation index	Pb(OH)$_2$(s) log IAP	Pb+2 Conc.
2.5	-6.279	1.871	0.00097	-6.565	1.585	0.00048
3.0	-5.26	2.89	0.00097	-5.541	2.609	0.00048
3.5	-4.254	3.896	0.00097	-4.532	3.618	0.00048
4.0	-3.251	4.899	0.00097	-3.529	4.621	0.00048
4.5	-2.251	5.899	0.00096	-2.528	5.622	0.00048
5.0	-1.251	6.899	0.00096	-1.529	6.621	0.00048
5.5	-0.253	7.897	0.00096	-0.53	7.62	0.00048
6.0	0.741	8.891	0.00094	0.463	8.613	0.00047
6.5	1.721	9.871	0.00090	1.443	9.593	0.00045
7.0	2.653	10.803	0.00076	2.383	10.533	0.00039
7.5	3.373	11.523	0.00039	3.183	11.333	0.00024
8.0	3.86	12.01	0.00012	3.723	11.873	0.00008

Table 4.9: Visual MINTEQ 3.1 analysis of Pb (II) at different pH continued.

pH	50 mg L^{-1}			25 mg L^{-1}		
	Pb(OH)$_2$(s) Saturation index	Pb(OH)$_2$(s) log IAP	Pb+2 Conc.	Pb(OH)$_2$(s) Saturation index	Pb(OH)$_2$(s) log IAP	Pb+2 Conc.
2.5	-6.857	1.293	0.00024	-7.153	0.997	0.00012
3.0	-5.83	2.32	0.00024	-6.123	2.027	0.00012
3.5	-4.818	3.332	0.00024	-5.108	3.042	0.00012
4.0	-3.813	4.337	0.00024	-4.103	4.047	0.00012
4.5	-2.812	5.338	0.00024	-3.101	5.049	0.00012
5.0	-1.812	6.338	0.00024	-2.101	6.049	0.00012
5.5	-0.814	7.336	0.00024	-1.103	7.047	0.00012
6.0	0.179	8.329	0.00024	-0.11	8.04	0.00012
6.5	1.159	9.309	0.00022	0.869	9.019	0.00011
7.0	2.099	10.249	0.00019	1.808	9.958	0.00010
7.5	2.934	11.084	0.00013	2.653	10.803	0.00007
8.0	3.547	11.697	0.00005	3.322	11.472	0.00003

4.4.6 Material Characteristics and adsorption mechanism

To understand the mechanisms of the removal of BPA and Pb (II) by PPAC and PPAC-MS 100, nitrogen adsorption-desorption isotherm, BET, XRD, FESEM-EDX and FTIR analysis were conducted.

First, the surface chemical characteristics of PPAC and PPAC-MS 100 were evaluated by use of FTIR (Figure 4.18). The peaks at 3737, 3729 and 3854 cm^{-1} indicated O-H stretching on PPAC and PPAC-MS 100. Asymmetric and symmetric C-H stretching vibration peaks were shown at 2924/2853 cm^{-1} for PPAC. The peak at 1556

cm^{-1} of PPAC indicated aromatic ring C=C while C-O-H group was shown at 1448 cm^{-1}. After magnesium silicate was impregnated on PPAC, C=C bond reduced and shifted to 1555cm^{-1}. Besides that, the peak of C-O-H group remained, but shifted to 1435cm^{-1}. Compared to PPAC, the peak at 1004 cm^{-1} corresponds to the asymmetric Si-O-Si or Si-O-Me (Me: metal) bond. After the adsorption in binary mode, peaks at 3369 and 3422 cm^{-1} with UPPAC-MS 100 and UPPAC, respectively, represent the OH group stretching vibration. Besides that, the peak at 1552 and 1551 cm^{-1} for UPPAC and UPPAC-MS 100, correspondingly, are characteristics of aromatic C=C bond. After BPA adsorption, the peak at 1445/1400 cm^{-1} for UPPAC/UPPAC-MS 100 greatly increased. These peaks correspond to the C-O-H bonds and the aromatic C=C bond and C-O-H were assigned as BPA compound. The new peak at 1740 cm^{-1} was recorded as C=O stretching from the carboxyl group on UPPAC. The peaks at 2927, 2855 and 2853 cm^{-1} on UPPAC and UPPAC-MS 100 indicated the C-H bond stretching due to the alkyl chain of BPA of the grafted side chains (Guang Choo, Tang et al., 2011). The peak at 763 cm^{-1} can be assigned as C-C bond stretching while the peak at 2960 cm^{-1} on PLB indicated asymmetric and symmetric C-H stretching. Strong peaks at 1594 and 1489 cm^{-1} were assigned for C=C aromatic bond and C-O-H group, respectively. The peaks at 844, 829, 1175 and 1145 cm^{-1} correspond the stretching for C-O and C-C bond in both rings (Ullah, Ahmad et al., 2016). Aromatic C=C (1594 cm^{-1}), C-O-H (1489 cm^{-1}), C-C (1175 cm^{-1}) and C-O bonds (844/829 cm^{-1}) in BPA molecule were strongly detected on PLB surface. Thus, an increase of pH in Pb (II) solution results in the precipitation as Pb(OH)$_2$(s) that can sink BPA by physical co-precipitation (Sridharan & Lee, 1972).
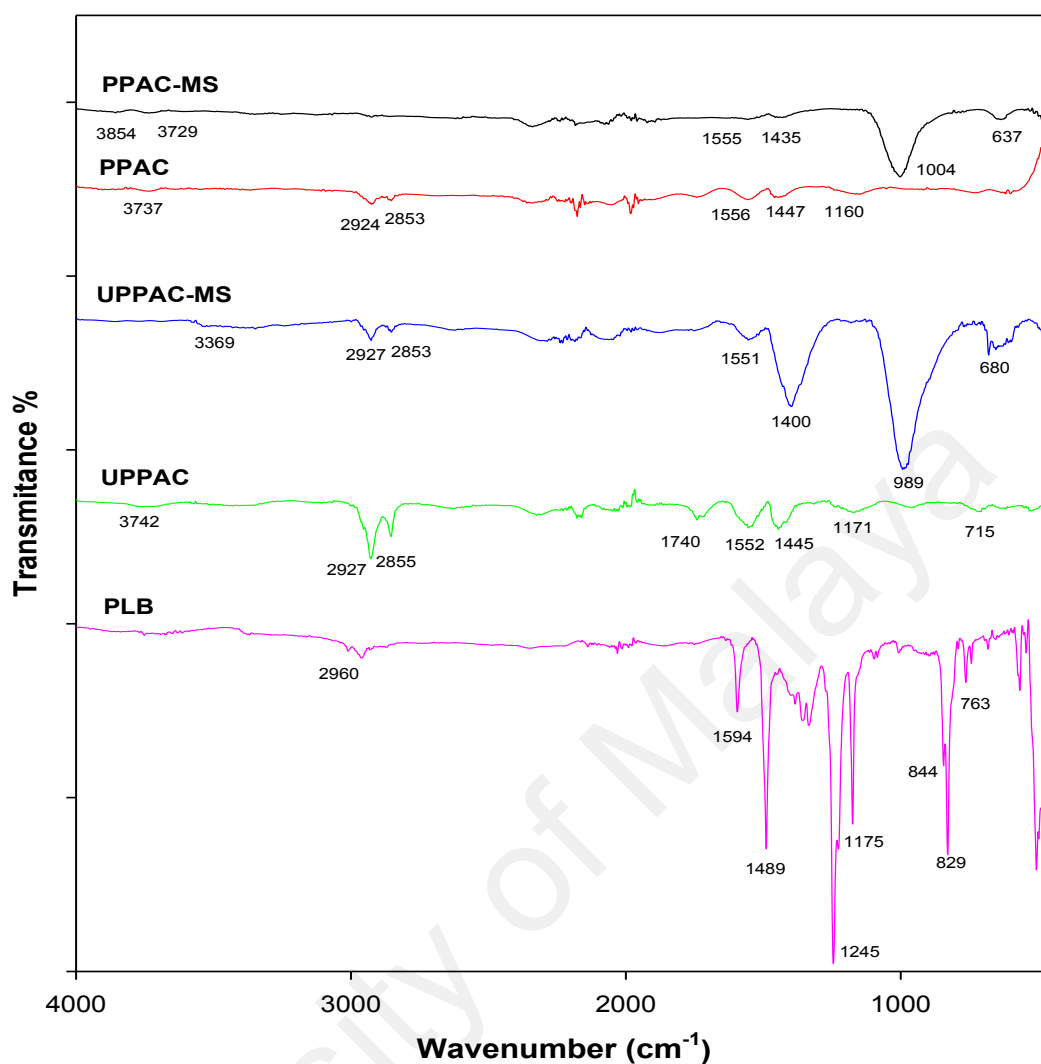
Figure 4.18:FTIR of PPAC, PPAC-MS 100, used PPAC and used PPAC-MS 100 in binary mode and PLB (precipitant of Pb (II) with BPA)

Nitrogen adsorption-desorption isotherms indicated that PPAC and PPAC-MS 100 were classified as type 1 and type 4 isotherms, respectively, according to International Union of Pure and Applied Chemistry (IUPAC) classification (Figure 4.19A). Type 1 isotherm has the characteristics for a highly micro-porous material. Especially, the marked knee at $0.02 \sim 0.2$ of P/P_0 and a low slope at $0.8 \sim 1.0$ of P/P_0 for PPAC represented significant microspores characteristics. Contrast to PPAC, PPAC-MS 100 had a high slope in $0.8 \sim 1.0$ of P/P_0, representing the existence of micro- and mesopore structures. PPAC-MS 100 exhibited a H4 hysteresis loop, in which the adsorption and desorption curves are separate and form parallel in $0.5 \sim 1.0$ of P/P_0. Figure 4.19 B illustrates the

pore size distributions of PPAC and PPAC-MS by BJH method. PPAC and PPAC-MS had a similar sharp peak at 32 Å with the FASS correction, indicating that the pore width at 32 Å increase after magnesium silicate impregnated on PPAC. Moreover, PPAC-MS had another pore ranging at 140 ~ 370 Å. BJH surface area and BJH pore volume of PPAC-MS 100 were higher than PPAC due to the formation of macro- and meso-pores formation on PPAC-MS 100 shown in Figure 4.19B. This is because the void spaces were formed by interwoven of $MgSiO_3$ on the surface of PPAC-MS 100 (Gui et al., 2014).

In order to explain the surface chemical composition of PPAC and PPAC-MS 100, XRD analysis was conducted (Figure 4.19C). PPAC had one strong peak at 29.5° assigned as graphite (JCPDS File no. 01-0640) and broad asymmetric peaks from 25° ~ 50°, corresponding to typical amorphous carbon activated by KOH (Gaya et al., 2015; Khalil, Jawaid et al., 2013). Meanwhile, the XRD analysis for PPAC-MS 100 presented the peaks at 20° and 60°, matching to magnesium hydroxide (JCPSD file no.07-0239) and peaks at 36° and 42° assigned as magnesium silicate (JCPDS file no. 07-0230) (Ding, Zhang et al., 2001; Lin, Wang et al., 2015). The XRD patterns for UPPAC and UPPAC-MS 100 obtained after binary mode adsorption were depicted in Figure 4.19D. UPPAC-MS 100 had significant sharp peaks at 19.9°, 20.9°, 24.7°, 27.4°, 32.3°, 34.2°, 36.1°, 42.6°, 44.2°, 53.9° and 58.2°, corresponding to hydrocerussite ($2PbCO_3 \cdot Pb(OH)_2$) (JCPDS file 13-131) (Figueiredo, Silva et al., 2006). The results infer that Pb (II) was removed by precipitation on PPAC-MS surface. Whiles, XRD pattern for UPPAC had a similar pattern for PPAC, but all peaks were reduced.

A

B (upper right panel)

C (left lower panel)

(a)

B (center panel)

D (right panel)

^ **Graphite**
* **MgOH**
+ **MgSiO₃**

H **Hydrocerussite**
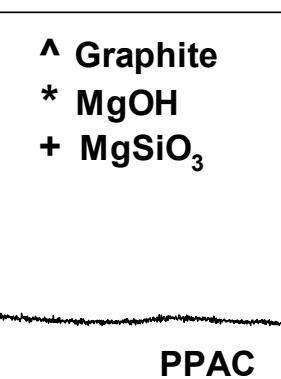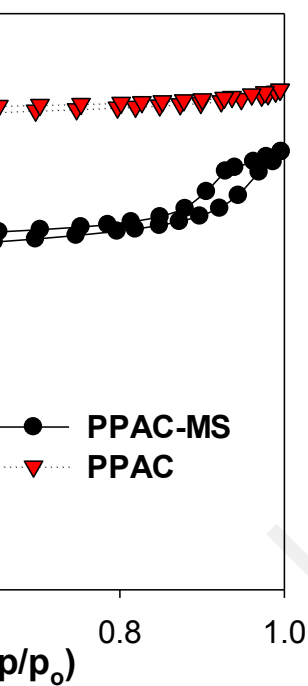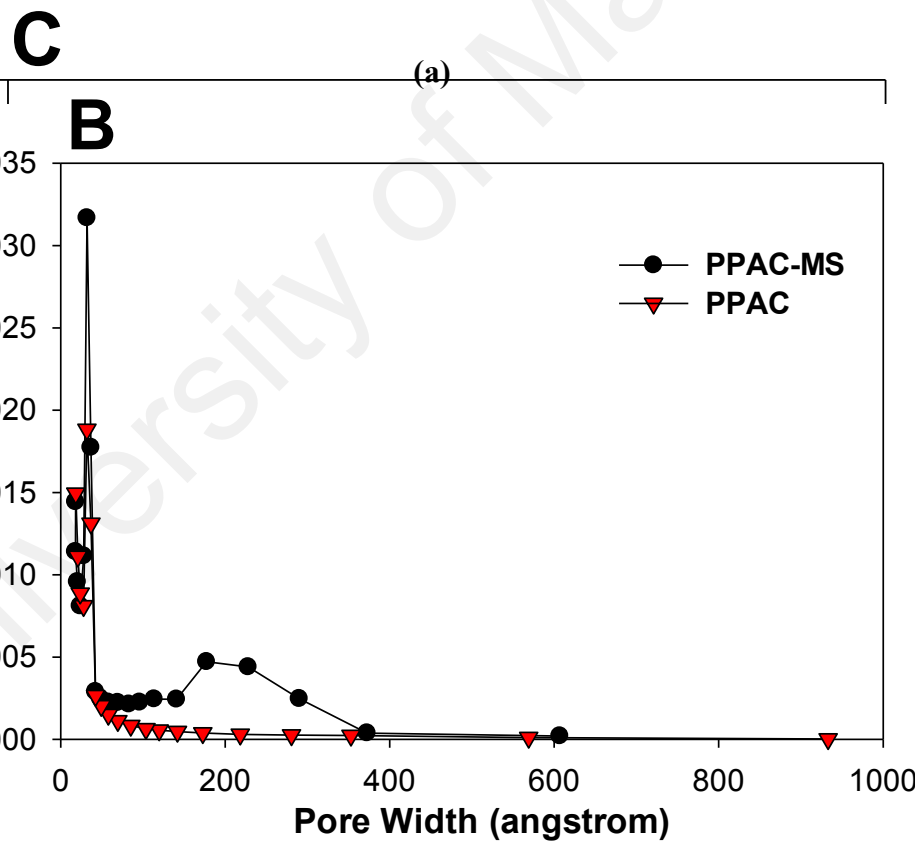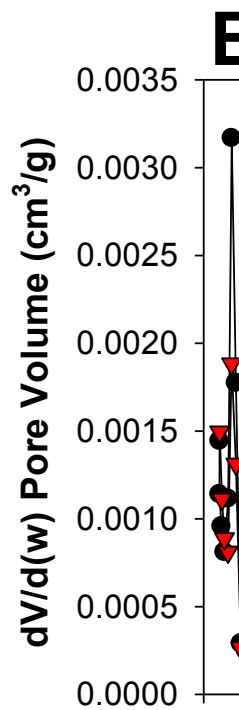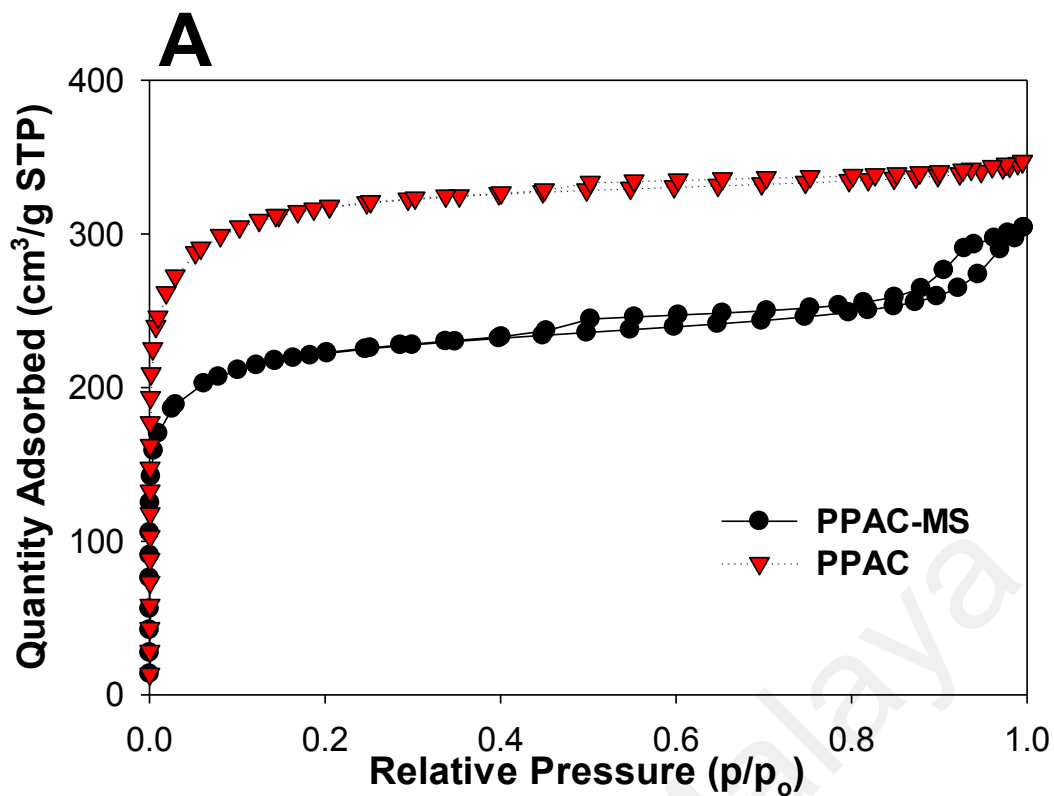
Figure 4.19 : (A) N2 gas adsorption-desorption isotherms of PPAC and PPAC-MS 100, (B) differential pore volume vs pore width with FAAS correction, (C) XRD for PPAC and PPAC-MS 100, (D) UPPAC and UPPAC-MS in binary mode

(b)

UPPAC

PPAC

87

C

^ **Graphite**

B

^ **Graphite**
* **MgOH**
+ **MgSiO₃**

PPAC

PPAC-MS

80

D

H **Hydrocerussite**

UPPAC

UPPAC-MS

20   40   60   80

2 Theta

(d)
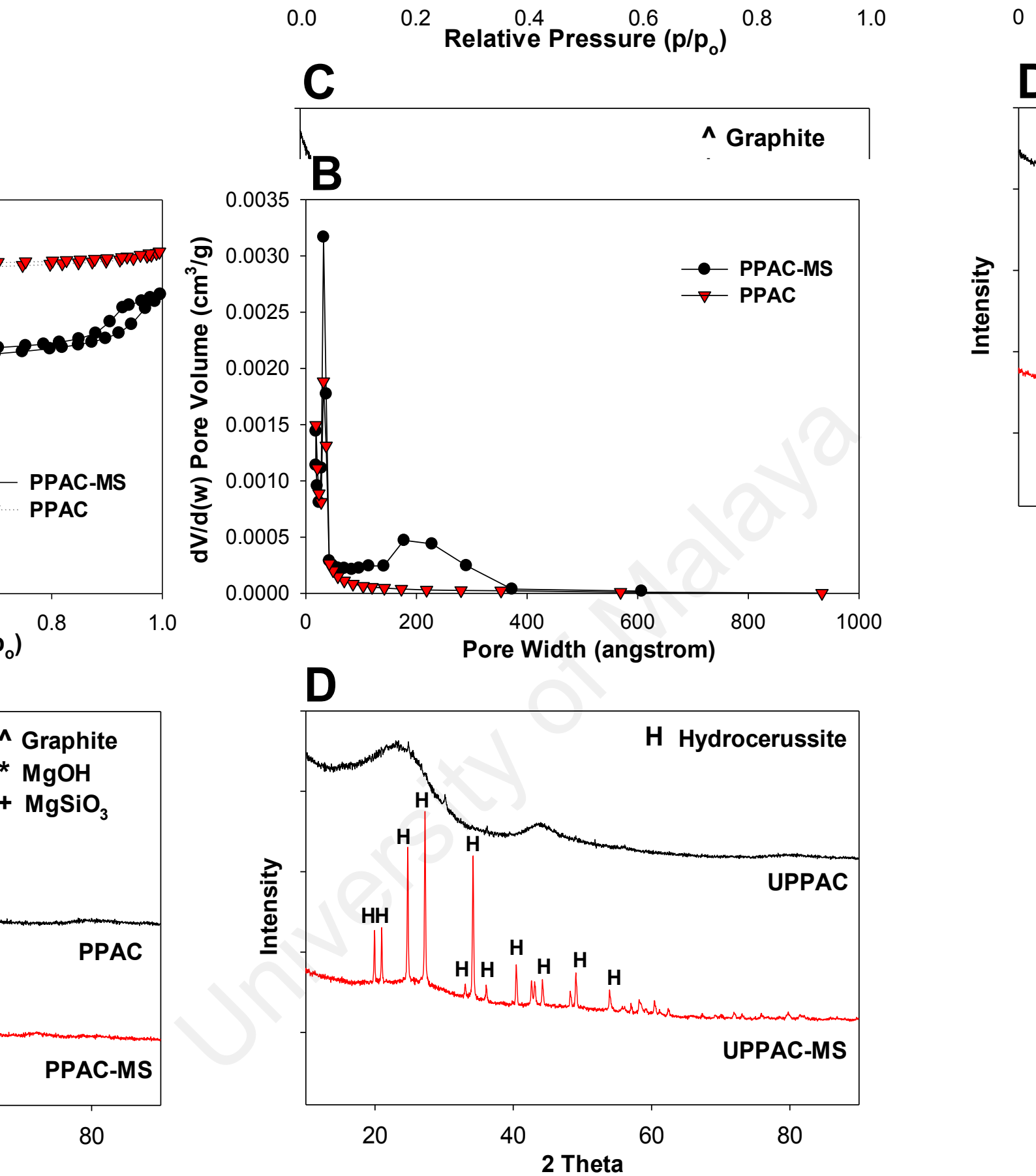
Figure 4.19, continued

The surface morphologies of PPAC and PPAC-MS 100 were analyzed by FESEM (Figure 4.20). PPAC had a smooth surface and consisted of porous structure (Figure4.20A and 4.20B). PPAC-MS 100 exhibited a rough surface with some particle agglomerate near the pore structure (Figure 4.20C). Elemental mapping (Figure 4.20D) for PPAC-MS show the Mg and Si were homogeneously dispersed on PPAC surface. As an interesting morphology, PPAC-MS 100 had a thin layer of $MgSiO_3$ without the clogging of external pores (Figure 5E). With a higher magnification, magnesium silicate exhibited a rough surface like sponge or thin plate mesh-like structure (Figure 4.20F). As Gui et al. (2014) reported that magnesium silicate forms petal-like structure under mild hypothermal preparation, this specific morphology might occur by the hydrothermal treatment. The results of EDX (Figure 4.20G) and elemental mapping represent that Mg and Si were homogeneously dispersed on the surface and their positions were shown at the similar location. Therefore, it infers that the thin layer is composed of magnesium silicate on PPAC-MS 100 as depicted in Figure 4.20G. After binary adsorption, thin sheet-like structured material was formed on the surface of UPPAC-MS 100 (Figure 4.21A and 4.21C). Based elemental mapping and EDX (Figure 4.21B and 4.21D), the thin sheet structure is hydrocerussite because the Pb and O elements match with the thin sheet structure location.
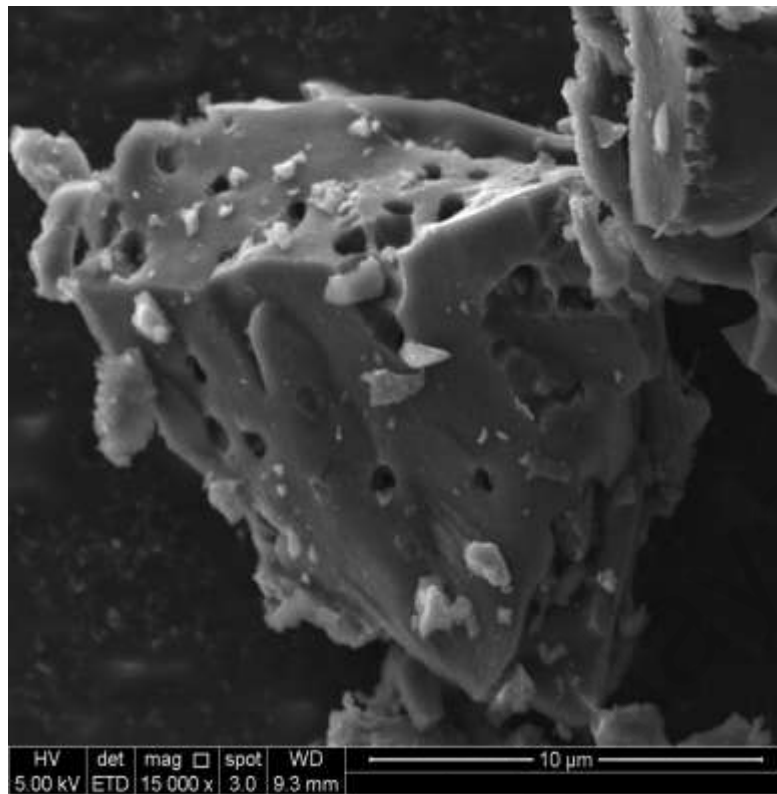
(a)
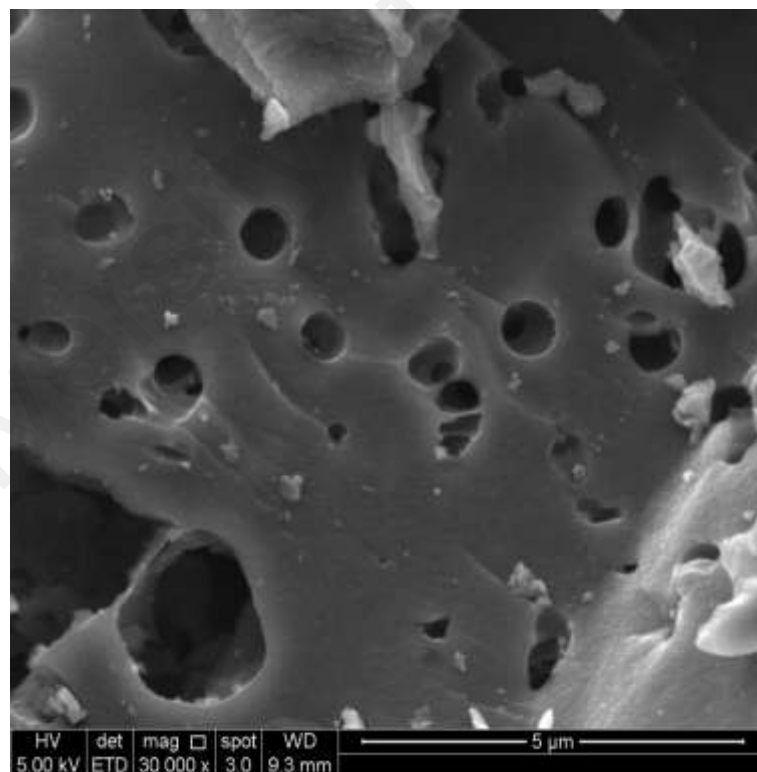
(b)

Figure 4.20: FESEM and EDS image of (A, B) PPAC, (C, D, E, F) PPAC-MS 100 and (G) element mapping for PPAC-MS 100
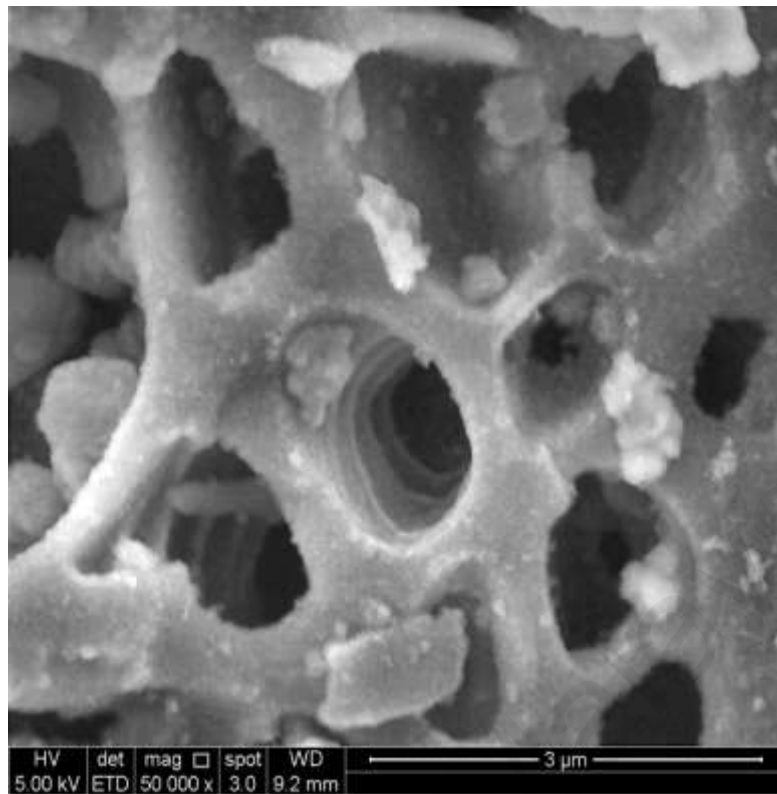
(c)
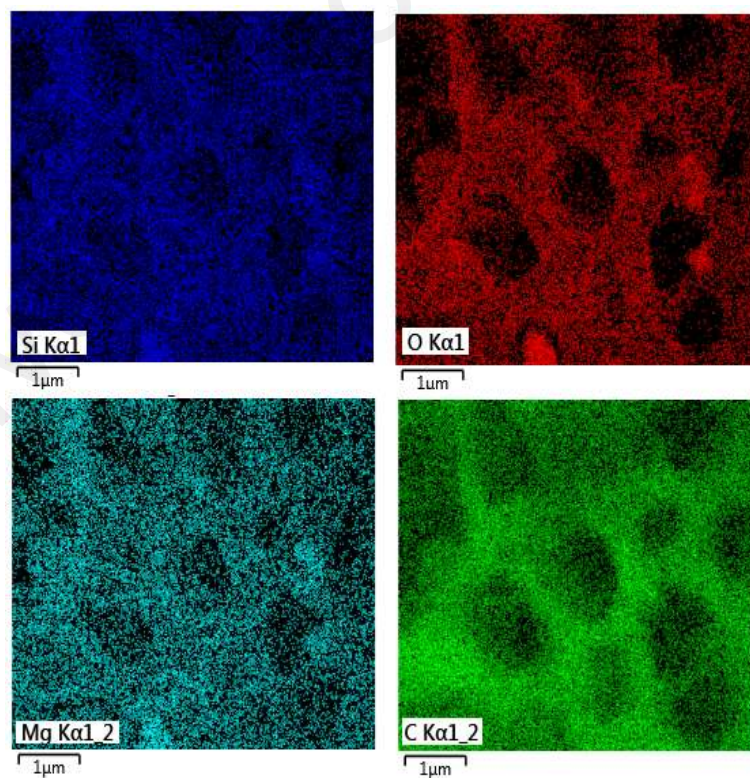
(d)

Figure 4.20, continued
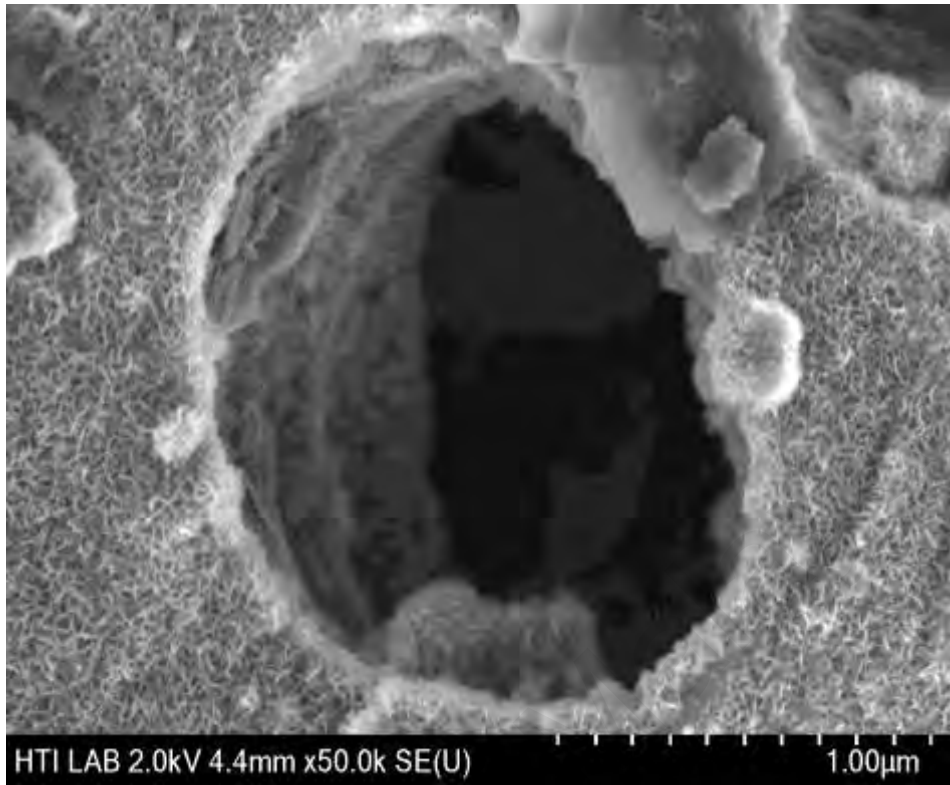
(e)
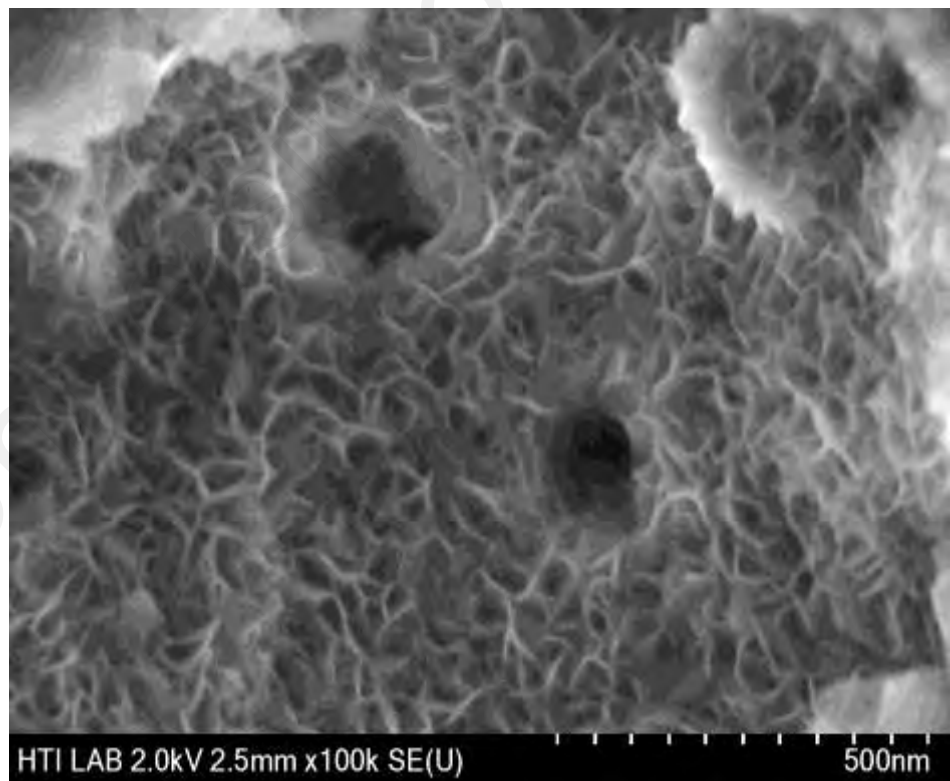
(f)

Figure 4.20, continued
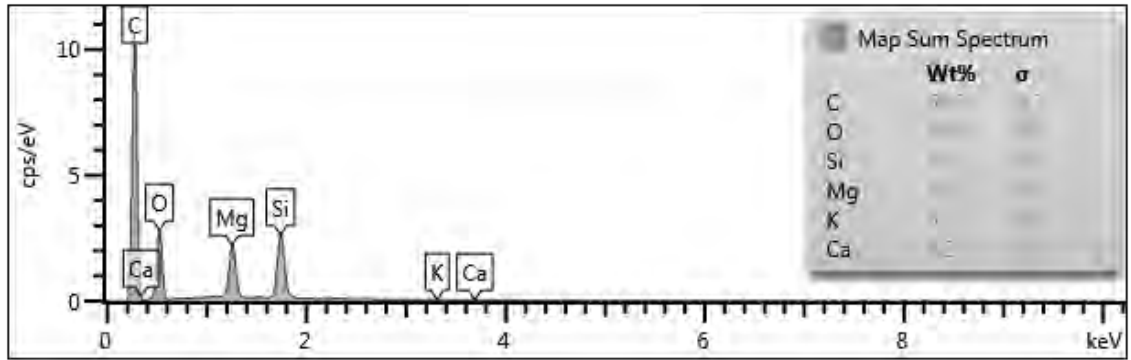
(g)

Figure 4.20, continued
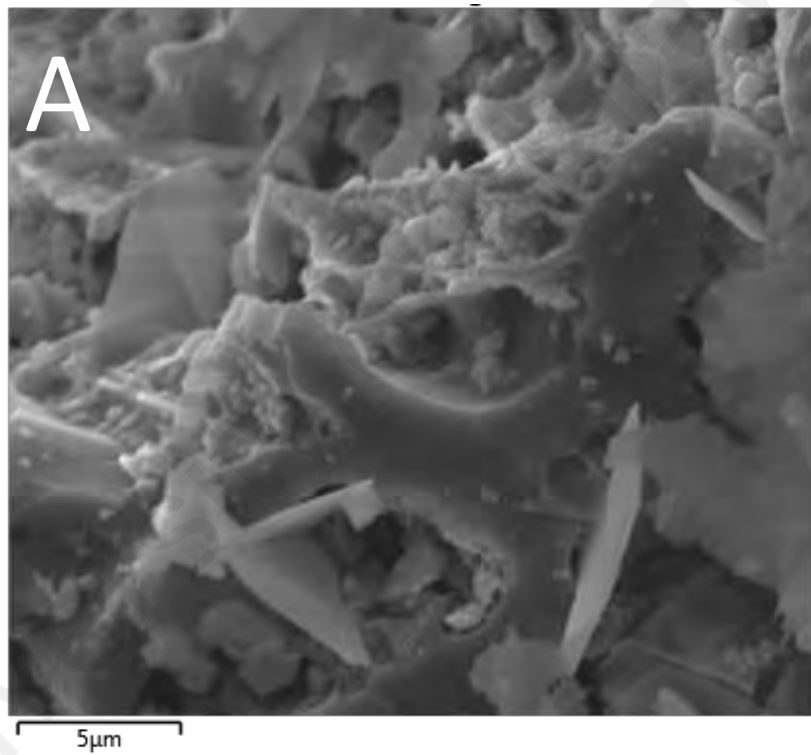
(a)

Figure 4.21: FESEM (A, C) and EDS images (B) of UPPAC-MS 100 obtained after the binary adsorption (D) element mapping for UPPAC-MS 100

Pb Mα1   O Kα1

5μm   5μm

Si Kα1   Mg Kα1_2

5μm   5μm
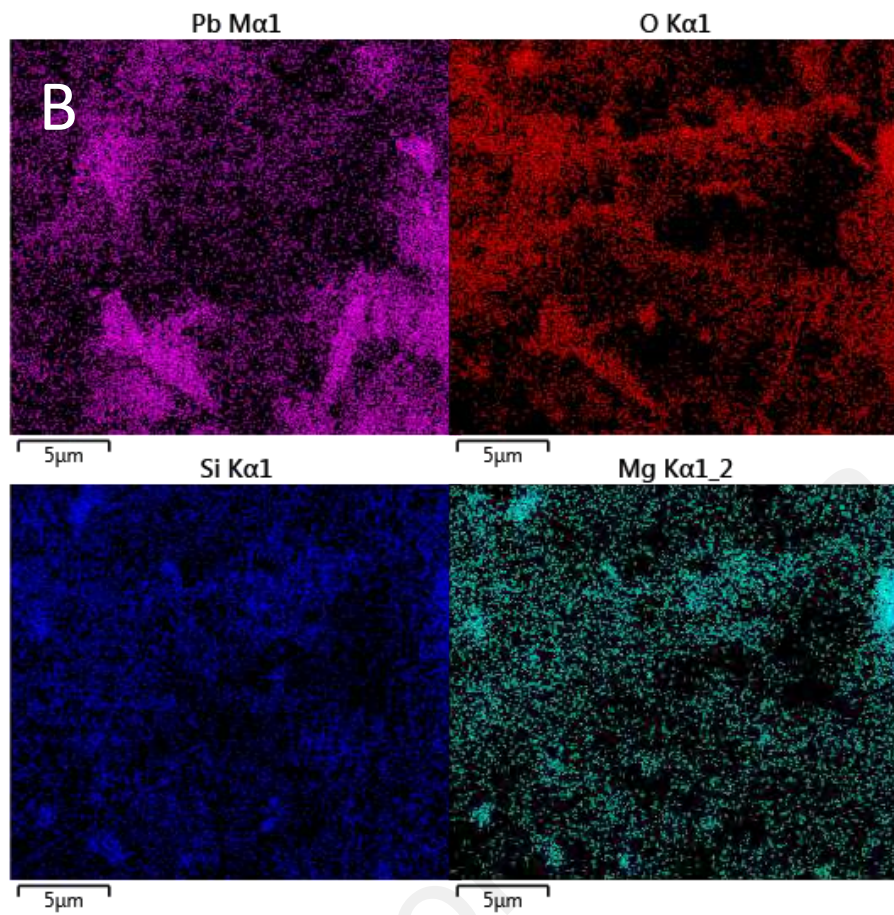
(b)
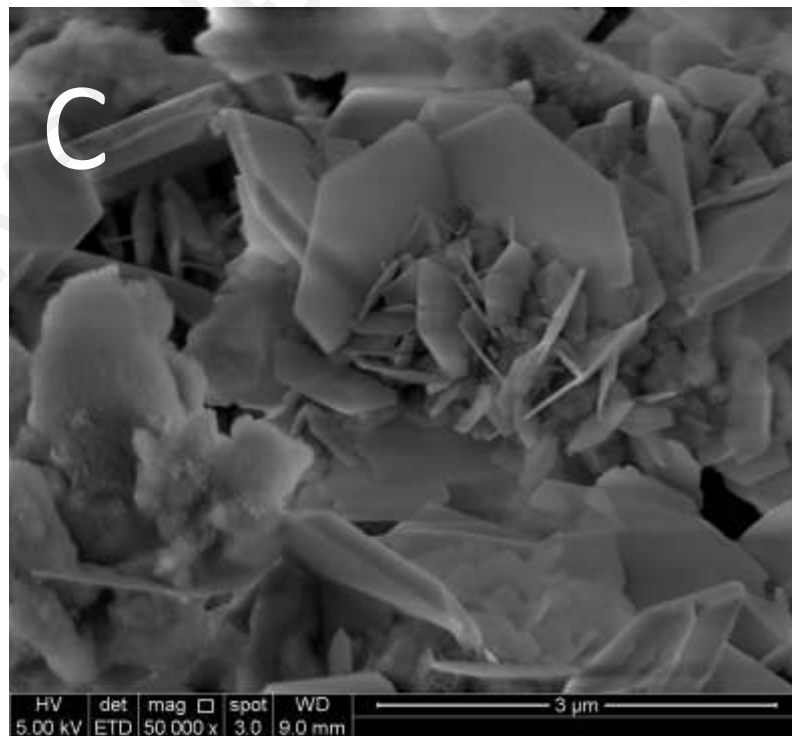
(c)

Figure 4.21, continued

94
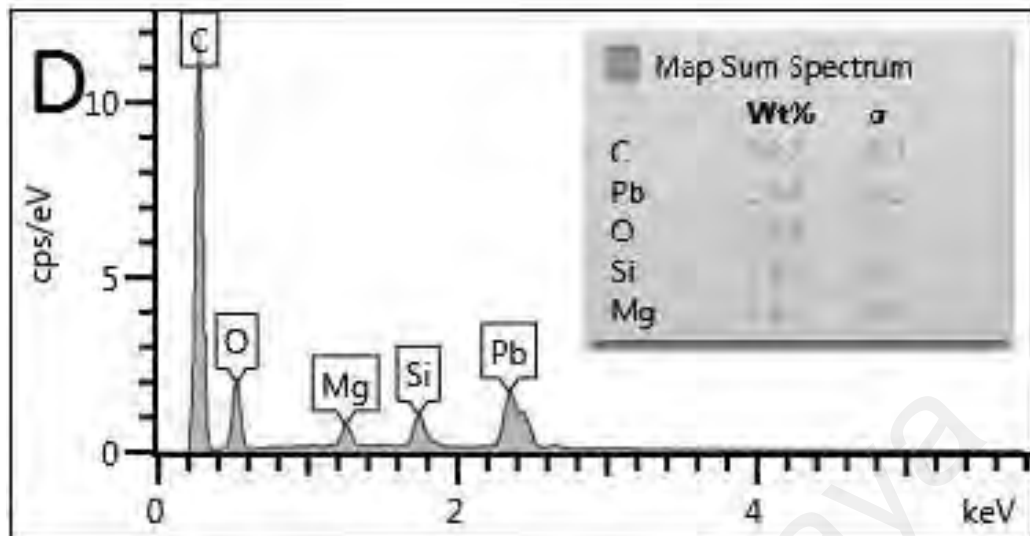
(d)

Figure 4.21, continued

Isotherm and kinetic adsorption results indicated that Pb (II) adsorption on PPAC-MS 100 is mainly involved with Si, Mg and hydroxide (OH⁻), because the adsorption capacities for Pb (II) in single mode is similar to those in binary mode. As another evidence, the present of BPA did not give any effect on the Pb (II) removal by PPAC-MS 100 in binary pollutant mode. In this study, the analytical results of FTIR, FESEM and XRD were utilized to investigate the mechanism of Pb (II) removal by PPAC-MS 100. Based on the description of previous section, the mechanism of Pb (II) removal can be proposed as precipitation and ion-exchange.

First, Pb (II) can be exchanged with Mg (II) due to the dissolution of $Mg(OH)_2$ from $MgSiO_3$ coated on PPAC-MS 100. Especially, the negative charge of Si-O formed on PPAC-MS 100 surface electro-statically attracts the positively charged Pb (II). Second, OH⁻ releases from the dissolution of magnesium hydroxide so that the increase of pH causes the precipitation of Pb (II). The FTIR result indicated the precipitation of Pb (II) as hydrocerussite $[Pb_3(CO_3)_2(OH)_2]$ (Kim & Herrera, 2010). This result was also

supported by the result of XRD, specifying that UPPAC-MS presented a XRD pattern of hydrocerussite in Figure 4D. Thus, the removal mechanism of Pb (II) by PPAC-MS 100 can be considered as the ion exchange followed by precipitation. As shown in the result of element mapping (Figure 4.21B), Pb (II) precipitation was occurred on the top of Pb (II) exchanged silicate because O, Pb and Si were detected at the similar location (Cao C.-Y., Qu et al., 2012). Thus, it can infer that Pb (II) precipitation might occur on the similar locations of ion exchange sites. Along with the result, the FTIR indicated that Si-O-Me bond was found on UPPAC-MS at peak 989 cm^{-1}, representing the occurrence of the bond of Pb (II) on Si-O. The surface reaction depicted for the removal mechanism of Pb (II) by PPAC-MS 100 can be shown below :

$$PPAC\text{-}Si\text{-}O\text{-}Mg\text{-}OH + Pb\ (II) \leftrightarrow AC\text{-}Si\text{-}O\text{-}Pb(OH) + Mg(II) + OH^{-} \qquad \text{(Ion Exchange)}$$

$$PPAC\text{-}Si\text{-}O\text{-}Pb(OH) + Pb(OH)_2 \leftrightarrow AC\text{-}Si\text{-}O\text{-}Pb\text{-}O\text{-}Pb(OH)_2 \qquad \text{(Precipitation)}$$

Meanwhile, the removal of BPA by PPAC might be happened by OH^{-} and carboxylic (COO^{-}) groups on PPAC surface. Thus, a decrease in the surface oxygen functional groups of activated carbon reduces the Pb (II) adsorption process. Pb (II) adsorption capacity by PPAC greatly decreased in binary mode and PPAC had similar adsorption capacities of BPA in both single and binary modes. Accordingly, it can be deduced that the oxygen functional group on PPAC surface might be covered by BPA to reduce the removal efficiency of Pb (II) since BPA has a priory in the adsorption surface.

The intermolecular force such as $\pi-\pi$ interaction could be the dominant mechanism for the adsorption of an organic compound consisting of aromatic or C=C double bond on graphene layer of activated carbon (Bautista-Toledo I. et al., 2005; Coughlin & Ezra, 1968). Secondly, OH group on activated carbon surface can form a hydrogen bond with BPA (Xu et al., 2012). FTIR results indicated that aromatic C=O

and C-O-H bonds were detected on UPPAC and UPPAC-MS 100 after binary adsorption. Thirdly, BPA can be co-precipitated during the precipitation of Pb on the surface of PPAC-MS 100 and PPAC in binary mode. Based on the results of BPA adsorption isotherms and kinetics, BPA adsorption increased with the present of Pb (II). However, PPAC had similar adsorption capacities of BPA in single and binary pollutant mode. Thus, BPA adsorption for PPAC has a priority compared to Pb (II) adsorption. Li et al. presented the adsorption of BPA to sediment increased in the existence of Pb (II) (Li J. et al., 2007). Sridharan and Lee (1972) found that iron salt can co-precipitate organic compound in lake water. In the result of FTIR (Figure 4.18), BPA peaks were found at UPPAC and UPPAC-MS 100 for binary mode. Overall, the mechanisms of BPA removal involved by PPAC-MS 100 and PPAC in binary mode are $\pi-\pi$ intermolecular force, hydrogen bond and co-precipitation as shown in Fig 4.22.
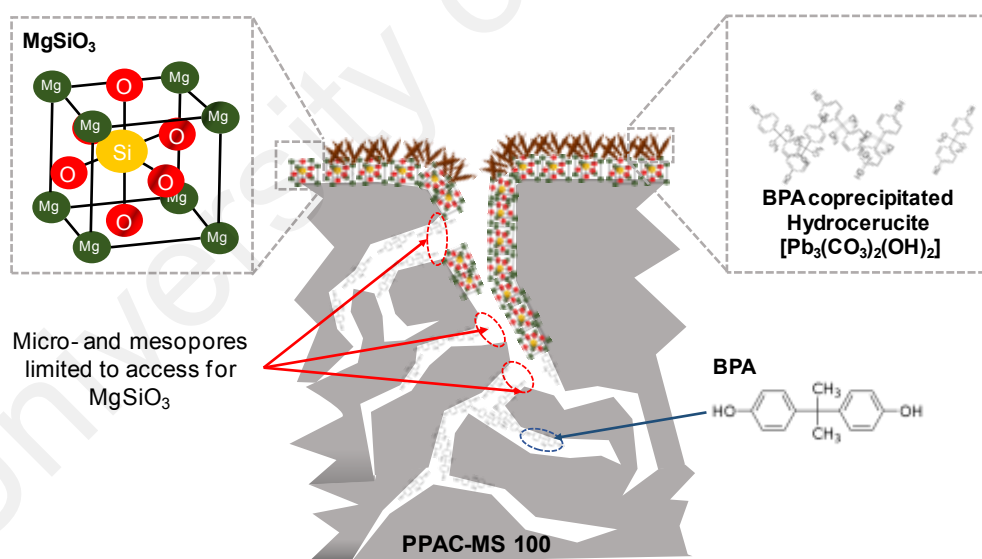
Figure 4.22: Schematics of possible BPA and Pb (II) adsorption mechanism

CHAPTER 5: CONCLUSION

5.1 Conclusion

The foremost aim of this thesis was to modify of the conventional PPAC for heavy metals wastewater treatment. The foresaid objective was successfully achieved by synthesizing meso-porous magnesium silicate from silicon powder using PPAC as a spinal. The conclusions for the adopted objective of this thesis are listed below:

- The fabrications of meso-porous adsorbent (PPAC-MS) was successfully achieved via simple and sustainable approach through mild hydrothermal treatment. The effects of impregnation ratio of $MgSiO_3$ on PPAC played crucial role for the performance of heavy metal removal.

- Physical and chemical characterizations of prepared adsorbents and commercial PPAC have been extensively investigated using FESEM-EDX, XRD, FTIR, and BET. The FESEM-EDX analyses of PPAC-MS proved that significant number of meso and marco-porous magnesium silicate was developed during the hydrothermal treatment process. Furthermore, the formation of these magnesium silicates formed a layer of plate-like structure without clogging the existing pore structure from PPAC.

- PPAC-MS shown comparatively better performance to PPAC by removing Zn (II), Al (III), As (V), Pb (II), Fe (II) and Cu (II). Adsorption of heavy metal ion onto PPAC and PPAC-MS is best represented by presudo-second-order kinetic models which indicated the adsorption processes were mainly chemisorptions. An increase in NaCl concentration decreased the adsorption capacity of PPAC-MS and PPAC. However, PPAC-MS had higher sensitivity on the cationic competition compared to PPAC for heavy metal removal. An increase in

solution pH increased the adsorption capacity of heavy metal due to the high amount of hydroxyl radical promoted the formation of metal hydroxide compound.

- The BPA and Pb (II) removal capacities by PPAC-MS and PPAC were compared to conclude that PPAC-MS had higher efficiencies of Pb (II) and BPA removal, especially in binary mode. The co-existence of heavy metals in solution significantly affected the removal of BPA for PPAC due to the competition between BPA and Pb (II). However, BPA did not promote any reduction of heavy metal adsorption for PPAC-MS.

- Regeneration by using magnesium solution is shown to be the best possible technique for reused the adsorbents for heavy metals wastewater treatment. Magnesium solution followed by thermal treatment performs excellent in the case of adsorbent loaded with organic and inorganic pollutants.

5.2 Recommendations

The following recommendations are to be considered for future research works.

- For industrially feasibility, a scale-up study is necessary in an appropriate continuous column reactor.

- Adsorption dynamic models for multi-pollutants should be undertaken as this given better understanding of sequences of competition effect in complex wastewater.

- The study on influence of numerous organic and inorganic compounds on the adsorption process could be further providing better understanding on the interaction between adsorbate and adsorbent.

- The amount of hydroxyl radicals from the dissolution of adsorbent could be quantitatively analyzed for additional information on the surface reaction.

- The study on disorder in adsorbents polymorphs using Raman spectroscopy.

REFERENCES

Ademiluyi, F. T., & David-West, E. O. (2012). Effect of chemical activation on the adsorption of heavy metals using activated carbons from waste materials. *ISRN Chemical Engineering, 2012*, 5. doi:10.5402/2012/674209

Ahluwalia, R. K., & Peng, J. K. (2009). Automotive hydrogen storage system using cryo-adsorption on activated carbon. *International Journal of Hydrogen Energy, 34*(13), 5476-5487. doi:http://dx.doi.org/10.1016/j.ijhydene.2009.05.023

Ahn, C. K., Park, D., Woo, S. H., & Park, J. M. (2009). Removal of cationic heavy metal from aqueous solution by activated carbon impregnated with anionic surfactants. *Journal of Hazardous Materials, 164*(2–3), 1130-1136. doi:http://dx.doi.org/10.1016/j.jhazmat.2008.09.036

Albroomi, H. I., Elsayed, M. A., Baraka, A., & Abdelmaged, M. A. (2017). Batch and fixed-bed adsorption of tartrazine azo-dye onto activated carbon prepared from apricot stones. *Applied Water Science, 7*(4), 2063-2074. doi:10.1007/s13201-016-0387-2

Amuda, O. S., Giwa, A. A., & Bello, I. A. (2007). Removal of heavy metal from industrial wastewater using modified activated coconut shell carbon. *Biochemical Engineering Journal, 36*(2), 174-181. doi:http://dx.doi.org/10.1016/j.bej.2007.02.013

Asfaram, A., Ghaedi, M., Hajati, S., & Goudarzi, A. (2015). Ternary dye adsorption onto MnO2 nanoparticle-loaded activated carbon: derivative spectrophotometry and modeling. *RSC Advances, 5*(88), 72300-72320. doi:10.1039/C5RA10815B

Bandyopadhyaya, R., Sivaiah, M. V., & Shankar, P. A. (2008). Silver-embedded granular activated carbon as an antibacterial medium for water purification. *Journal of Chemical Technology & Biotechnology, 83*(8), 1177-1180. doi:10.1002/jctb.1985

Barakat, M. A. (2011). New trends in removing heavy metals from industrial wastewater. *Arabian Journal of Chemistry, 4*(4), 361-377. doi:http://dx.doi.org/10.1016/j.arabjc.2010.07.019

Barth, A. (2007). Infrared spectroscopy of proteins. *Biochimica et Biophysica Acta (BBA) - Bioenergetics, 1767*(9), 1073-1101. doi:http://dx.doi.org/10.1016/j.bbabio.2007.06.004

Bartzas, G., Komnitsas, K., & Paspaliaris, I. (2006). Laboratory evaluation of Fe0 barriers to treat acidic leachates. *Minerals Engineering, 19*(5), 505-514. doi:10.1016/j.mineng.2005.09.032

Bautista-Toledo, I., Ferro-García, M. A., Rivera-Utrilla, J., Moreno-Castilla, C., & Vegas Fernández, F. J. (2005). Bisphenol A removal from water by activated carbon. Effects of carbon characteristics and solution chemistry. *Environmental Science & Technology, 39*(16), 6246-6250. doi:10.1021/es0481169

Bautista-Toledo, M. I., Rivera-Utrilla, J., Ocampo-Pérez, R., Carrasco-Marín, F., & Sánchez-Polo, M. (2014). Cooperative adsorption of bisphenol-A and chromium(III) ions from water on activated carbons prepared from olive-mill waste. *Carbon, 73*, 338-350. doi:http://dx.doi.org/10.1016/j.carbon.2014.02.073

Beckner, M., & Dailly, A. (2016). A pilot study of activated carbon and metal–organic frameworks for methane storage. *Applied Energy, 162*, 506-514. doi:http://dx.doi.org/10.1016/j.apenergy.2015.10.110

Biloé, S., Goetz, V., & Guillot, A. (2002). Optimal design of an activated carbon for an adsorbed natural gas storage system. *Carbon, 40*(8), 1295-1308. doi:http://dx.doi.org/10.1016/S0008-6223(01)00287-1

Bonvin, F., Jost, L., Randin, L., Bonvin, E., & Kohn, T. (2016). Super-fine powdered activated carbon (SPAC) for efficient removal of micropollutants from wastewater treatment plant effluent. *Water Research, 90*, 90-99. doi:10.1016/j.watres.2015.12.001

Brady, T. A., Rostam-Abadi, M., & Rood, M. J. (1996). Applications for activated carbons from waste tires: natural gas storage and air pollution control. *Gas Separation & Purification, 10*(2), 97-102. doi:http://dx.doi.org/10.1016/0950-4214(96)00007-2

Brar, S. K., Verma, M., Tyagi, R. D., & Surampalli, R. Y. (2010). Engineered nanoparticles in wastewater and wastewater sludge – Evidence and impacts. *Waste Management, 30*(3), 504-520. doi:http://dx.doi.org/10.1016/j.wasman.2009.10.012

Canadian Council of Resource and Environment Ministers. (2007). Canadian water quality guidelines for the protection of aquatic life: Summary table.*: Canadian environmental quality guidelines*. Canadian Council of Ministers of the Environment, Winnipeg.

Cao, C.-Y., Qu, J., Wei, F., Liu, H., & Song, W.-G. (2012). Superb adsorption capacity and mechanism of flowerlike magnesium oxide nanostructures for lead and cadmium ions. *ACS Applied Material Interfaces, 4*(8), 4283-4287. doi:10.1021/am300972z

Cao, H., Zheng, H., Yin, J., Lu, Y., Wu, S., Wu, X., & Li, B. (2010). Mg(OH)2 complex nanostructures with superhydrophobicity and flame retardant effects. *The Journal of Physical Chemistry C, 114*(41), 17362-17368. doi:10.1021/jp107216z

Caraballo, M. A., Rötting, T. S., Macías, F., Nieto, J. M., & Ayora, C. (2009). Field multi-step limestone and MgO passive system to treat acid mine drainage with high metal concentrations. *Applied Geochemistry, 24*(12), 2301-2311. doi:10.1016/j.apgeochem.2009.09.007

Caraballo, M. A., Rotting, T. S., & Silva, V. (2010). Implementation of an MgO-based metal removal step in the passive treatment system of Shilbottle, UK: column experiments. *Journal of Hazard Material, 181*(1-3), 923-930. doi:10.1016/j.jhazmat.2010.05.100

Cataldo, S., Gianguzza, A., Milea, D., Muratore, N., & Pettignano, A. (2016). Pb (II) adsorption by a novel activated carbon – alginate composite material. A kinetic and equilibrium study. *International Journal of Biological Macromolecules*. doi:http://dx.doi.org/10.1016/j.ijbiomac.2016.07.099

Chen, W., Parette, R., Zou, J., Cannon, F. S., & Dempsey, B. A. (2007). Arsenic removal by iron-modified activated carbon. *Water Research, 41*(9), 1851-1858. doi:http://dx.doi.org/10.1016/j.watres.2007.01.052

Chibuike, G. U., & Obiora, S. C. (2014). Heavy Metal Polluted Soils: Effect on plants and bioremediation methods. *Applied and Environmental Soil Science, 2014*, 1-12. doi:10.1155/2014/752708

Choi, B.-U., Choi, D.-K., Lee, Y.-W., Lee, B.-K., & Kim, S.-H. (2003). Adsorption equilibria of methane, ethane, ethylene, nitrogen, and hydrogen onto activated carbon. *Journal of Chemical & Engineering Data, 48*(3), 603-607. doi:10.1021/je020161d

Choi, K.-J., Kim, S.-G., & Kim, S.-H. (2008). Removal of antibiotics by coagulation and granular activated carbon filtration. *Journal of Hazardous Materials, 151*(1), 38-43. doi:http://dx.doi.org/10.1016/j.jhazmat.2007.05.059

Choi, K. J., Kim, S. G., Kim, C. W., & Kim, S. H. (2005). Effects of activated carbon types and service life on removal of endocrine disrupting chemicals: amitrol, nonylphenol, and bisphenol-A. *Chemosphere, 58*(11), 1535-1545. doi:http://dx.doi.org/10.1016/j.chemosphere.2004.11.080

Choi, K. J., Kim, S. G., Kim, C. W., & Park, J. K. (2006). Removal efficiencies of endocrine disrupting chemicals by coagulation/flocculation, ozonation, powdered/granular activated carbon adsorption, and chlorination. *Korean Journal of Chemical Engineering, 23*(3), 399-408. doi:10.1007/bf02706741

Coughlin, R. W., & Ezra, F. S. (1968). Role of surface acidity in the adsorption of organic pollutants on the surface of carbon. *Environmental Science & Technology, 2*(4), 291-297. doi:10.1021/es60016a002

Cybelle Morales Futalan, Wan-Chi Tsai, Shiow-Shyung Lin, Kuo-Jung Hsien, Maria Lourdes Dalida , & Wan, M.-W. (2012). Copper, nickel and lead adsorption from aqueous solution using chitosan-immobilized on bentonite in a ternary system. *Sustainable Environmental Research, 22(6)*, 345-355 doi:140.116.228.7

Dabrowski, A., Hubicki, Z., Podkościelny, P., & Robens, E. (2004). Selective removal of the heavy metal ions from waters and industrial wastewaters by ion-exchange method. *Chemosphere, 56*(2), 91-106. doi:http://dx.doi.org/10.1016/j.chemosphere.2004.03.006

Dai, X.-D., Liu, X.-M., Xing, W., Qian, L., Qiao, K., & Yan, Z.-F. (2009). Natural gas storage on activated carbon modified by metal oxides. *Journal of Porous Materials, 16*(1), 27-32. doi:10.1007/s10934-007-9164-9

de la Casa-Lillo, M. A., Lamari-Darkrim, F., Cazorla-Amorós, D., & Linares-Solano, A. (2002). Hydrogen storage in activated carbons and activated carbon fibers. *The Journal of Physical Chemistry B, 106*(42), 10930-10934. doi:10.1021/jp014543m

Dhaouadi, H., Chaabane, H., & Touati, F. (2011). Mg (OH) 2 nanorods synthesized by a facile hydrothermal method in the presence of CTAB. *Nano-Micro Letters, 3*(3), 153-159.

Ding, Y., Zhang, G., Wu, H., Hai, B., Wang, L., & Qian, Y. (2001). Nanoscale magnesium hydroxide and magnesium oxide powders: control over size, shape, and structure via hydrothermal synthesis. *Chemistry of Materials, 13*(2), 435-440. doi:10.1021/cm000607e

Djilani, C., Zaghdoudi, R., Djazi, F., Bouchekima, B., Lallam, A., Modarressi, A., & Rogalski, M. (2015). Adsorption of dyes on activated carbon prepared from apricot stones and commercial activated carbon. *Journal of the Taiwan Institute of Chemical Engineers, 53*, 112-121. doi:http://dx.doi.org/10.1016/j.jtice.2015.02.025

El-Sharkawy, I. I., Mansour, M. H., Awad, M. M., & El-Ashry, R. (2015). Investigation of natural gas storage through activated carbon. *Journal of Chemical & Engineering Data, 60*(11), 3215-3223. doi:10.1021/acs.jced.5b00430

Fan, T.-T., Wang, Y.-J., Li, C.-B., He, J.-Z., Gao, J., Zhou, D.-M. Sparks, D. L. (2016). Effect of organic matter on sorption of Zn on soil: elucidation by wien effect measurements and EXAFS spectroscopy. *Environmental Science & Technology, 50*(6), 2931-2937. doi:10.1021/acs.est.5b05281

Figueiredo, M. O., Silva, T. P., & Veiga, J. P. (2006). A XANES study of the structural role of lead in glazes from decorated tiles, XVI to XVIII century manufacture. *Applied Physics A, 83*(2), 209-211. doi:10.1007/s00339-006-3509-0

Freundlich, H. M. F. (1906). Over the Adsorption in Solution. *The Journal of Physical Chemistry, 57*, 385-471.

Fulazzaky, M. A., & Omar, R. (2012). Removal of oil and grease contamination from stream water using the granular activated carbon block filter. *Clean Technologies and Environmental Policy, 14*(5), 965-971. doi:10.1007/s10098-012-0471-8

Gaya, U. I., Otene, E., & Abdullah, A. H. (2015). Adsorption of aqueous Cd (II) and Pb (II) on activated carbon nanopores prepared by chemical activation of doum palm shell. *SpringerPlus, 4*, 458. doi:10.1186/s40064-015-1256-4

Gholidoust, A., Atkinson, J. D., & Hashisho, Z. (2017). Enhancing CO_2 Adsorption via Amine-Impregnated Activated Carbon from Oil Sands Coke. *Energy & Fuels, 31*(2), 1756-1763. doi:10.1021/acs.energyfuels.6b02800

Goetz, E. R., & Riefler, R. G. (2014). Performance of steel slag leach beds in acid mine drainage treatment. *Chemical Engineering Journal, 240*, 579-588. doi:10.1016/j.cej.2013.10.080

Gong, Z., Alef, K., Wilke, B.-M., & Li, P. (2007). Activated carbon adsorption of PAHs from vegetable oil used in soil remediation. *Journal of Hazardous Materials, 143*(1), 372-378. doi:http://dx.doi.org/10.1016/j.jhazmat.2006.09.037

Greenberg, A. E., Clesceri, L. S., Eaton, A. D., American Public Health, A., American Water Works, A., & Water Environment, F. (1992). *Standard methods for the examination of water and wastewater*. Washington, DC: American Public Health Association.

Guang Choo, E. S., Tang, X., Sheng, Y., Shuter, B., & Xue, J. (2011). Controlled loading of superparamagnetic nanoparticles in fluorescent nanogels as effective T2-weighted MRI contrast agents. *Journal of Materials Chemistry, 21*(7), 2310-2319. doi:10.1039/C0JM03232H

Gui, C. X., Wang, Q. Q., Hao, S. M., Qu, J., Huang, P. P., Cao, C. Y., Yu, Z. Z. (2014). Sandwichlike magnesium silicate/reduced graphene oxide nanocomposite for enhanced Pb(II) and methylene blue adsorption. *ACS Applied Material Interfaces, 6*(16), 14653-14659. doi:10.1021/am503997e

Hameed, B. H., & El-Khaiary, M. I. (2008). Malachite green adsorption by rattan sawdust: Isotherm, kinetic and mechanism modeling. *Journal of Hazardous Materials, 159*(2–3), 574-579. doi:http://dx.doi.org/10.1016/j.jhazmat.2008.02.054

Hassouna, D., Hedia, C., & Fathi, T. (2011). Mg(OH)2 Nanorods Synthesized by A Facile Hydrothermal Method in the Presence of CTAB. *Nano-Micro Letters, 3*(3), 153-159. doi:10.5101/nml.v3i3.p153-159

Hayes, K. F., Papelis, C., & Leckie, J. O. (1988). Modeling ionic strength effects on anion adsorption at hydrous oxide/solution interfaces. *Journal of Colloid and Interface Science, 125*(2), 717-726. doi:http://dx.doi.org/10.1016/0021-9797(88)90039-2

Heviánková, S., Bestová, I., & Kyncl, M. (2014). The application of wood ash as a reagent in acid mine drainage treatment. *Miner. Eng., 56*, 109-111. doi:http://doi.org/10.1016/j.mineng.2013.10.032

Hu, L., Shi, L., Hong, H., Li, M., Bao, Q., Tang, J., Gu, H. (2010). Catalytic epoxidation of stilbene with FePt@Cu nanowires and molecular oxygen. *Chemical Communications, 46*(45), 8591-8593. doi:10.1039/C0CC03204B

Jafari, R., Tanguy, P. A., & Chaouki, J. (2012). Characterization of Minimum Impeller Speed for Suspension of Solids in Liquid at High Solid Concentration, Using Gamma-Ray Densitometry. *International Journal of Chemical Engineering, 2012*, 15. doi:10.1155/2012/945314

Jais, F. M., Ibrahim, S., Yoon, Y., & Jang, M. (2016). Enhanced arsenate removal by lanthanum and nano–magnetite composite incorporated palm shell waste–based activated carbon. *Separation and Purification Technology, 169*, 93-102. doi:http://dx.doi.org/10.1016/j.seppur.2016.05.034

Johnson, P. D., Watson, M. A., Brown, J., & Jefcoat, I. A. (2002). Peanut hull pellets as a single use sorbent for the capture of Cu(II) from wastewater. *Waste Management, 22*(5), 471-480. doi:http://dx.doi.org/10.1016/S0956-053X(01)00036-8

Kadirvelu, K., Faur-Brasquet, C., & Cloirec, P. L. (2000). Removal of Cu (II), Pb (II), and Ni(II) by adsorption onto activated carbon cloths. *Langmuir, 16*(22), 8404-8409. doi:10.1021/la0004810

Kadirvelu, K., Thamaraiselvi, K., & Namasivayam, C. (2001). Removal of heavy metals from industrial wastewaters by adsorption onto activated carbon prepared from an agricultural solid waste. *Bioresource Technology, 76*(1), 63-65. doi:http://dx.doi.org/10.1016/S0960-8524(00)00072-9

Kalyoncu Ergüler, G. (2015). Investigation the applicability of eggshell for the treatment of a contaminated mining site. *Minerals Engineering, 76*, 10-19. doi:10.1016/j.mineng.2015.02.002

Kapaj, S., Peterson, H., Liber, K., & Bhattacharya, P. (2006). Human health effects from chronic arsenic poisoning--a review. *Journal of Environmetal Science & Health, A Toxic and Hazard Substance Environmetal Engineering, 41*(10), 2399-2428. doi:10.1080/10934520600873571

Karnib, M., Kabbani, A., Holail, H., & Olama, Z. (2014). Heavy metals removal using activated carbon, silica and silica activated carbon composite. *Energy Procedia, 50*, 113-120. doi:http://dx.doi.org/10.1016/j.egypro.2014.06.014

Khalil, H. P. S. A., Jawaid, M., Firoozian, P., Rashid, U., Islam, A., & Akil, H. M. (2013). Activated carbon from various agricultural wastes by chemical activation with KOH: preparation and characterization. *Journal of Biobased Materials and Bioenergy, 7*(6), 708-714. doi:10.1166/jbmb.2013.1379

Khodaie, M., Ghasemi, N., Moradi, B., & Rahimi, M. (2013). Removal of methylene blue from wastewater by adsorption onto $ZnCl_2$ activated corn husk carbon equilibrium studies. *Journal of Chemistry, 2013*, 6. doi:10.1155/2013/383985

Khraisheh, M. A. M., Al-Degs, Y. S., Allen, S. J., & Ahmad, M. N. (2002). Elucidation of controlling steps of reactive dye adsorption on activated carbon. *Industrial & Engineering Chemistry Research, 41*(6), 1651-1657. doi:10.1021/ie000942c

Kilmer, M. K., & Bouldin, J. L. (2016). Detection of lead (Pb) in three environmental matrices of the cache river watershed, Arkansas. *Bulletin of Environmental Contamination and Toxicology, 96*(6), 744-749. doi:10.1007/s00128-016-1743-5

Kim, E. J., & Herrera, J. E. (2010). Characteristics of lead corrosion scales formed during drinking water distribution and their potential influence on the release of lead and other contaminants. *Environmental Science & Technology, 44*(16), 6054-6061. doi:10.1021/es101328u

Koduru, J. R., Lingamdinne, L. P., Singh, J., & Choo, K.-H. (2016). Effective removal of bisphenol A (BPA) from water using a goethite/activated carbon composite. *Process Safety and Environmental Protection, 103*, 87-96. doi:http://dx.doi.org/10.1016/j.psep.2016.06.038

Langmuir, I. (1918). The adsorption of gases on plane surface of glass, mica and platinum. *Journal of the American Chemical Society, 40*(9), 1361-1403. doi:10.1021/ja02242a004

Lee, S., Liao, C., Song, G.-J., Ra, K., Kannan, K., & Moon, H.-B. (2015). Emission of bisphenol analogues including bisphenol A and bisphenol F from wastewater treatment plants in Korea. *Chemosphere, 119*, 1000-1006. doi:http://dx.doi.org/10.1016/j.chemosphere.2014.09.011

Leghouchi, E., Laib, E., & Guerbet, M. (2008). Evaluation of chromium contamination in water, sediment and vegetation caused by the tannery of Jijel (Algeria): a case study. *Environmental Monitoring and Assessment, 153*(1), 111. doi:10.1007/s10661-008-0341-3

Li, B., Luo, X., Zhu, Y., & Wang, X. (2015). Immobilization of Cu(II) in KIT-6 supported Co3O4 and catalytic performance for epoxidation of styrene. *Applied Surface Science, 359*, 609-620. doi:http://dx.doi.org/10.1016/j.apsusc.2015.10.131

Li, J., Zhou, B., Shao, J., Yang, Q., Liu, Y., & Cai, W. (2007). Influence of the presence of heavy metals and surface-active compounds on the sorption of bisphenol A to sediment. *Chemosphere, 68*(7), 1298-1303. doi:http://dx.doi.org/10.1016/j.chemosphere.2007.01.045

Li, S., Zhang, G., Wang, P., Zheng, H., & Zheng, Y. (2016). Microwave-enhanced Mn-Fenton process for the removal of BPA in water. *Chemical Engineering Journal, 294*, 371-379. doi:http://dx.doi.org/10.1016/j.cej.2016.03.006

Li, Y., Ben, T., Zhang, B., Fu, Y., & Qiu, S. (2013). Ultrahigh gas storage both at low and high pressures in KOH-activated carbonized porous aromatic frameworks. *3*, 2420. doi:10.1038/srep02420

Liao, J., Wen, Z., Ru, X., Chen, J., Wu, H., & Wei, C. (2016). Distribution and migration of heavy metals in soil and crops affected by acid mine drainage: Public health implications in Guangdong Province, China. *Ecotoxicology Environmental and Safety, 124*, 460-469. doi:10.1016/j.ecoenv.2015.11.023

Liao, P., Yuan, S., Zhang, W., Tong, M., & Wang, K. (2012). Mechanistic aspects of nitrogen-heterocyclic compound adsorption on bamboo charcoal. *Journal of Colloid and Interface Science, 382*(1), 74-81. doi:http://dx.doi.org/10.1016/j.jcis.2012.05.052

Lin, N., Wang, L., Zhou, J., Zhou, J., Han, Y., Zhu, Y., Cao, C. (2015). A Si/Ge nanocomposite prepared by a one-step solid-state metathesis reaction and its enhanced electrochemical performance. *Journal of Materials Chemistry A, 3*(21), 11199-11202. doi:10.1039/C5TA02216A

Linares, N., Silvestre-Albero, A. M., Serrano, E., Silvestre-Albero, J., & Garcia-Martinez, J. (2014). Mesoporous materials for clean energy technologies. *Chemical Society Reviews, 43*(22), 7681-7717. doi:10.1039/C3CS60435G

Lindsay, M. B. J., Ptacek, C. J., Blowes, D. W., & Gould, W. D. (2008). Zero-valent iron and organic carbon mixtures for remediation of acid mine drainage: Batch experiments. *Applied Geochemistry, 23*(8), 2214-2225. doi:10.1016/j.apgeochem.2008.03.005

Liu, C., Wu, P., Zhu, Y., & Tran, L. (2016). Simultaneous adsorption of Cd(II) and BPA on amphoteric surfactant activated montmorillonite. *Chemosphere, 144*, 1026-1032. doi:10.1016/j.chemosphere.2015.09.063

Lu, H., Wang, J., Stoller, M., Wang, T., Bao, Y., & Hao, H. (2016). An overview of nanomaterials for water and wastewater treatment. *Advances in Materials Science and Engineering, 2016*, 10. doi:10.1155/2016/4964828

Lua, A. C., & Guo, J. (2001). Microporous oil-palm-shell activated carbon prepared by physical activation for gas-phase adsorption. *Langmuir, 17*(22), 7112-7117. doi:10.1021/la010290c

Ma, J., Zhu, Z., Chen, B., Yang, M., Zhou, H., Li, C., Chen, J. (2013). One-pot, large-scale synthesis of magnetic activated carbon nanotubes and their applications for arsenic removal. *Journal of Materials Chemistry A, 1*(15), 4662-4666. doi:10.1039/C3TA10329C

Maarof, H. I., Ajeel, M. A., Daud, W. M. A. W., & Aroua, M. K. (2017). Electrochemical properties and electrode reversibility studies of palm shell activated carbon for heavy metal removal. *Electrochimica Acta, 249*, 96-103. doi:http://dx.doi.org/10.1016/j.electacta.2017.07.171

Madzin, Z., Shai-in, M. F., & Kusin, F. M. (2015). Comparing heavy metal mobility in active and abandoned mining sites at Bestari Jaya, Selangor. *Procedia Environmental Sciences, 30*, 232-237. doi:http://dx.doi.org/10.1016/j.proenv.2015.10.042

Mahmoud, M. E., Khalifa, M. A., El Wakeel, Y. M., Header, M. S., & Abdel-Fattah, T. M. (2017). Engineered nano-magnetic iron oxide-urea-activated carbon nanolayer sorbent for potential removal of uranium (VI) from aqueous solution. *Journal of Nuclear Materials, 487*, 13-22. doi:http://dx.doi.org/10.1016/j.jnucmat.2017.01.046

Malik, P. K. (2004). Dye removal from wastewater using activated carbon developed from sawdust: adsorption equilibrium and kinetics. *Journal of Hazardous Materials, 113*(1), 81-88. doi:http://dx.doi.org/10.1016/j.jhazmat.2004.05.022

Mobasherpour, I., Salahi, E., & Ebrahimi, M. (2014). Thermodynamics and kinetics of adsorption of Cu(II) from aqueous solutions onto multi-walled carbon nanotubes. *Journal of Saudi Chemical Society, 18*(6), 792-801. doi:http://dx.doi.org/10.1016/j.jscs.2011.09.006

Mohapatra, D. P., Brar, S. K., Tyagi, R. D., & Surampalli, R. Y. (2011). Occurrence of bisphenol A in wastewater and wastewater sludge of CUQ treatment plant. *Journal of Xenobiotics, 1*(1), 3. doi:10.4081/xeno.2011.e3

Mopoung, S., Moonsri, P., Palas, W., & Khumpai, S. (2015). Characterization and properties of activated carbon prepared from tamarind seeds by KOH activation for Fe (III) adsorption from aqueous solution. *The Scientific World Journal, 2015*, 9. doi:10.1155/2015/415961

Mudga V, M., Mudgal A, Singh RB, Mishra (2010). Effect of toxic metals on human health. *The Open Nutraceuticals Journal, 3: 94-99.*

Name, T., & Sheridan, C. (2014). Remediation of acid mine drainage using metallurgical slags. *Minerals Engineering, 64*, 15-22. doi:10.1016/j.mineng.2014.03.024

Nekouei, F., Kargarzadeh, H., Nekouei, S., Tyagi, I., Agarwal, S., & Kumar Gupta, V. (2016). Preparation of Nickel hydroxide nanoplates modified activated carbon for Malachite Green removal from solutions: Kinetic, thermodynamic, isotherm and antibacterial studies. *Process Safety and Environmental Protection, 102*, 85-97. doi:http://dx.doi.org/10.1016/j.psep.2016.02.011

Nouri, L., Ghodbane, I., Hamdaoui, O., & Chiha, M. (2007). Batch sorption dynamics and equilibrium for the removal of cadmium ions from aqueous phase using wheat bran. *Journal of Hazardous Materials, 149*(1), 115-125. doi:http://dx.doi.org/10.1016/j.jhazmat.2007.03.055

Ojedokun, A. T., & Bello, O. S. (2017). Kinetic modeling of liquid-phase adsorption of Congo red dye using guava leaf-based activated carbon. *Applied Water Science, 7*(4), 1965-1977. doi:10.1007/s13201-015-0375-y

Ou, Q., Zhou, L., Zhao, S., Geng, H., Hao, J., Xu, Y.,Chen, X. (2012). Self-templated synthesis of bifunctional Fe_3O_4@MgSiO3 magnetic sub-microspheres for toxic metal ions removal. *Chemical Engineering Journal, 180*, 121-127. doi:http://dx.doi.org/10.1016/j.cej.2011.11.022

Paggiaro, R., Bénard, P., & Polifke, W. (2010). Cryo-adsorptive hydrogen storage on activated carbon. I: Thermodynamic analysis of adsorption vessels and comparison with liquid and compressed gas hydrogen storage. *International Journal of Hydrogen Energy, 35*(2), 638-647. doi:http://dx.doi.org/10.1016/j.ijhydene.2009.10.108

Pei, L.-Z., Yin, W.-Y., Wang, J.-F., Chen, J., Fan, C.-G., & Zhang, Q.-F. (2010). Low temperature synthesis of magnesium oxide and spinel powders by a sol-gel process. *Materials Research, 13*, 339-343.

Perera, P. A. C. T., Sundarabarathy, T. V., Sivananthawerl, T., Kodithuwakku, S. P., & Edirisinghe, U. (2016). Arsenic and cadmium contamination in water, sediments and fish is a consequence of paddy cultivation: evidence of river pollution in Sri Lanka. *Achievements in the Life Sciences, 10*(2), 144-160. doi:https://doi.org/10.1016/j.als.2016.11.002

Przepiórski, J., Czyżewski, A., Pietrzak, R., & Morawski, A. W. (2013). MgO/CaO-loaded activated carbon for carbon dioxide capture: practical aspects of use. *Industrial & Engineering Chemistry Research, 52*(20), 6669-6677. doi:10.1021/ie302848r

Przepiórski, J., Czyżewski, A., Pietrzak, R., & Tryba, B. (2013). MgO/CaO-loaded porous carbons for carbon dioxide capture. *Journal of Thermal Analysis and Calorimetry, 111*(1), 357-364. doi:10.1007/s10973-012-2354-y

Rafiq, Z., Nazir, R., Durr e, S., Shah, M. R., & Ali, S. (2014). Utilization of magnesium and zinc oxide nano-adsorbents as potential materials for treatment of copper electroplating industry wastewater. *Journal of Environmental Chemical Engineering, 2*(1), 642-651. doi:http://dx.doi.org/10.1016/j.jece.2013.11.004

Ramesh, T., Rajalakshmi, N., & Dhathathreyan, K. S. (2017). Synthesis and characterization of activated carbon from jute fibers for hydrogen storage. *Renewable Energy Environment Sustainble, 2*, 4.

Reza, R. A., & Ahmaruzzaman, M. (2015). A novel synthesis of Fe_2O_3@activated carbon composite and its exploitation for the elimination of carcinogenic textile dye from an aqueous phase. *RSC Advances, 5*(14), 10575-10586. doi:10.1039/C4RA13601B

Reza, R. A., Ahmaruzzaman, M., Sil, A. K., & Gupta, V. K. (2014). Comparative Adsorption Behavior of Ibuprofen and Clofibric Acid onto Microwave Assisted Activated Bamboo Waste. *Industrial & Engineering Chemistry Research, 53*(22), 9331-9339. doi:10.1021/ie404162p

Saeidi, N., Parvini, M., & Niavarani, Z. (2015). High surface area and mesoporous graphene/activated carbon composite for adsorption of Pb(II) from wastewater. *Journal of Environmental Chemical Engineering, 3*(4, Part A), 2697-2706. doi:http://dx.doi.org/10.1016/j.jece.2015.09.023

Sánchez-Rodas, D., Luis Gómez-Ariza, J., Giráldez, I., Velasco, A., & Morales, E. (2005). Arsenic speciation in river and estuarine waters from southwest Spain. *Science of The Total Environment, 345*(1), 207-217. doi:https://doi.org/10.1016/j.scitotenv.2004.10.029

Sathishkumar, M., Binupriya, A. R., Kavitha, D., Selvakumar, R., Sheema, K. K., Choi, J. G., & Yun, S. E. (2008). Organic micro-pollutant removal in liquid-phase using carbonized silk cotton hull. *Journal of Environmental Sciences, 20*(9), 1046-1054. doi:http://dx.doi.org/10.1016/S1001-0742(08)62148-8

Sathivel, S., & Prinyawiwatkul, W. (2004). Adsorption of FFA in crude catfish oil onto chitosan, activated carbon, and activated earth: A kinetics study. *Journal of the American Oil Chemists' Society, 81*(5), 493-496. doi:10.1007/s11746-004-0929-0

Sawana, R., Somasundar, Y., Iyer, V. S., & Baruwati, B. (2017). Ceria modified activated carbon: an efficient arsenic removal adsorbent for drinking water purification. *Applied Water Science, 7*(3), 1223-1230. doi:10.1007/s13201-016-0398-z

Sethia, G., & Sayari, A. (2016). Activated carbon with optimum pore size distribution for hydrogen storage. *Carbon, 99*, 289-294. doi:http://dx.doi.org/10.1016/j.carbon.2015.12.032

Sharma, Y. C., Srivastava, V., Singh, V. K., Kaul, S. N., & Weng, C. H. (2009). Nano‐adsorbents for the removal of metallic pollutants from water and wastewater. *Environmental Technology, 30*(6), 583-609. doi:10.1080/09593330902838080

Shekinah, P., Kadirvelu, K., Kanmani, P., Senthilkumar, P., & Subburam, V. (2002). Adsorption of lead(II) from aqueous solution by activated carbon prepared from Eichhornia. *Journal of Chemical Technology & Biotechnology, 77*(4), 458-464. doi:10.1002/jctb.576

Shi, Z., Neoh, K. G., & Kang, E. T. (2007). Antibacterial and adsorption characteristics of activated carbon functionalized with quaternary ammonium moieties. *Industrial & Engineering Chemistry Research, 46*(2), 439-445. doi:10.1021/ie0608096

Shukla, S. R., & Pai, R. S. (2005). Adsorption of Cu (II), Ni (II) and Zn (II) on dye loaded groundnut shells and sawdust. *Separation and Purification Technology, 43*(1), 1-8. doi:http://dx.doi.org/10.1016/j.seppur.2004.09.003

Silvani, L., Vrchotova, B., Kastanek, P., Demnerova, K., Pettiti, I., & Papini, M. P. (2017). Characterizing biochar as alternative sorbent for oil spill remediation. *7*, 43912. doi:10.1038/srep43912

Simate, G. S., & Ndlovu, S. (2014). Acid mine drainage: challenges and opportunities. *Journal of Environmental Chemical Engineering, 2*(3), 1785-1803. doi:10.1016/j.jece.2014.07.021

Singh, K. P., Mohan, D., Sinha, S., Tondon, G. S., & Gosh, D. (2003). Color removal from wastewater using low-cost activated carbon derived from agricultural waste material. *Industrial & Engineering Chemistry Research, 42*(9), 1965-1976. doi:10.1021/ie020800d

Sircar, S., Golden, T. C., & Rao, M. B. (1996). Activated carbon for gas separation and storage. *Carbon, 34*(1), 1-12. doi:http://dx.doi.org/10.1016/0008-6223(95)00128-X

Soni, H., & Padmaja, P. (2014). Palm shell based activated carbon for removal of bisphenol A: an equilibrium, kinetic and thermodynamic study. *Journal of Porous Materials, 21*(3), 275-284. doi:10.1007/s10934-013-9772-5

Sridharan, N., & Lee, G. F. (1972). Coprecipitation of organic compounds from lake water by iron salts. *Environmental Science & Technology, 6*(12), 1031-1033. doi:10.1021/es60071a005

Sun, J., Rood, M. J., Rostam-Abadi, M., & Lizzio, A. A. (1996). Natural gas storage with activated carbon from a bituminous coal. *Gas Separation & Purification, 10*(2), 91-96. doi:http://dx.doi.org/10.1016/0950-4214(96)00009-6

Sun, Y., Yang, G., Wang, Y.-S., & Zhang, J.-P. (2011). Production of activated carbon by K2CO3 activation treatment of furfural production waste and its application in gas storage. *Environmental Progress & Sustainable Energy, 30*(4), 648-657. doi:10.1002/ep.10503

Tangahu, B. V., Sheikh Abdullah, S. R., Basri, H., Idris, M., Anuar, N., & Mukhlisin, M. (2011). A Review on heavy metals (As, Pb, and Hg) uptake by plants through phytoremediation. *International Journal of Chemical Engineering, 2011*, 31. doi:10.1155/2011/939161

Tanghe, T., & Verstraete, W. (2001). Adsorption of nonylphenol onto granular activated carbon. *Water, Air, and Soil Pollution, 131*(1), 61-72. doi:10.1023/a:1011966914827

Tao, Q., Zhu, J., Frost, R. L., Bostrom, T. E., Wellard, R. M., Wei, J.,He, H. (2010). silylation of layered double hydroxides via a calcination−rehydration route. *Langmuir, 26*(4), 2769-2773. doi:10.1021/la902812g

Tchounwou, P. B., Yedjou, C. G., Patlolla, A. K., & Sutton, D. J. (2012). Heavy metal toxicity and the environment. In A. Luch (Ed.), *Molecular, Clinical and Environmental Toxicology: Volume 3: Environmental Toxicology* (pp. 133-164). Basel: Springer Basel.

Tjokronegoro, M. H., & Roosmini, D. (2010). Study of mercury pollution at Bantarpanjang area (Citarum River) using biomarker. In A. Sumi, K. Fukushi, R. Honda, & K. M. Hassan (Eds.), *Sustainability in Food and Water: An Asian Perspective* (pp. 201-208). Dordrecht: Springer Netherlands.

Tsai, W. T., Chang, C. Y., Wang, S. Y., Chang, C. F., Chien, S. F., & Sun, H. F. (2001). Cleaner production of carbon adsorbents by utilizing agricultural waste corn cob. *Resources, Conservation and Recycling, 32*(1), 43-53. doi:http://dx.doi.org/10.1016/S0921-3449(00)00093-8

Ullah, R., Ahmad, I., & Zheng, Y. (2016). Fourier Transform Infrared Spectroscopy of Bisphenol. *Journal of Spectroscopy, 2016*, 5. doi:10.1155/2016/2073613

Vasiliev,L.L., Kanonchik, L. E., Kulakov, A. G., & Mishkins, D. A.(2007) Activated Carbon and hydrogen adsoorption storage. In T. N. Veziroglu, S. Y. Zaginaichenko, D. V. Schur, B. Baranowski, A. P. Shpak, V. V. Skorokhod, & A. Kale (Eds.), *Hydrogen Materials Science and Chemistry of Carbon Nanomaterials* (pp. 633-651). Dordrecht: Springer Netherlands.

Velazquez-Jimenez, L. H., Hurt, R. H., Matos, J., & Rangel-Mendez, J. R. (2014). Zirconium–carbon hybrid sorbent for removal of fluoride from water: Oxalic Acid Mediated Zr(IV) Assembly and Adsorption Mechanism. *Environmental Science & Technology, 48*(2), 1166-1174. doi:10.1021/es403929b

Viana, R. B., da Silva, A. B. F., & Pimentel, A. S. (2012). Infrared Spectroscopy of Anionic, Cationic, and Zwitterionic Surfactants. *Advances in Physical Chemistry, 2012*, 14. doi:10.1155/2012/903272

Wambu, E. W., Omwoyo, W. N., & Akenga, T. (2016). Excessive copper(II) and zinc(II) levels in drinkable water sources in areas along the lake Victoria Shorelines in Siaya County, Kenya. *Bulletin of Environmental Contamination and Toxicology, 96*(1), 96-101. doi:10.1007/s00128-015-1690-6

Wang, K., Zhao, J., Li, H., Zhang, X., & Shi, H. (2016). Removal of cadmium (II) from aqueous solution by granular activated carbon supported magnesium hydroxide. *Journal of the Taiwan Institute of Chemical Engineers, 61*, 287-291. doi:http://dx.doi.org/10.1016/j.jtice.2016.01.006

Wang, M. C., Sheng, G. D., & Qiu, Y. P. (2015). A novel manganese-oxide/biochar composite for efficient removal of lead(II) from aqueous solutions. *International Journal of Environmental Science and Technology, 12*(5), 1719-1726. doi:10.1007/s13762-014-0538-7

Wang, P., Ye, Y., Liang, D., Sun, H., Liu, J., Tian, Z., & Liang, C. (2016). Layered mesoporous Mg(OH)$_2$/GO nanosheet composite for efficient removal of water contaminants. *RSC Advances, 6*(32), 26977-26983. doi:10.1039/C6RA02914K

Watzlaf, G. R., Schroeder, K. T., & Kairies, C. L. (2000). Long term performance of Anoxic Limestone Drains. *Mine Water and the Environment, 19*(2), 98-110. doi:10.1007/BF02687258

Wilkin, R. T., & McNeil, M. S. (2003). Laboratory evaluation of zero-valent iron to treat water impacted by acid mine drainage. *Chemosphere, 53*(7), 715-725. doi:10.1016/s0045-6535(03)00512-5

Xu, J., Wang, L., & Zhu, Y. (2012). Decontamination of Bisphenol A from aqueous solution by graphene adsorption. *Langmuir, 28*(22), 8418-8425. doi:10.1021/la301476p

Yakout, S. M., & Borai, E. H. (2014). Adsorption behavior of cadmium onto natural chabazite: batch and column investigations. *Desalination and Water Treatment, 52*(22-24), 4212-4222. doi:10.1080/19443994.2013.803938

Yamanaka, H., Moriyoshi, K., Ohmoto, T., Ohe, T., & Sakai, K. (2008). Efficient microbial degradation of bisphenol A in the presence of activated carbon. *Journal of Bioscience and Bioengineering, 105*(2), 157-160. doi:http://dx.doi.org/10.1263/jbb.105.157

Yang, L., Wu, S., & Chen, J. P. (2007). Modification of activated carbon by polyaniline for enhanced adsorption of aqueous arsenate. *Industrial & Engineering Chemistry Research, 46*(7), 2133-2140. doi:10.1021/ie0611352

Yang, X., Li, Q., Tang, Z., Zhang, W., Yu, G., Shen, Q., & Zhao, F.-J. (2017). Heavy metal concentrations and arsenic speciation in animal manure composts in China. *Waste Management, 64*, 333-339. doi:https://doi.org/10.1016/j.wasman.2017.03.015

Yang, Y., Xie, Y., Pang, L., Li, M., Song, X., Wen, J., & Zhao, H. (2013). Preparation of reduced graphene oxide/poly(acrylamide) nanocomposite and its adsorption of Pb (II) and methylene blue. *Langmuir, 29*(34), 10727-10736. doi:10.1021/la401940z

Yantasee, W., Lin, Y., Fryxell, G. E., Alford, K. L., Busche, B. J., & Johnson, C. D. (2004). Selective removal of copper(II) from aqueous solutions Using fine-grained activated carbon functionalized with amine. *Industrial & Engineering Chemistry Research, 43*(11), 2759-2764. doi:10.1021/ie030182g

Yoon, K. Y., Byeon, J. H., Park, C. W., & Hwang, J. (2008). Antimicrobiale effect of silver particles on bacterial contamination of activated carbon fibers. *Environmental Science & Technology, 42*(4), 1251-1255. doi:10.1021/es0720199

Yu, Y., Hu, Z., Chen, Z., Yang, J., Gao, H., & Chen, Z. (2016). Organically-modified magnesium silicate nanocomposites for high-performance heavy metal removal. *RSC Advances, 6*(100), 97523-97531. doi:10.1039/C6RA20181D

Zhang, K., Li, H., Xu, X., & Yu, H. (2016). Facile and efficient synthesis of nitrogen-functionalized graphene oxide as a copper adsorbent and its application. *Industrial & Engineering Chemistry Research, 55*(8), 2328-2335. doi:10.1021/acs.iecr.5b04095

Zhang, Y. X., Huang, M., Li, F., & Wen, Z. Q. (2013). Controlled synthesis of hierarchical CuO nanostructures for electrochemical capacitor electrodes. *International Journal of Electrochemistry Science, 8*, 8645-8661.

LIST OF PUBLICATIONS AND PAPERS PRESENTED

Paper Published

1. Choe Earn Choong, Shaliza Ibrahim, Yeomin Yoon, Min Jang (2018). Removal of lead and bisphenol A using magnesium silicate impregnated palm-shell waste powdered activated carbon: Comparative studies on single and binary pollutant adsorption, Ecotoxicology and Environmental Safety, Volume 148: 142-151.

2. Choe Earn Choong, Shaliza Ibrahim, Min Jang, Gooyong Lee (2018). One-pot synthesis and characterization of magnesium silicate impregnated palm-shell-waste activated carbons and removal of copper in solution. Metals, volume 8(10):741.

Publication in preparation

1. Choe Earn Choong, Shaliza Ibrahim, Min Jang (2018). Fluoride adsorption using magnesium silicate modified activated carbon powder: Isotherm, kinetic and mechanism of adsorption.